AD-A057 645 ILLINOIS UNIV AT URBANA-CHAMPAIGN COORDINATED SCIENCE LAB F/G 20/12
ANNEALING STUDIES OF BERYLLIUM IN GALLIUM ARSENIDE AND GALLIUM --ETC(U)
DEC 77 W V MCLEVIGE DAAB07-72-C-0259
UNCLASSIFIED R-802 NL

1 OF 2
AD
A057 645

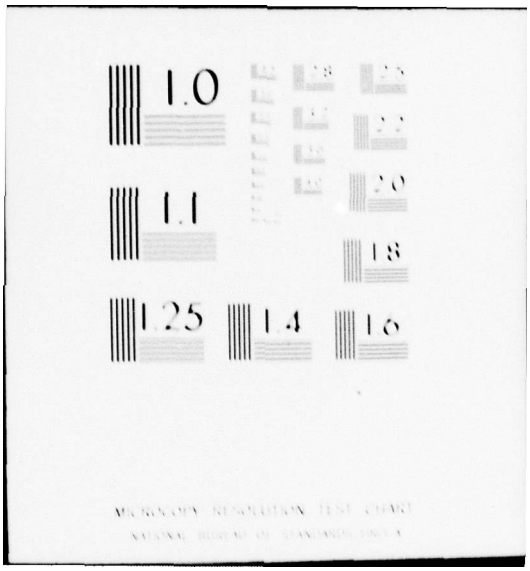
1.0
1.1
1.25
1.4
1.6
2.0
1.8

LEVEL II

REPORT R-802 DECEMBER, 1977 UILU-ENG 77-2249

CSL COORDINATED SCIENCE LABORATORY

ANNEALING STUDIES OF BERYLLIUM IN GALLIUM ARSENIDE AND GALLIUM ARSENIDE PHOSPHIDE

WILLIAM VICTOR McLEVIGE

UNIVERSITY OF ILLINOIS - URBANA, ILLINOIS

UNCLASSIFIED

SECURITY CLASSIFICATION OF THIS PAGE (When Data Entered)

REPORT DOCUMENTATION PAGE	READ INSTRUCTIONS BEFORE COMPLETING FORM
1. REPORT NUMBER	2. GOVT ACCESSION NO. / 3. RECIPIENT'S CATALOG NUMBER
4. TITLE (and Subtitle): ANNEALING STUDIES OF BERYLLIUM IN GALLIUM ARSENIDE AND GALLIUM ARSENIDE PHOSPHIDE	5. TYPE OF REPORT & PERIOD COVERED: Technical Report
	6. PERFORMING ORG. REPORT NUMBER: R-802, UILU-ENG-77-2249
7. AUTHOR(s): William Victor McLevige	8. CONTRACT OR GRANT NUMBER(s): DAAB-07-72-C-0259; N00014-76-C-0806; Monsanto Company
9. PERFORMING ORGANIZATION NAME AND ADDRESS: Coordinated Science Laboratory, University of Illinois at Urbana-Champaign, Urbana, Illinois 61801	10. PROGRAM ELEMENT, PROJECT, TASK AREA & WORK UNIT NUMBERS
11. CONTROLLING OFFICE NAME AND ADDRESS: Joint Services Electronics Program	12. REPORT DATE: December, 1977
	13. NUMBER OF PAGES: 101
14. MONITORING AGENCY NAME & ADDRESS (if different from Controlling Office): Doctoral thesis, 114p.	15. SECURITY CLASS. (of this report): UNCLASSIFIED
	15a. DECLASSIFICATION/DOWNGRADING SCHEDULE

16. DISTRIBUTION STATEMENT (of this Report)

Approved for public release; distribution unlimited

17. DISTRIBUTION STATEMENT (of the abstract entered in Block 20, if different from Report)

18. SUPPLEMENTARY NOTES

19. KEY WORDS (Continue on reverse side if necessary and identify by block number)

Ion Implantation
Semiconductors
Gallium Arsenide

78 15 08 069

20. ABSTRACT (Continue on reverse side if necessary and identify by block number)

Differential resistivity and Hall effect measurements, secondary ion mass spectrometry (SIMS), and low temperature (5°K) photoluminescence are utilized to study the annealing behavior of ion-implanted beryllium in GaAs and $GaAs_{(0.6)}P_{(0.4)}$, and of beryllium incorporated in GaAs during growth by molecular beam epitaxy (MBE).

DD FORM 1 JAN 73 1473 EDITION OF 1 NOV 65 IS OBSOLETE

097700

UNCLASSIFIED LB

SECURITY CLASSIFICATION OF THIS PAGE (When Data Entered)

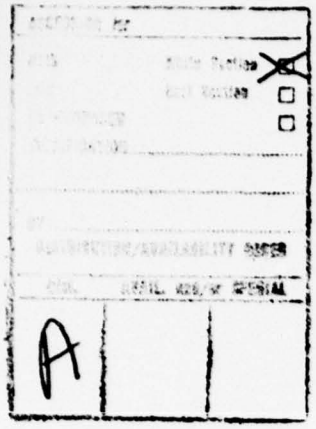

LEVEL II

UILU-ENG 77-2249

ANNEALING STUDIES OF BERYLLIUM IN GALLIUM ARSENIDE AND GALLIUM ARSENIDE PHOSPHIDE

by

William Victor McLevige

This work was supported in part by the Joint Services Electronics Program (U.S. Army, U.S. Navy and U.S. Air Force) under Contract DAAB-07-72-C-0259; the Office of Navy Research under Contract ONR N00014-76-C-0806; and by the Monsanto Company.

Approved for public release. Distribution unlimited.

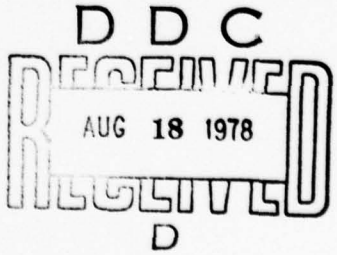

ANNEALING STUDIES OF BERYLLIUM IN GALLIUM ARSENIDE AND GALLIUM ARSENIDE PHOSPHIDE

BY

WILLIAM VICTOR McLEVIGE

B.S., University of Illinois, 1974
M.S., University of Illinois, 1975

THESIS

Submitted in partial fulfillment of the requirements
for the degree of Doctor of Philosophy in Electrical Engineering
in the Graduate College of the
University of Illinois at Urbana-Champaign, 1978

Thesis Advisor: B. G. Streetman

Urbana, Illinois

ANNEALING STUDIES OF BERYLLIUM IN GALLIUM ARSENIDE AND GALLIUM ARSENIDE PHOSPHIDE

William Victor McLevige, Ph.D.
Coordinated Science Laboratory and
Department of Electrical Engineering
University of Illinois at Urbana-Champaign, 1978

Differential resistivity and Hall effect measurements, secondary ion mass spectrometry (SIMS), and low temperature ($5^{o}K$) photoluminescence are utilized to study the annealing behavior of ion-implanted beryllium in GaAs and $GaAs_{0.6}P_{0.4}$, and of beryllium incorporated in GaAs during growth by molecular beam epitaxy (MBE).

For low fluence implants in GaAs, an electrical activation of 90-100% and no significant diffusion is observed for annealing at $900^{o}C$ with Si_3N_4 encapsulation. However, higher fluences result in a substantial redistribution of the implanted Be during the anneal, including outdiffusion into the encapsulant for Be surface concentrations above $\sim 1 \times 10^{18}$ cm^{-3}. Excellent agreement between the electrical and atomic profiles indicates that 85-100% of the Be remaining after annealing is electrically active. Implants into heated substrates and two-step anneals fail to significantly affect the diffusion of implanted Be in GaAs, indicating the diffusion is not a simple damage-related phenomenon, but instead involves a complex combination of defect and concentration-dependent effects. The diffusion coefficient of implanted Be in GaAs at $900^{o}C$ is estimated to be approximately two orders of magnitude smaller than that reported for Zn diffusion in GaAs.

The annealing behavior of Be-implanted $GaAs_{0.6}P_{0.4}$ is similar to that for Be-implanted GaAs. However, greater dependences of the electrical activation and diffusion on temperature, defects, and

surface-related effects are observed in the ternary. The low temperature (600-700°C) electrical activation of implanted Be in $GaAs_{0.6}P_{0.4}$ is substantially less than that in GaAs, and significant redistribution effects occur in the ternary alloy during 900°C annealing even for low fluence Be implants.

Substantial differences are observed between the annealing properties of Be-implanted GaAs and material doped with Be during MBE growth. Net acceptor concentrations of $\sim 3.5 \times 10^{19}$ cm^{-3} are obtainable in Be-doped MBE GaAs even after a 900°C, 1/2 hr anneal. Such a doping level is nearly one order of magnitude higher than can be achieved with Be implantation and similar annealing. The 900°C Be diffusion coefficient in Be-doped MBE GaAs is two orders of magnitude lower than that observed for implanted Be of equal concentration ($2\text{-}3 \times 10^{19}$ cm^{-3}). Only a slight concentration-dependence is observed in the diffusion of Be introduced during MBE-growth of GaAs, in contrast to an approximately square-law concentration dependence for the diffusion coefficient of implanted Be.

ACKNOWLEDGMENT

The author is especially grateful to Professor B. G. Streetman and Dr. P. K. Chatterjee for their encouragement, guidance, friendship, and inspiration that made this work possible.

He is greatly indebted to Dr. J. Comas of Naval Research Laboratory and L. Plew of Naval Weapons Support Center for performing the SIMS measurements presented here, and to Dr. M. Ilegems of Bell Laboratories for growing the Be-doped MBE GaAs layers investigated in this work. He wishes to thank Dr. D. Shaw of Texas Instruments, Dr. D. L. Kuene and Dr. D. E. Hill of Monsanto, Dr. R. Behrig and Dr. A. Moysenko of Raytheon, and Dr. J. A. Hutchby of NASA Langley for generously providing the VPE GaAs and $GaAs_{1-x}P_x$ crystals used in this work.

The author immensely appreciates the assistance and friendship of his colleagues M. J. Helix, Dr. K. V. Vaidyanathan, G. T. Marcyk, D. J. Wolford, M. Y. Tsai, T. H. Yu, A. J. Zaremba, Dr. A. J. Rosa, S. S. Chan, and Dr. D. R. Myers. He also thanks the many members of the professional staff of Coordinated Science Laboratory for their invaluable support throughout the course of this work.

The author also wishes to express his sincere gratitude to his wife Sandy, for sharing her love, her dreams, and her aspirations. Above all, the author would like to express his deep appreciation of the inner guidance and blessings of that force which has been known by so many names. In the words of Joe Henry:

> And the spirit fills the darkness of the heavens
> It fills the endless yearning of the soul
> It lives within a star too far to dream of
> It lives within each part and is the whole
> It's the fire and the wings that fly us home.

TABLE OF CONTENTS

CHAPTER Page

1. INTRODUCTION

Considerable interest in the use of the beryllium acceptor in III-V compounds has been generated by recent studies of the high electrical and optical activity exhibited by Be-implanted GaAs and $GaAs_{0.6}P_{0.4}$ [1-9]. Because of difficulties associated with the rapid diffusion of Zn [10,11], the conventional p-type dopant in GaAs and $GaAs_{1-x}P_x$, much attention has been focused on Be implantation for device applications requiring precise doping control. It has been found that extremely low leakage currents, high breakdown voltages, and greatly reduced lateral diffusion are obtainable in planar Be-implanted GaAs and $GaAs_{0.6}P_{0.4}$ p-n junctions [4,11,12]. High quality optical waveguides [13], varactors [14], detectors [15], FETs [16], and light-emitting diodes [17] have been fabricated in various III-V compounds by Be implantation.

Although these successes are very encouraging, ion implantation has certain associated complications which must be thoroughly studied and understood if its full potential as a doping technique is to be realized. Substantial lattice damage is created during the implantation process, especially for high dose implants. To reorder the crystal lattice and to activate the implanted impurity, a high temperature annealing process must be carried out. The implanted impurity must become substitutional on the correct lattice site in order to be electrically and optically active. Significant diffusion of the implanted impurity may take place during the anneal. Although not necessarily undesirable, such redistribution effects must be well understood in order to fabricate devices having specific doping profiles.

Although the annealing procedure is relatively straightforward for Si, considerable problems are encountered in the III-V compounds because of dissociation of the constituents. In the case of GaAs, surface decomposition can be severe at temperatures as low as 600°C [18]. It is therefore necessary to protect the surface with a suitable encapsulant such as chemical-vapor (CVD) or rf-plasma deposited or sputtered Si_3N_4 [19-20], or to perform the anneal in a carefully controlled ambient [21]. Various other encapsulants have been investigated, including SiO_2 [22] and AlN [23]. In this work, rf-plasma deposited Si_3N_4 has been used because it has been found to be a better mask against Ga outdiffusion than CVD SiO_2 [20,24].

Since Be is a very light ion, it is ideally suited for fairly deep implantation, with less lattice damage than is typical of a heavier ion. Although Be has been diffused into GaAs from a source evaporated onto the surface [25], implantation is a much more controllable process. Previous photoluminescence [2,3,5] and electrical [8] measurements of implanted Be have shown that this impurity is a shallow acceptor with an ionization energy of 28.4 meV in GaAs and 35 $\pm$ 3 meV in $GaAs_{0.6}P_{0.4}$.

Some disagreement has appeared in the literature regarding the optimum annealing conditions necessary to achieve proper lattice restructuring and electrical activation of the implanted Be. Early work in Be-implanted GaAs by Hunsperger *et al.* [1] and more recent studies by Zölch *et al.* [26] have indicated maximum electrical activation occurs at annealing temperatures of 600-700°C. These findings were in conflict with those of Chatterjee *et al.* [7,27], who found a continuous increase in the electrical activation of Be-implanted GaAs in annealing from 600 to 900°C, along with a striking increase in the optical activation of the implanted

Be as seen in low temperature (6°K) photoluminescence [2].

In this work, a thorough study of the electrical and optical activation and the annealing behavior of implanted Be in GaAs and $GaAs_{0.6}P_{0.4}$ has been carried out, to resolve the conflicts mentioned above and to gain a better understanding of the annealing and diffusion properties of implanted Be in these materials. Low temperature (5°K) photoluminescence was employed to study the optical activation of implanted Be and residual damage not evident in electrical properties. Profiles of the electrically active carrier distribution were obtained by performing differential resistivity and Hall effect measurements in conjunction with chemical etching for removal of successive layers. Secondary ion mass spectrometry (SIMS) was used to determine the Be atomic distribution. SIMS Be atomic profiles were compared with the net acceptor distributions found from electrical measurements for a wide range of implant doses and anneal temperatures and times.

Beryllium has also been investigated [28] as a possible p-type dopant in molecular beam epitaxial (MBE) growth of III-V compounds. MBE [29] is an epitaxial growth technique involving the simultaneous deposition of one or more thermal molecular beams on a crystalline surface under ultra-high vacuum conditions. Device quality single-crystals with precisely controlled dimensions can be grown, and the fabrication of electronic devices with ultra-thin planar structures such as superlattices [30], microwave oscillators [31], and double-heterojunction lasers [32] has been demonstrated with MBE. However, because of high vapor pressures and very low sticking coefficients ($< 10^{-5}$), elements such as Zn [33], Cd [33], and Mg [34] are difficult, if not impossible, to use in conventional MBE systems. Although a substantially higher sticking coefficient (3×10^{-2}) has been reported in

GaAs for ionized Zn [35], recent work by Ilegems [28] indicates Be may become the preferred acceptor in MBE growth of III-V compounds. Be was found to have a unity sticking coefficient in GaAs, and p-type doping levels of up to 5×10^{19} cm^{-3} were obtained. Electrical profiles determined by the differential capacitance technique established a very low diffusion coefficient for Be in GaAs of $\leq 10^{-15}$ cm^2/sec at 800°C for Be concentrations near 10^{17} cm^{-3}.

Part of the present work, done in collaboration with M. Ilegems of Bell Laboratories, includes differential resistivity and Hall effect measurements and SIMS, employed to obtain electrical carrier and atomic distribution profiles and study the properties of MBE GaAs doped with high Be concentrations during growth. The annealing behavior of Be-doped MBE GaAs is compared with that of Be-implanted vapor phase epitaxial (VPE) GaAs.

2. EXPERIMENTAL PROCEDURES

2.1. Implantation

Ion implantation is now a standard technique of doping semiconductors, and has been extensively reviewed in the literature [36-38]. Briefly, the implantation process consists of forming a plasma containing ions of the desired impurity, accelerating the ions to a high energy, selecting the desired ions by mass separation, and directing them uniformly onto a substrate. A schematic diagram of the 300 keV Accelerators, Inc. 300-MP ion implanter used in this work is shown in Fig. 2.1. Be implantations were performed by utilizing a cold cathode source with a Be exit canal which was sputtered during a BF_3 discharge to generate Be ions. Typical scanned Be currents obtained were 1.2 - 1.5 μA. To avoid channeling effects, all substrates were tilted 7° from the incident ion beam.

A theory describing the nuclear and electronic stopping processes that occur during implantation has been developed by Lindhard, Scharff, and Schiott (LSS) [39-40]. This theory predicts the implanted impurity distribution N(x) can be approximated by a Gaussian of the form

$$N(x) = \frac{4000\ N_{\square}}{\Delta R_p} \exp \frac{-(x-R_p)^2}{2\ \Delta R_p^2} \qquad (2.1)$$

where R_p is the projected ion range (microns), ΔR_p is the projected standard deviation (microns), $N_{\square}$ is the total ion fluence (ions/cm^2), and N(x) is the implanted impurity concentration (atoms/cm^3) as a function of depth x (microns). A computer program [41] has been used to perform the LSS calculations, and values of the projected range, standard deviation, and stopping powers for Be ions in GaAs and $GaAs_{0.6}P_{0.4}$ for various implantation energies are tabulated in Appendix 1.

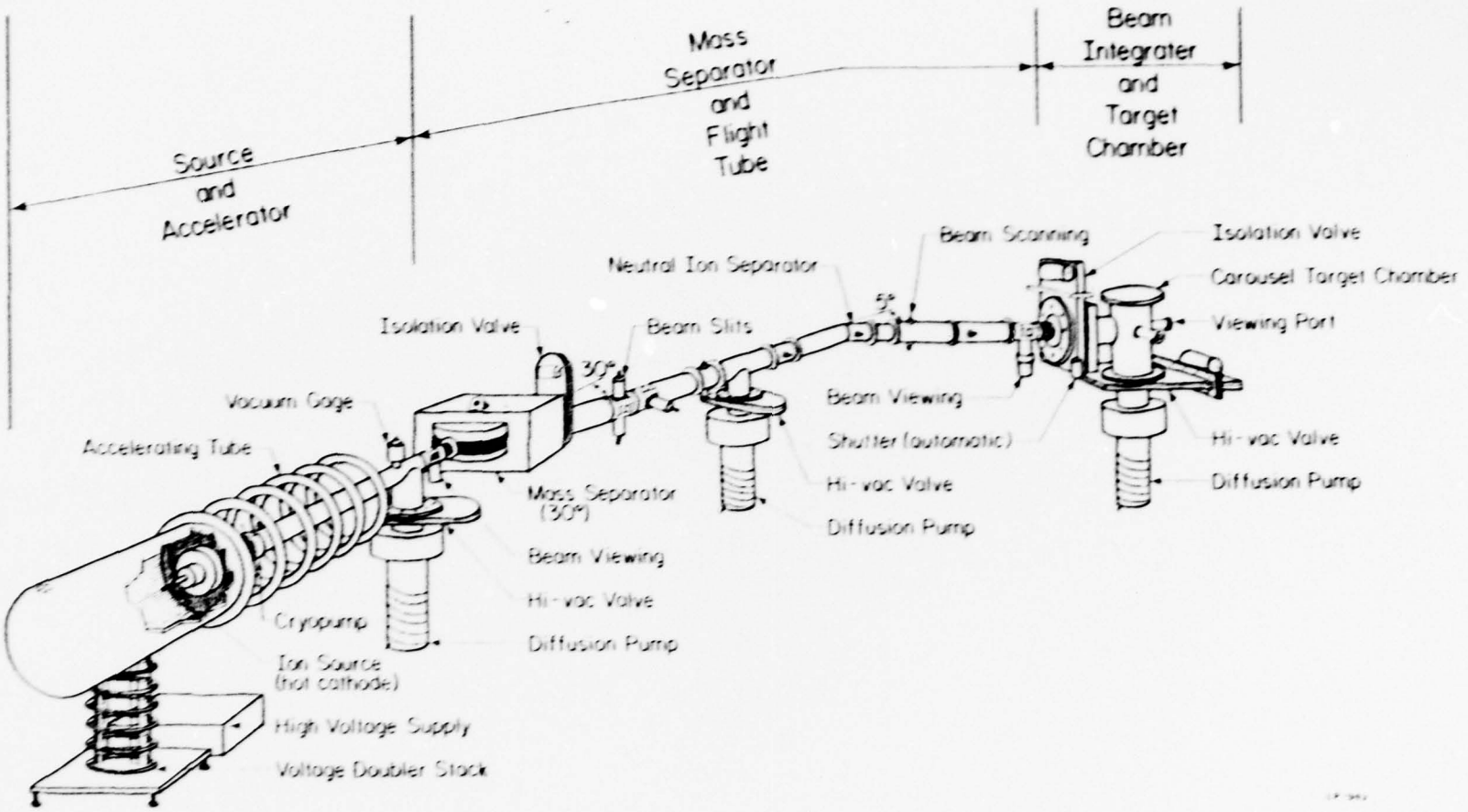

Fig. 2.1. Schematic diagram of the ion implantation system.

2.2. Encapsulation and Annealing

It has been verified by several workers [19,20,24] that Si_3N_4 encapsulation is a reliable technique for annealing of implanted GaAs. The Si_3N_4 films used in this work were obtained by an rf-plasma deposition process [42,43], for which a schematic diagram is shown in Fig. 2.2. The sample chamber is diffusion pumped (3×10^{-6} torr) prior to deposition to prevent oxygen contamination. In an earlier version of the system the mass flowmeters were not present and the gas flow rates were set by monitoring the pressure in the sample chamber. The pressure was first stabilized at 125 microns with 2% SiH_4 in Ar, and then brought up to 400 microns with N_2. In the present system the flow rates are 11 standard cubic centimeters per minute (sccm) of 2% SiH_4 in Ar and 50 sccm of N_2. To deposit Si_3N_4, the flow rates are set, the sample is quickly (< 10 sec) brought up to 450°C, and the plasma is initiated. Deposition time was ~ 15 min for the ~ 1000 Å films typically utilized. Although nearly all of the Si_3N_4 films used in this work were deposited at 450°C, excellent films have also been obtained with deposition temperatures as low as 300°C. No resulting differences in the electrical characteristics of the implanted layers after annealing were observed for the lower Si_3N_4 deposition temperatures.

The cleanliness of the sample surface was found to be critically important in ensuring proper adherence of the Si_3N_4 films. The procedure which gave best results involved ultrasonic cleaning in solvents, followed by an HCl rinse, and finally letting the sample grow a thin native oxide in deionized water for ~ 5 min prior to deposition. A Si_3N_4 layer was deposited on both sides of all samples before annealing.

The anneals for this study were performed in an 18" TransTemp

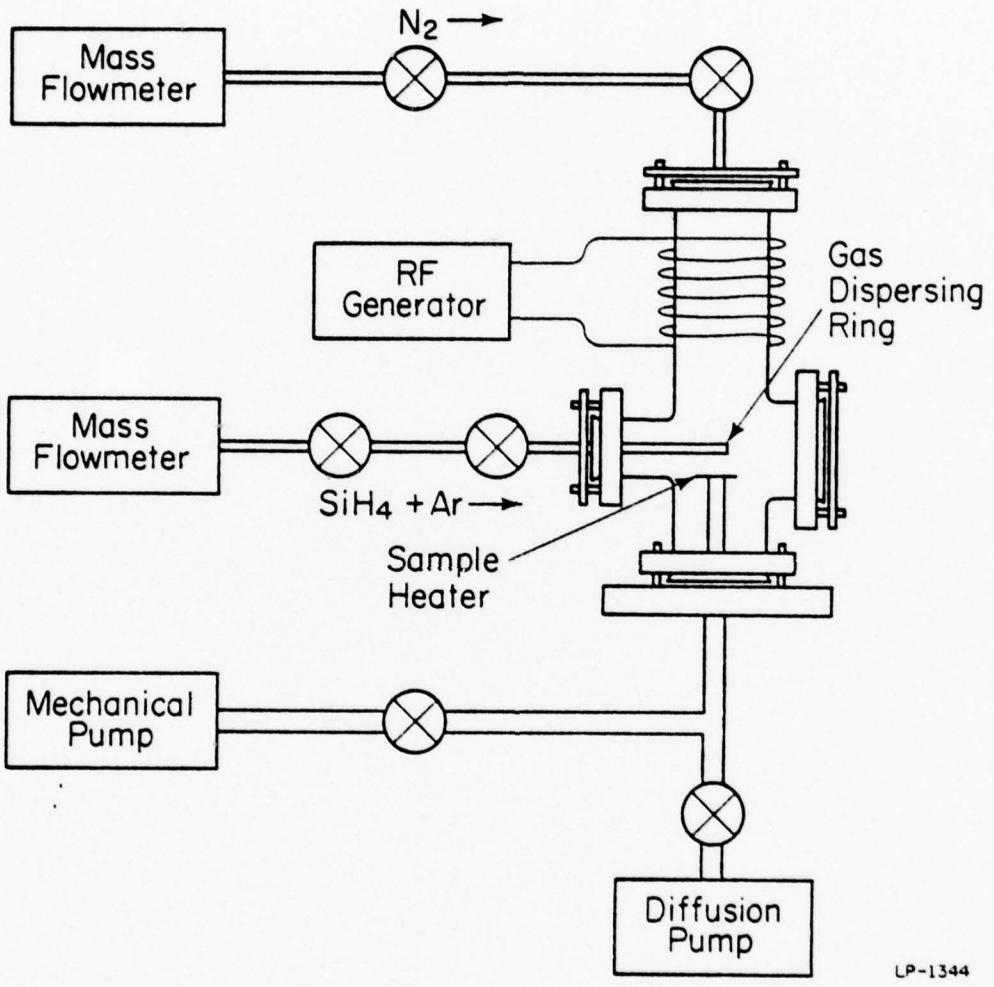

Fig. 2.2. Schematic diagram of the rf-plasma Si_3N_4 deposition system.

furnace with flowing forming gas (4% H_2 in N_2). The sample temperature was monitored by using a chromel-alumel thermocouple and a Fluke 2100A digital thermometer.

2.3. Photoluminescence

Low temperature photoluminescence is an extremely sensitive research tool for examining radiative processes in GaAs and $GaAs_{1-x}P_x$. The technique involves the generation of electron-hole pairs near the sample surface by the absorption of photons with energy greater than the bandgap of the material. The resulting excess carriers diffuse away from the surface and recombine by various characteristic radiative and non-radiative processes. The energy and intensity of the emitted luminescence gives information regarding the nature and extent of impurities and defects present in the crystal. Photoluminescence is an especially good technique for studying the annealing of implanted layers, because it can be used to monitor impurity substitution and lattice reordering. An excellent discussion of the theoretical and experimental aspects of photoluminescence, including a review of previous studies in GaAs, has been presented by Bebb and Williams [44,45].

A schematic diagram of the front-face photoluminescence apparatus utilized in this study is shown in Fig. 2.3. The photoluminescence in GaAs was excited by the focused 20 mW 5145 Å line from a Coherent Radiation Model 52G Argon-Krypton laser. The 4880 Å line was used for $GaAs_{0.6}P_{0.4}$. Samples for these measurements were compressed into indium-wetted copper heat sinks [46] and were held at ~ 5°K in a Janis "Super Varitemp" gas-exchange type liquid helium cryostat. The temperature was monitored by a calibrated Ge resistance thermometer. Spectra were recorded using a

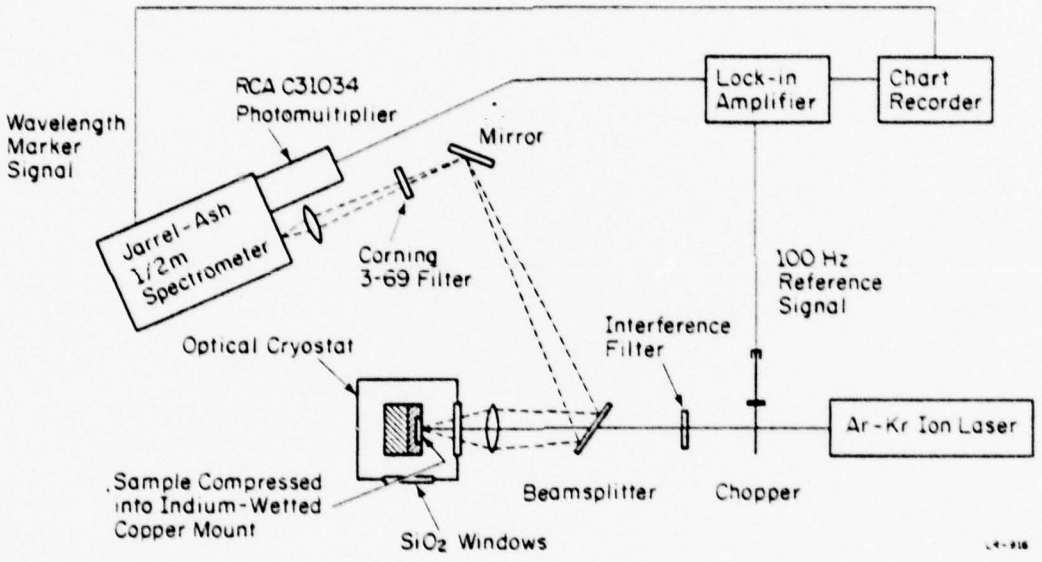

Fig. 2.3. Schematic diagram of the photoluminescence apparatus.

Jarrel-Ash 1/2 meter scanning spectrometer and an RCA C31034 GaAs photocathode.

2.4. Electrical Profiling

A common method of profiling implanted or diffused layers in semiconductors is the use of chemical etching or anodic oxidation and stripping of successive layers in conjunction with differential resistivity and Hall effect measurements [47-50]. In this work a versatile system [51] in which each step of the profiling process can be accomplished without removing the sample from its mounting, involving photolithographic techniques, or soldering the electrical contacts, has been implemented. Hall effect data is obtained through the use of the double ac method [52-55], which has the advantage of greater sensitivity and signal-to-noise ratio compared with conventional methods. Hall measurements using the dc technique are hampered with various thermoelectric and misalignment effects which must be averaged out by permutation of field and current. With the double ac method this averaging is accomplished automatically, so that only a single measurement of the Hall voltage is necessary. This greatly facilitates the profiling of implanted layers in semiconductors, in which many successive Hall effect measurements must be made. Since this technique employs separate frequencies for sample current and magnetic field, the Hall voltage appears at the heterodyne frequencies instead of at the excitation frequency as in the dc or single ac Hall effect. The use of phase sensitive lock-in detection results in excellent sensitivity and noise rejection.

2.4.1. Double ac Hall Apparatus

The block diagram of the double ac Hall system used in this work is shown in Fig. 2.4, with the corresponding circuit schematic given in

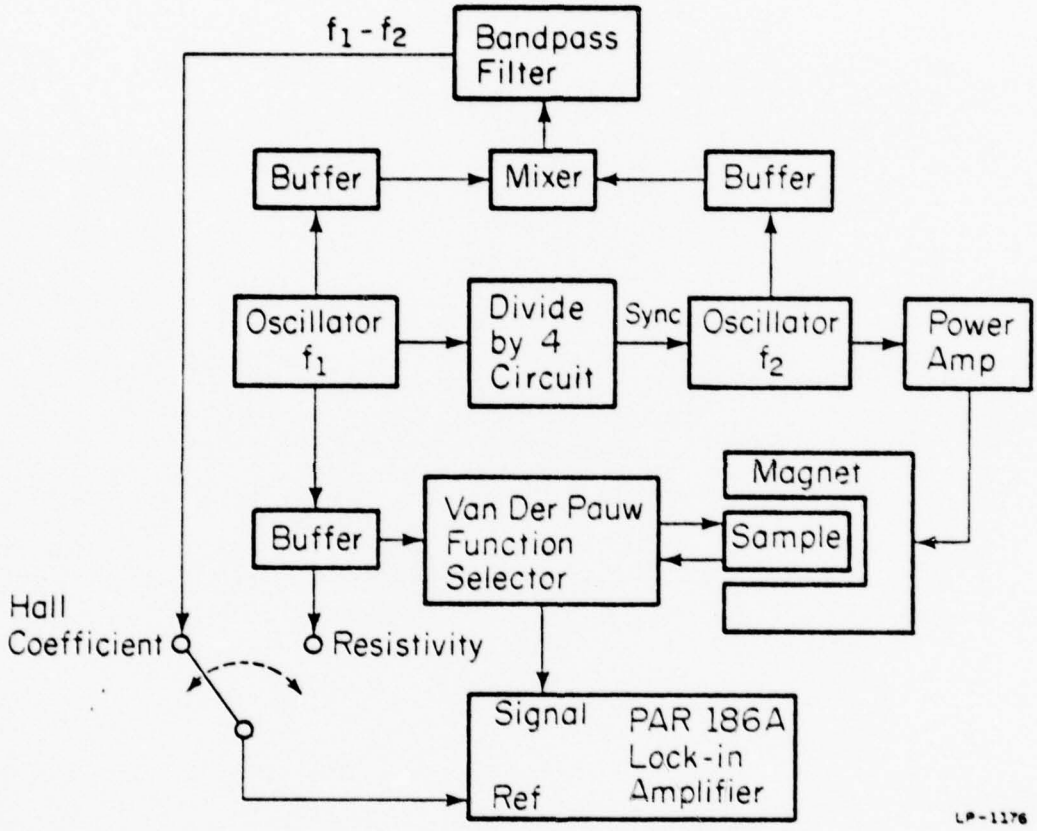

Fig. 2.4. Block diagram of the double ac Hall system.

Fig. 2.5. A sample current frequency (f_1) of 1 kHz and magnetic field frequency (f_2) of 250 Hz were chosen to give a wide frequency separation for proper suppression by the lock-in amplifier. The Hall voltage is detected at the difference frequency ($f_1 - f_2$) of 750 Hz. These choices of frequencies differ from those used by other authors. Russell and Wahlig [52] utilized 10 Hz as the Hall voltage frequency. Kaneda et al. [53] used 125 Hz, whereas Altwein et al. [55] experimented with 10 to 100 Hz. A noticeable improvement resulting from a wider frequency separation between the Hall voltage and the sample current was observed. Buffer stages are placed between the mixer and both oscillators and also before the current inputs to the sample. These additional isolation measures, along with careful shielding of all leads, result in significant noise reduction. In addition, the spectral purity of the reference waveform was found to be of critical importance in diminishing the noise level competing with the Hall signal. In practice three stages of tuned active filters are employed to generate the 750 Hz reference. The final two stages are the reference channels of PAR JB-5 and HR-8 lock-in amplifiers.

Because of the unusually high sensitivity of the double ac method and the PAR 186A lock-in amplifier used to detect the Hall signal, large magnetic fields are not necessary. In this system, a field of 200 gauss (rms) is employed. The magnetic field was determined by measuring the voltage induced in a 5-turn test coil inserted in the magnet. The calibration was checked by comparing observed double ac Hall coefficients with values obtained from dc Hall measurements.

The sample holder, shown in Fig. 2.6, fits inside a solenoidal magnet constructed by winding 7100 turns of 30 gauge transformer wire on a

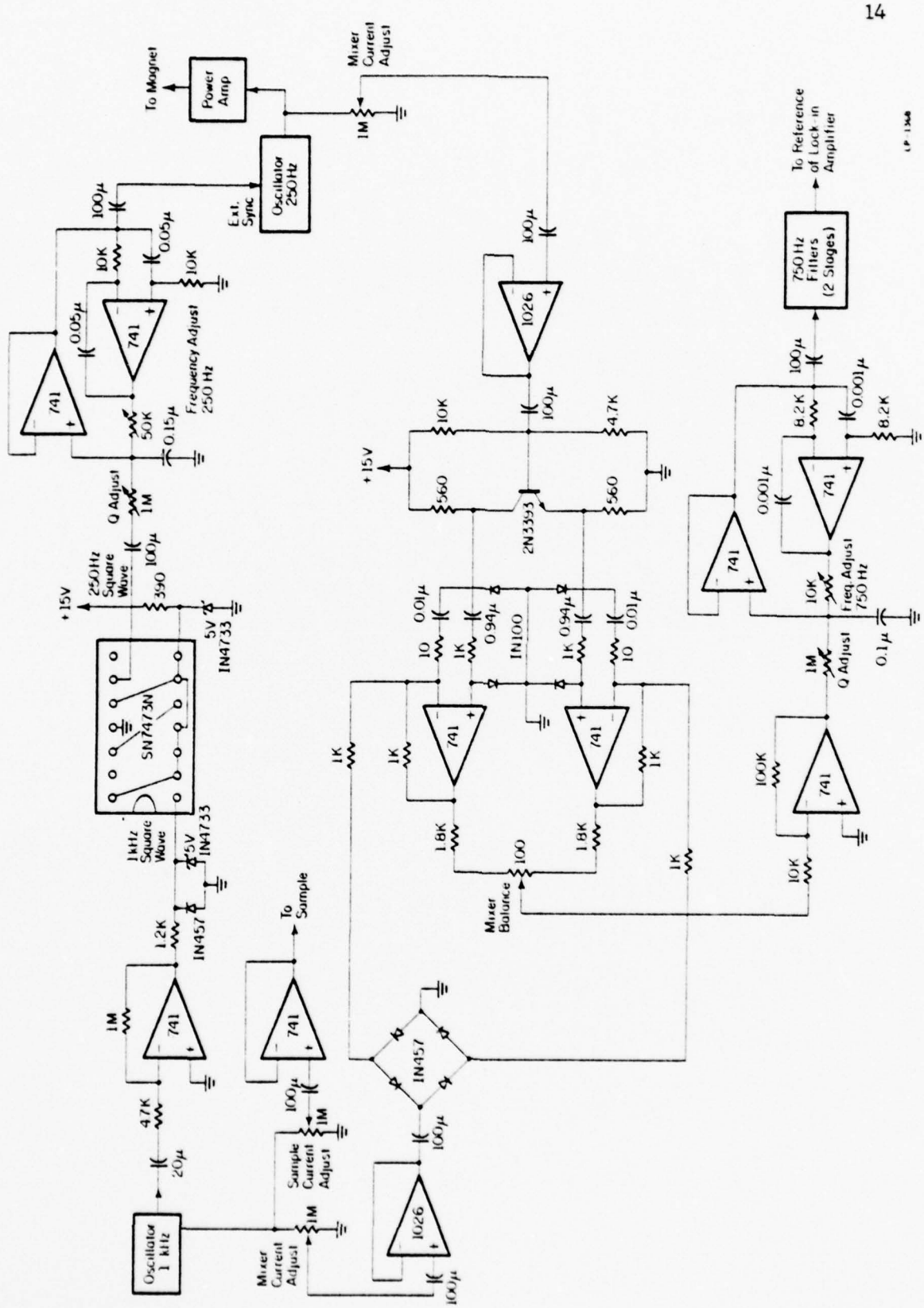

Fig. 2.5. Circuit diagram of the double ac Hall system.

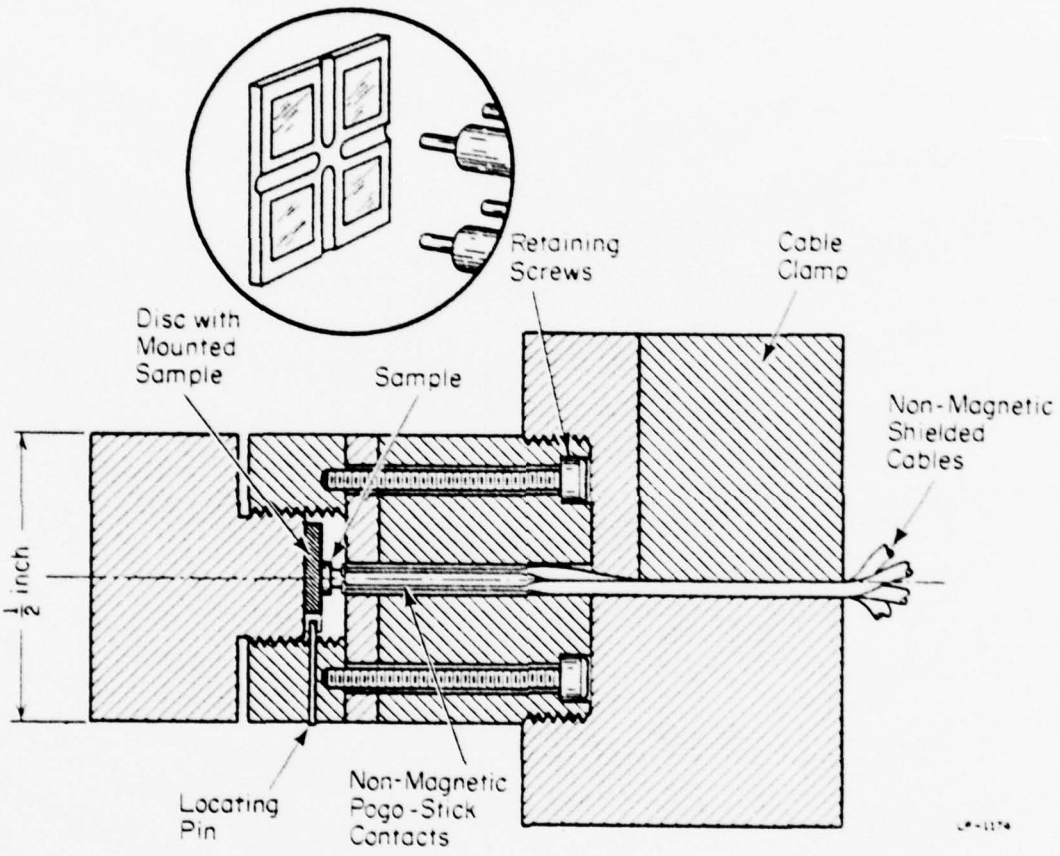

Fig. 2.6. Cross-sectional view of the sample holder used for double ac van der Pauw measurements. The inset shows the sample configuration and the spring-loaded contacts in the holder.

bakelite spool 1 inch long. Machined from nylon, the sample holder is designed to hold the nylon discs on which the samples are mounted. A locating pin automatically aligns the discs in the holder. Electrical contact is made by four non-magnetic spring-mounted "pogo-stick" contacts, which are manufactured by Pylon Co., Attleboro, MA. The repetitive measurements necessary in profiling an electrically active impurity distribution in a semiconductor are greatly facilitated by this sample holder design. The mounted sample can be quickly removed from the holder, etched, and reinserted for another measurement.

A problem associated with this design is the tendency of the metal-to-metal contact between the "pogo-sticks" of the sample holder and the evaporated contact pads on the sample to be noisy if the contacts are not clean and free of surface oxide. Although not noticeable during resistivity measurements, this noise is occasionally important in the Hall voltage. A time constant of one second or longer on the lock-in amplifier is necessary in such cases. A second problem, not well understood, is that the zero-field voltage ranges from 0 to 20% of the Hall voltage. Ideally, in a double ac Hall measurement, there should be no zero-field voltage. This voltage is most sensitive to changes in the reference signal, and is therefore apparently due to some slight distortion in the reference waveform which is not detectable on an oscilloscope trace. In practice, the Hall voltage is measured as the difference between the observed voltages with the sample in and out of the magnet.

2.4.2. Processing of the Samples

Electrical contacts to the samples for profile studies were formed by evaporating Ag-Mn [56] through a shadow mask. Contacts were sintered

at 330°C in flowing H_2 for 1 min. Measurement samples were ~ 120 mils square, with the contact pads arranged to have 60 mils between centers. The van der Pauw geometry [57,58] was defined by lightly sandblasting grooves through a stainless-steel mask 3 mil thick. Samples were secured to the mask by means of glycol phthalate during the sandblasting, and no resulting degradation of the p-n junction characteristics was observed. Insulating varnish (GE 7031) was used to mount the samples on 325 mil diameter nylon discs for measurements.

Successive layer removal of GaAs and $GaAs_{0.6}P_{0.4}$ was accomplished using a chemical etch consisting of equal parts H_2SO_4 and 30% H_2O_2 diluted in H_2O at room temperature. This etch did not significantly affect the Ag-Mn contacts, so no protection of the contacts during etching was necessary. The etch rate was chosen to give 25-30 measurement steps for each sample profiled. For GaAs, a 1:1:60 etch resulted in an etch rate of ~ 600 Å/min, whereas a 1:1:100 mixture etched at ~ 350 Å/min. Wide fluctuations in the etch rate for $GaAs_{0.6}P_{0.4}$ were observed, with an etch of 1:1:6 resulting in an etch rate of 500-800 Å/min, depending on the age and purity of the chemicals involved, and possibly concentration and damage dependent effects. To minimize uncertainty due to variation in the etch rate, etched step heights were measured periodically during the experiment. Apiezon W (black wax) dots of ~ 1 mm diameter were placed in several places near the edges of each sample, and the resulting etched step height was measured every 5000 - 7000 Å using a Sloan Dektak profilometer.

2.4.3. Data Analysis

For double ac van der Pauw measurements, the sheet resistivity ρ_s and sheet Hall coefficient R_s are given by

$$\rho_s = \frac{\pi}{\ln 2} \frac{V_{ABCD} + V_{BCDA}}{2} f\left(\frac{V_{ABCD}}{V_{BCDA}}\right) \tag{2.2}$$

and

$$R_s = \frac{\sqrt{2}\ \Delta V_{BDAC}\ (\text{rms})}{B(\text{rms})\ I(\text{rms})} \tag{2.3}$$

With the four contacts labeled consecutively, V_{ABCD} represents the voltage between contacts A and B with current I passed between contacts C and D. The symbols V_{BCDA} and ΔV_{BDAC} are defined similarly, with ΔV_{BDAC} the Hall voltage in a magnetic field B. The correction factor $f\left(\frac{V_{ABCD}}{V_{BCDA}}\right)$ has been tabulated by van der Pauw [57].

The interpretation of differential resistivity and Hall effect measurements in determining the electrically active carrier distribution is discussed by Mayer et al. [38,47]. The results presented below can be derived using the Boltzmann transport equation [59], or obtained from an equivalent circuit analysis [60]. The sheet resistivities before and after stripping a layer of thickness d_j are denoted by ρ_{s_j} and $\rho_{s_{j-1}}$, respectively; similarly, R_{s_j} and $R_{s_{j-1}}$ are used for the sheet Hall coefficients. Then the average mobility μ_j of the layer is given by

$$\mu_j = \frac{R_{s_j}}{\rho_{s_j}} + \frac{R_{s_{j-1}}}{\rho_{s_{j-1}}} - \frac{R_{s_{j-1}} - R_{s_j}}{\rho_{s_{j-1}} - \rho_{s_j}} \tag{2.4}$$

and the average carrier concentration is given by

$$n_j = \frac{\frac{1}{\rho_{s_j}} - \frac{1}{\rho_{s_{j-1}}}}{e d_j \mu_j} \tag{2.5}$$

In this analysis, the ratio of Hall mobility to conductivity mobility has been taken to be unity. Any error arising from such an approximation is expected to be slight [61], and for the high doping levels studied in this work, is much less than the experimental uncertainties.

The profiles obtained from differential resistivity and Hall effect measurements are extremely sensitive to scatter in the experimental data points. The procedure followed in this study was to plot by hand the data for sheet resistivity and sheet Hall coefficient on semi-log graph paper, and to draw a smoothed curve through these data points. Points were then taken from this smoothed curve and fed into a computer program which performs the calculations given by equations (2.4) and (2.5). The computer programs used for this analysis are given in Appendix 2.

All of the electrical profiles presented in this work are smoothed averages of data obtained from two or more identically processed samples. The error bars indicated with these profiles approximate the extent of the scatter in the data.

2.5. Atomic Profiling

The beryllium atomic profiles presented in this work were measured by secondary ion mass spectrometry (SIMS) [62,63] using the Cameca IMS 300 ion microanalyzer at the Naval Weapons Support Center, Crane, IN. In this technique, the sample surface is sputtered with a primary beam of ions, such as O_2^+ or Ar^+. The sputtered atoms which become ionized (i.e., secondary ions) are extracted and pass through a mass analyzer. Under well controlled conditions, the current produced by these ions at the output of the detection system of the mass analyzer is proportional to the concentration of the investigated species in the sample. By monitoring the secondary ion

current with time during sputtering, the concentration profile can then be obtained.

A schematic diagram of the SIMS apparatus used for this work is shown in Fig. 2.7. This system has been discussed in detail elsewhere [62], so only a brief summary is included here. The ion microanalyzer consists of four main parts: an ion gun to produce the primary ion beam that sputters the sample, the collection optics for extraction and acceleration of the emitted secondary ions, a mass and energy filtering system for selecting the desired ion species, and a detection-display system for observing the chosen secondary ion signal. The mass analyzer is a double-pass system, whereby the ions travel through a magnetic prism twice. Momentum filtering is achieved by the first deflection through the magnet. The electrostatic mirror (Fig. 2.7) then acts as a low energy filter, since high energy ions will hit the mirror instead of being reflected. The reflected ions again enter the magnet to be mass separated, following a trajectory symmetrical to the previous one. This type of mass analyzer is necessary to achieve the needed mass resolution for SIMS.

For the profiles presented in this work, O_2^+ primary ion beam currents ranging from 0.5 to 1.25 μA were employed. The beam was rastered to sputter an area 500 x 500 microns. The collection optics were set such that only the $^9Be^+$ secondary ion signal from the center of the sputtered crater was monitored.

The SIMS data were calibrated in terms of Be concentration by integrating the area under the unannealed profile and setting it equal to the implanted dose. Depth scales were established from Dektak measurements of the sputtered craters. The uniformity of the sputtering rate was

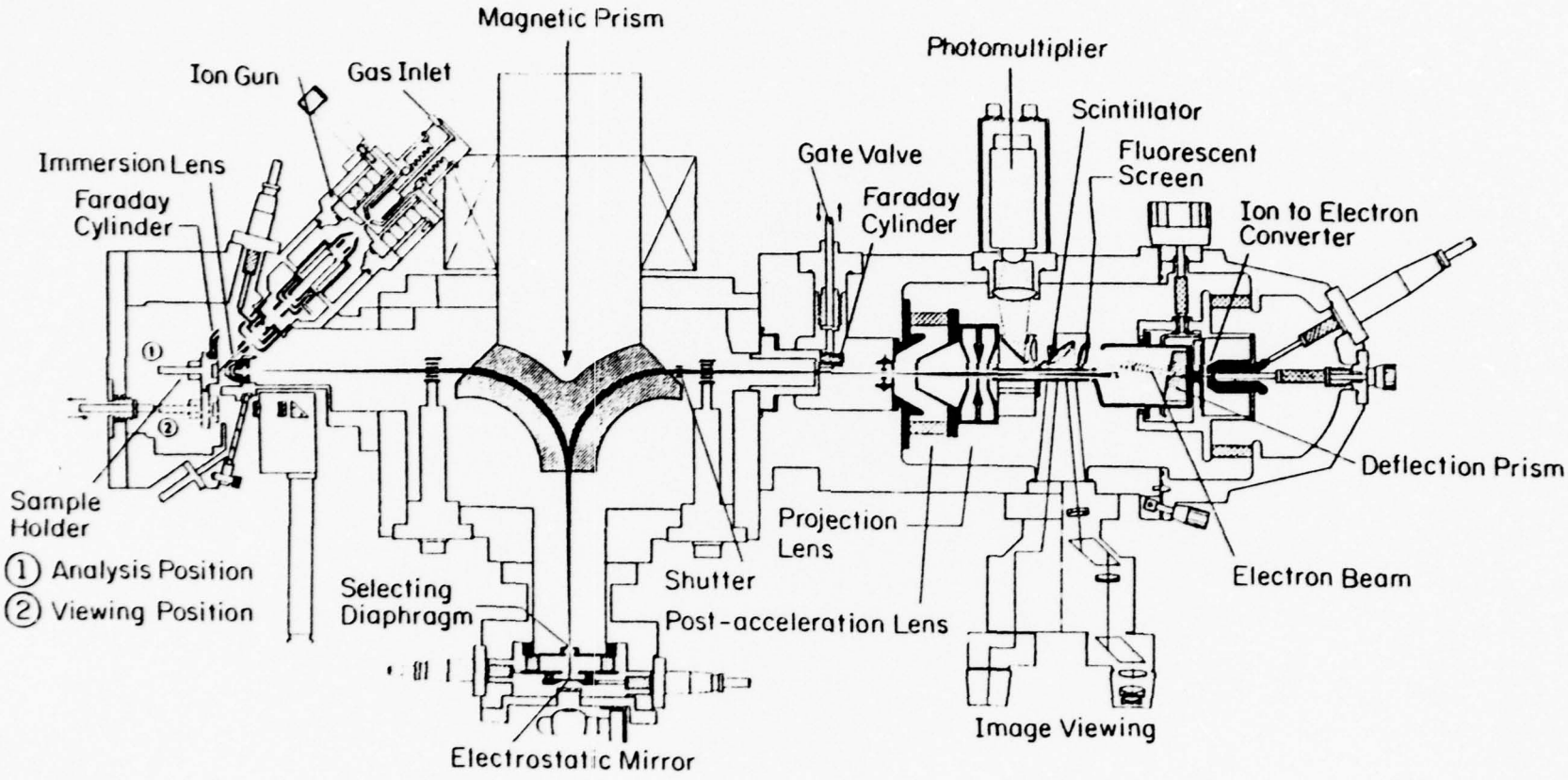

Fig. 2.7. Schematic diagram of the ion microanalyzer used in secondary ion mass spectrometry (SIMS) studies.

verified by monitoring the $^{71}Ga^{+}$ signal during profiling. The validity of SIMS Be atomic profiles in GaAs has been further substantiated by parallel studies using $^{9}Be(p,\alpha)^{6}Li$ nuclear-reaction methods [64]. Reproducibility from run to run on the same sample was generally within 15%. In most cases, the SIMS profiles presented here are averages of data from two or more runs.

3. ANNEALING STUDIES OF Be-IMPLANTED GaAs

Vapor-phase epitaxial (VPE) GaAs obtained from two sources, Texas Instruments and Raytheon, were used in this study. Epitaxial n-type layers grown on either n^+ or Cr-doped substrates were investigated, and no substrate-dependent effects were observed. Background donor concentrations in the various VPE samples utilized ranged from ~ 10^{14} to 5 x 10^{15} cm^{-3}.

3.1 Photoluminescence Results

Low temperature photoluminescence (5°K) is an extremely sensitive technique for studying the optical properties and lattice recovery of implanted layers. In the original isochronal anneal study of Be-implanted GaAs by Chatterjee *et al.*[2] the integrated intensity of the Be-related (band-to-acceptor) luminescence band at 1.493 eV was observed to increase dramatically as a function of anneal temperature for Be fluences from 5 x 10^{12} to 5 x 10^{13} cm^{-2} at 130 keV. This result indicates that an anneal temperature of 900°C is necessary to achieve maximum Be optical activation and lattice recovery. In this work we have further substantiated this conclusion and extended the results to include higher dose Be implants.

Figure 3.1 shows the variation of the integrated intensity of the Be-related luminescence band at 1.493 eV for samples implanted at 250 keV for fluences from 5 x 10^{13} to 1 x 10^{15} cm^{-2} and annealed at temperatures from 600 to 900°C for 30 minutes using Si_3N_4 encapsulation. To ensure the luminescence observed is from the region of peak Be concentration and highest implantation damage, ~ 3000 Å were etched from the surface after the anneal. The results presented in Fig. 3.1 were duplicated in samples

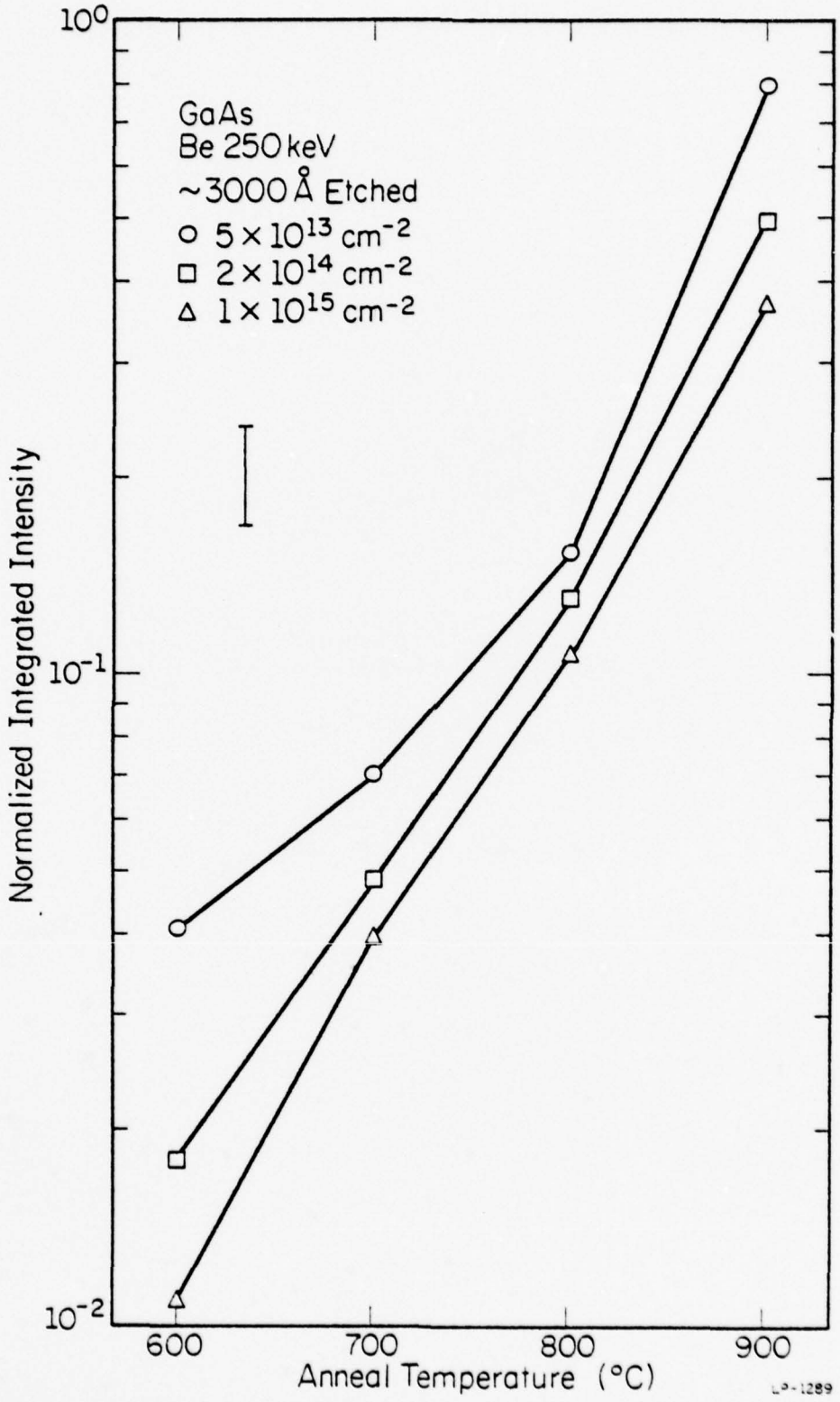

Fig. 3.1. Normalized integrated intensity of Be-related luminescence as a function of 1/2 hr isochronal anneal temperature for the fluences shown.

from both Texas Instruments and Raytheon. The data points shown are actually averages of data taken from these two sets of samples. Normalization has been done with respect to the total integrated intensity of the band-edge luminescence of an unimplanted sample.

As is evident from Fig. 3.1, an anneal temperature of 900°C is unquestionably necessary for maximum Be optical activation and lattice recovery. The increase in the integrated intensity between 600 and 900°C anneals becomes even more pronounced as the implant fluence is increased, due to the greater extent of the lattice damage caused by heavier dose implants. As noted by Chatterjee et al. [2], for low Be fluences (5×10^{12} - 5×10^{13} cm^{-2} at 130 keV) the band-to-acceptor luminescence observed for 900°C anneals scales with the implanted dose. However, as shown in Fig. 3.1, the integrated intensity decreases for successive fluences above 5×10^{13} cm^{-2}. This indicates that for heavy dose implants, some residual lattice damage may be unannealable even at 900°C.

An isothermal anneal study was also carried out to investigate the effect of annealing time on the observed photoluminescence. The general trend observed in 900°C anneals from 2 minutes to 2 hours was a monotonic increase in integrated intensity with a saturation in the intensity occurring for anneals of 1 hour or more. A 900°C anneal for 5 min (measured from the time the sample temperature reached 875°C) resulted in an integrated intensity roughly equivalent to an 800°C, 1/2 hour anneal. An anneal of 900°C for 1/2 hour appears to be optimum, since the reliability of the Si_3N_4 encapsulant decreases with longer anneal times.

3.2. Electrical and Atomic Profiles

3.2.1. Temperature and Time Dependence

Electrical carrier concentration profiles, shown in Fig. 3.2, were obtained from differential resistivity and Hall effect measurements on GaAs samples Be-implanted at 250 keV to a fluence of 5×10^{13} cm^{-2} and annealed for 1/2 hr at various temperatures from 600 to 900°C. The dashed line indicates the as-implanted Be distribution predicted by LSS theory [39]. The lower graph shows the mobility variation as a function of depth. No significant differences in the mobilities were observed for the three anneal temperatures studied, so only the 900°C points are plotted. The dashed line on the mobility graph represents a Brooks-Herring [65,66] calculation based on the measured impurity distribution and an assumed lattice-limited mobility of 400 cm^2/V-sec. Although the Brooks-Herring formula is a semi-empirical approximation, the calculation indicates no anomalous mobility variations resulting from the implantation.

Measurement of the integrated area under each of the carrier distribution profiles in Fig. 3.2 gives activation efficiency estimates of 80, 85, and 95% for the 600, 700, and 900°C anneals, respectively. Considering the experimental uncertainties involved in such profiling measurements, these results are in good agreement with earlier data reported by Chatterjee et al. [7,27], apart from the 600°C activation, which is somewhat higher in the present case. It should also be noted the mobility values are quite high (200-300 cm^2/V-sec) and that little diffusion of the implanted Be takes place for these concentrations ($\leq 10^{18}$ cm^{-3}).

In Fig. 3.3 carrier concentration and mobility profiles are shown for a Be fluence of 1×10^{15} cm^{-2} at 250 keV. The samples were annealed for 1/2 hr with Si_3N_4 encapsulation at the temperatures shown. In this

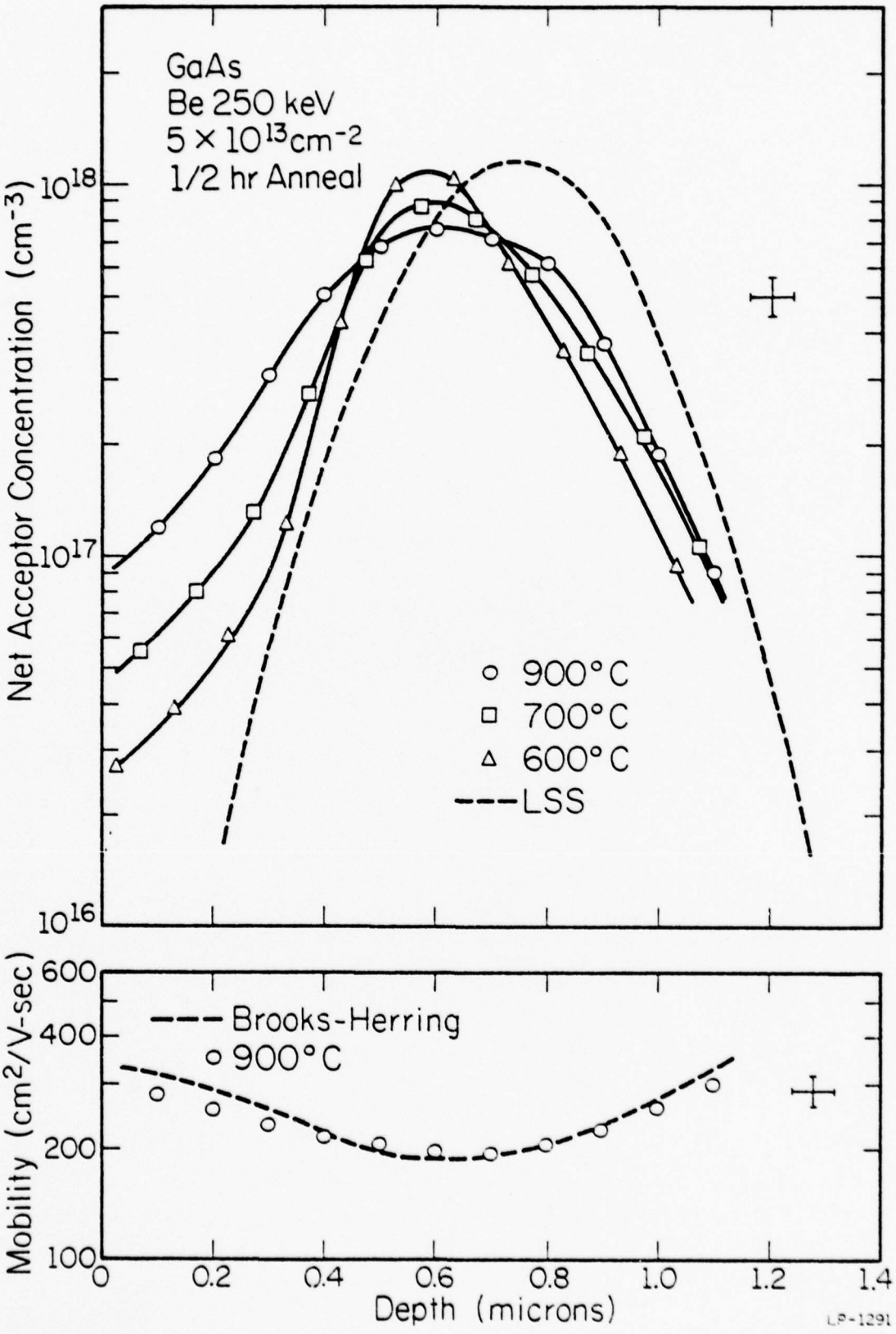

Fig. 3.2. Electrical concentration and mobility profiles for the low fluence implant and isochronal anneals shown.

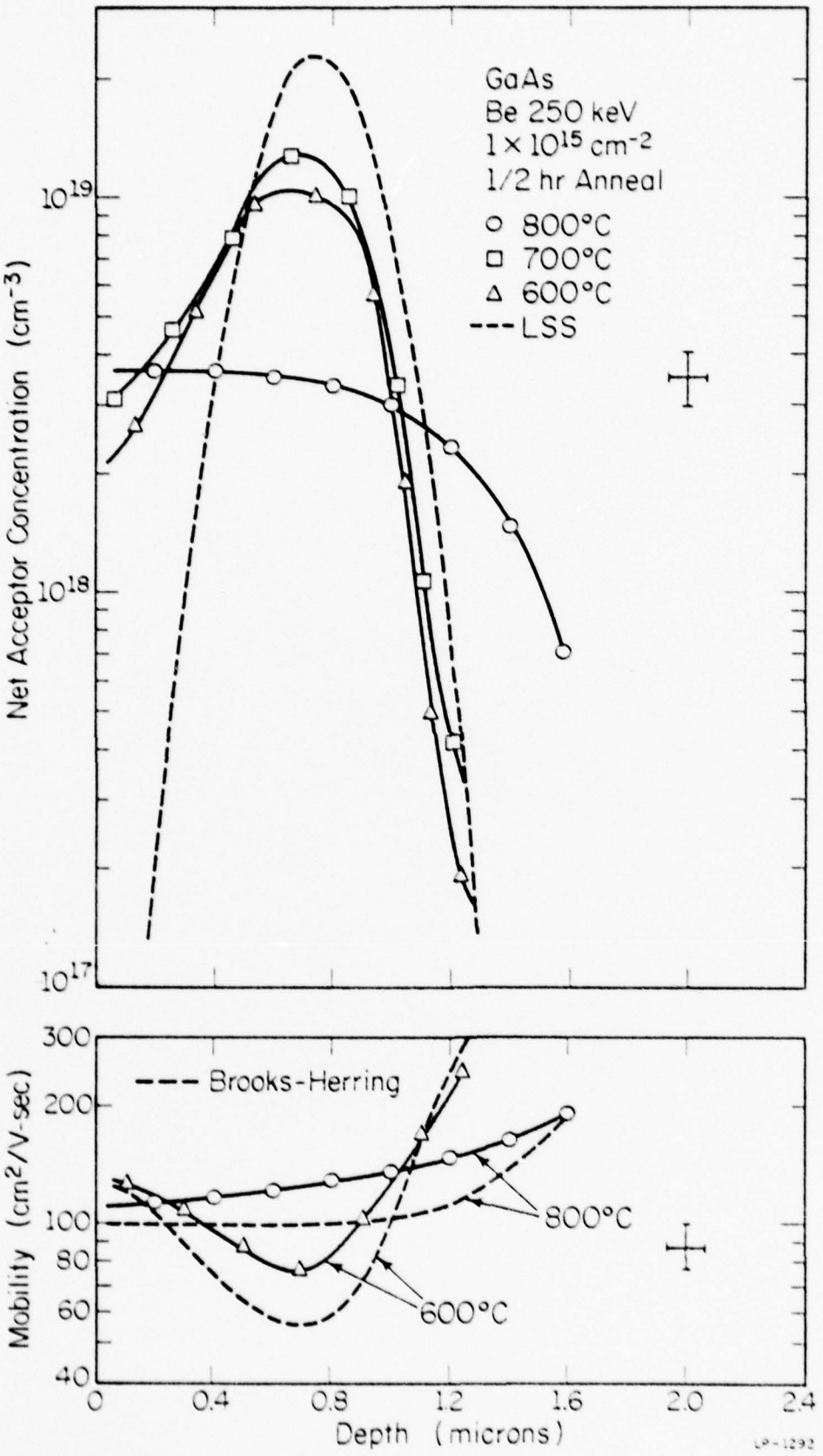

Fig. 3.3. Electrical concentration and mobility profiles for the high fluence implant and isochronal anneals shown.

case the highest hole concentration occurs for the 700°C anneal with an activation of 75%, although the 600°C profile is quite similar with an activation of 70%. In contrast with the results of Fig. 3.2, a drastic redistribution of the implanted Be is found at 800°C in this higher fluence case. The activation has been reduced to 50%, and significant indiffusion has occurred. The decrease in activation at higher temperatures is due to outdiffusion of Be into the Si_3N_4 encapsulant during the anneal. Such outdiffusion was first observed in SIMS profiling by Comas and Plew [67, 68], and will be discussed in detail in Sec. 3.2.2.

No significant differences are observed in the profiles for 800 and 900°C, 1/2 hr anneals, indicating the diffusion mechanism is highly concentration dependent. The diffusion rate is extremely fast for concentrations above ~ 5×10^{18} cm^{-3} when the temperature is near or above 800°C, and is much slower for lower concentrations and anneal temperatures.

Mobility values are again extremely good, in this case slightly higher than that predicted by Brooks-Herring theory. Numerous variations from this theory have been observed experimentally [66], so these results are not surprising. The high electrical activation and high mobility found even for 600°C anneals indicates the requirements for good electrical activation are much less stringent than those for optical activation. For applications in which only electrical activation is desired, anneal temperatures of 600-700°C may be sufficient. However, the photoluminescence results indicate that optoelectronic devices fabricated with Be implantation will require an anneal temperature of 900°C for successful removal of residual lattice damage.

The peak concentration in Fig. 3.2 for the 600°C profile corresponds closely with the value predicted by LSS. In Figs. 3.2 and 3.3 the

position of the peak appears 10-20% shallower than the projected range given by LSS. A further comparison of LSS with SIMS Be atomic distributions will be discussed in Sec. 3.2.2.

The data presented in Fig. 3.3 are in agreement with previous work reported by Hunsperger et al. [1] and Zölch et al. [26], who also observed a decrease in activation for anneal temperatures above 700°C for higher dose Be implantations. The lower activation for 600-700°C anneals first reported by Chatterjee et al. [7,27] has not been reproduced. Reasons for this discrepancy are not clear, although improvements in the Si_3N_4 encapsulant may result in the present better activation. There is no substantial difference, however, between the 900°C activation noted by Chatterjee et al. [7,27] and the present findings.

An isothermal anneal study was carried out to investigate the effect of annealing time on the resulting profile. For low doses ($\leq 5 \times 10^{13}$ cm^{-2}) corresponding to impurity concentrations of less than $\sim 10^{18}$ cm^{-3}, no appreciable diffusion with time is detected. For higher doses, however, the effect of annealing time on the electrical carrier concentration profile is striking. Profiles of a 1×10^{15} cm^{-2} Be fluence at 250 keV annealed at 900°C with Si_3N_4 encapsulation for various times from 5 min to 1 hr are presented in Fig. 3.4. The implanted Be diffuses rapidly during the first 5 min of annealing, and then diffuses slowly for concentrations less than $\sim 5 \times 10^{18}$ cm^{-3}. A continuous indiffusion of Be is observed, with a junction depth of ~ 2 microns for a 1 hr anneal at 900°C. Activation efficiencies for 5, 30, and 60 min anneals at 900°C are 65, 50, and 40%, respectively. The decrease in activation with anneal time is again related to the loss of Be into the Si_3N_4 encapsulant.

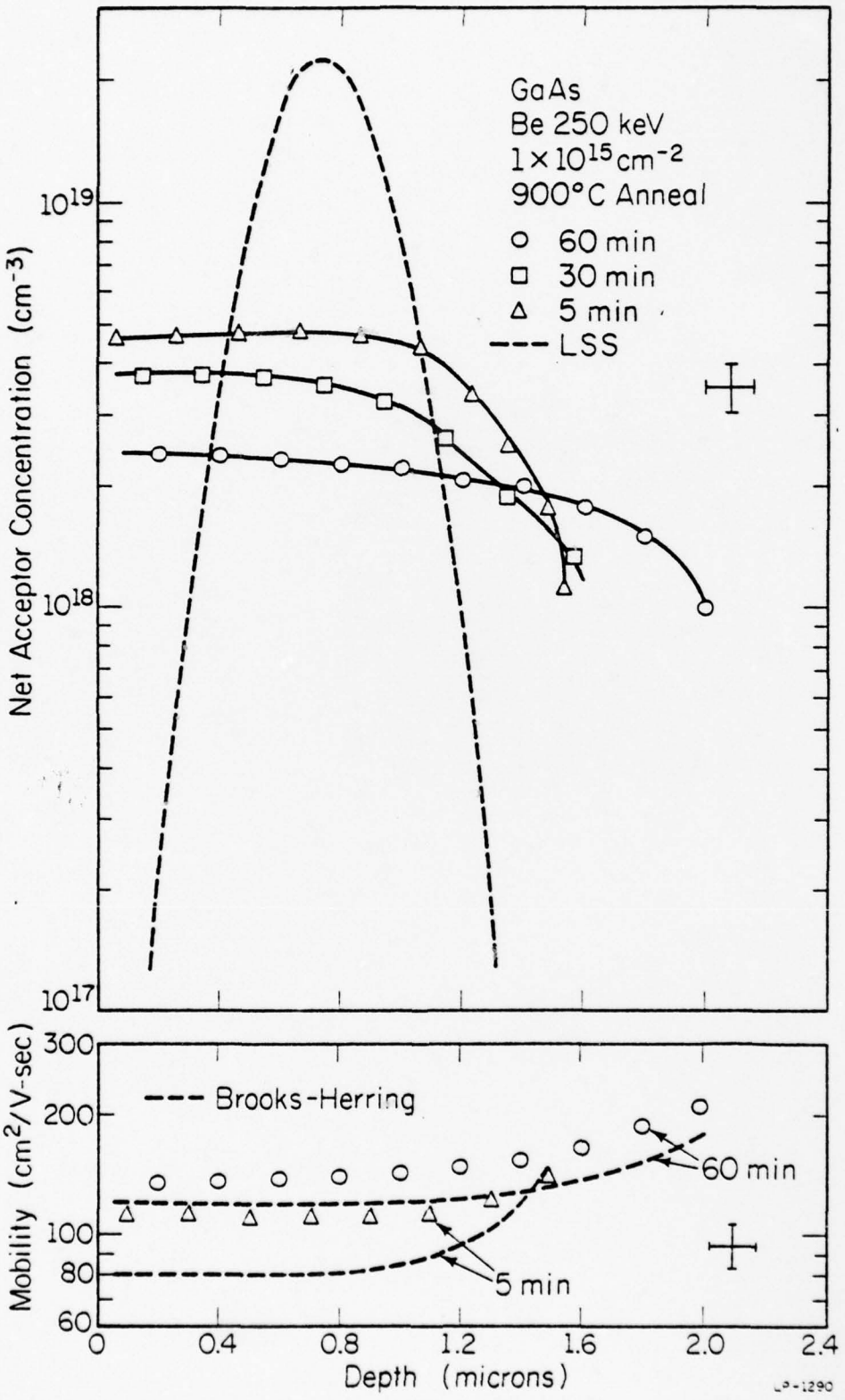

Fig. 3.4. Electrical concentration and mobility profiles for the high fluence implant and isothermal anneals shown.

The diffusion fronts in the electrical profiles shown in Fig. 3.4 are believed to be extremely sharp. Accurate data points are difficult to obtain in such close proximity with a p-n junction, but a sharp drop-off has consistently been found for high fluence implants annealed at 900°C. This will be substantiated by SIMS Be atomic profiles presented in the following section.

3.2.2. Concentration Dependence and Outdiffusion

In Fig. 3.5 the SIMS Be atomic distribution for a 250 keV, 10^{15} cm^{-2} implant is compared with the profile predicted by LSS theory [39]. This figure also shows the Be atomic distribution after annealing for 1/2 hr at 900°C, and the corresponding electrical profile determined from differential Hall effect measurements. In this high dose case a substantial redistribution of the implanted Be takes place during the anneal, and the electrical activation has been reduced to 50% of the implanted dose. However, the integrated area under the SIMS annealed Be atomic profile is also ~ 50% of the implanted dose. Such close agreement between the atomic distribution and the electrical data indicates that, to within an experimental uncertainty of ~ 15%, all of the Be remaining in the GaAs after the anneal is electrically active. No evidence of effects such as large Be precipitates or defect compensation is observed. Previously reported SIMS profiles [67], obtained when anneals were performed using either chemical-vapor deposited SiO_2 or sputtered Si_3N_4, exhibited a large pileup of Be at the surface which extended ~ 1000 Å into the sample. This surface pileup is absent for properly deposited Si_3N_4 films [42].

It is clear from Fig. 3.5 that significant differences exist between LSS theory and the SIMS unannealed Be profile. The Be distribution

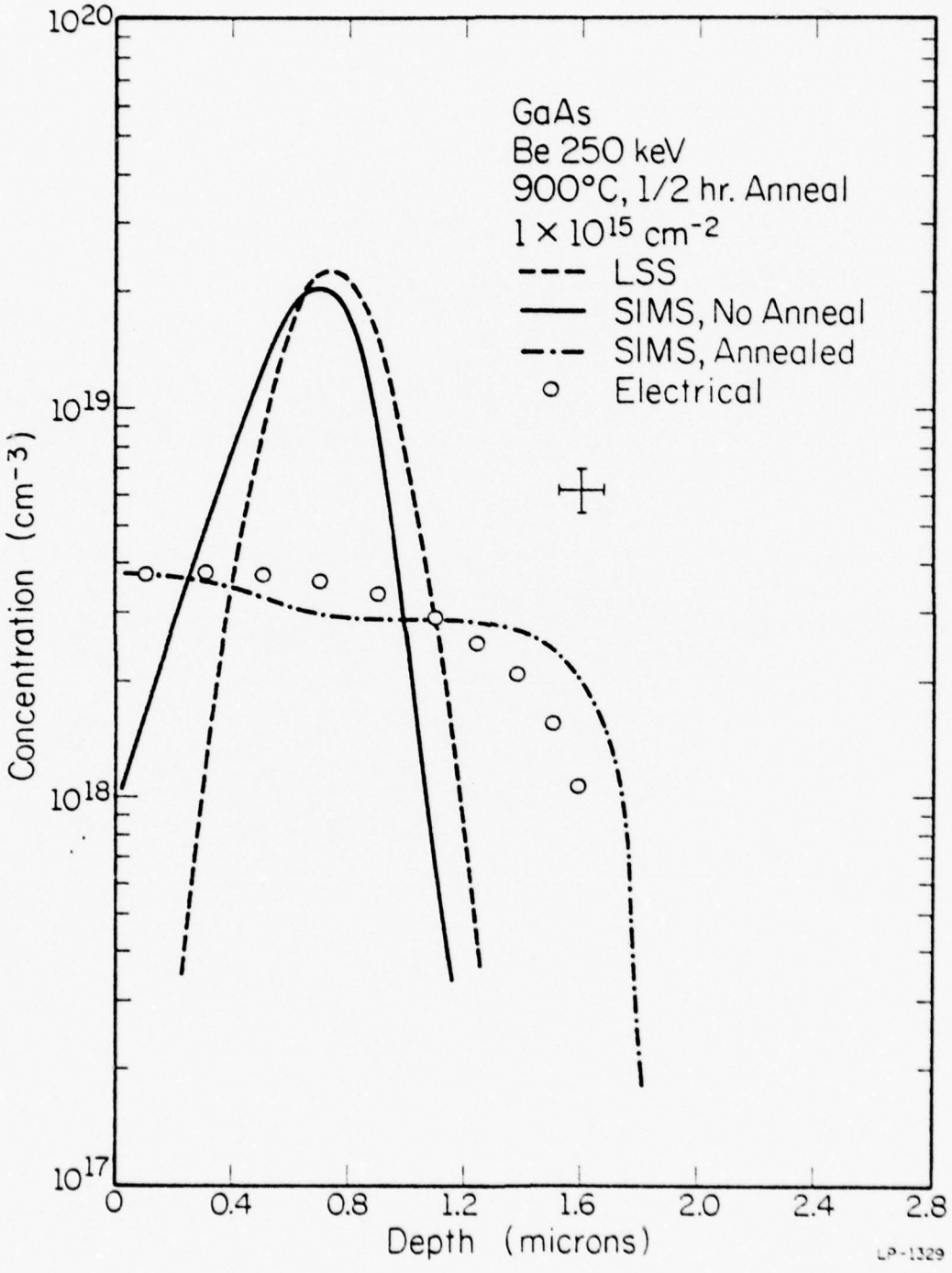

Fig. 3.5. Comparison of as-implanted SIMS Be profile with theoretical distribution (LSS), and comparison of SIMS data with net acceptor concentration profile after annealing for the high fluence implant shown.

is skewed considerably toward the surface, and the projected range is ~20% shallower than predicted by LSS. This skewness has consistently been observed in SIMS Be atomic profiles of unannealed samples implanted with fluences from 10^{13} to 10^{16} cm^{-2} at both 100 and 250 keV [69]. Such deviations from a simple LSS Gaussian are often observed for other implanted impurities, most notably for B in Si. In such cases, calculations of the third and higher moments of the distribution have been necessary to accurately predict the implanted profile [70,71].

To investigate the outdiffusion of Be into the Si_3N_4 encapsulant during annealing, SIMS profiles were obtained by sputtering through both the Si_3N_4 and the GaAs surface. The result for a 100 keV Be fluence of 2×10^{14} cm^{-2} is plotted in Fig. 3.6. The data clearly indicate the presence of Be in the Si_3N_4 layer. Due to differences in the secondary ion yield of Be in GaAs and Si_3N_4, however, it is not possible to directly compare concentrations in the two regions. The high secondary ion signals at the Si_3N_4 surface and at the GaAs-Si_3N_4 interface are in part artifacts of the SIMS technique, probably caused by thin oxide layers and other inhomogeneities often present at such boundaries, which affect the secondary ion yield. It does appear, however, that the interface acts as a source for Be diffusion into the Si_3N_4 during annealing. The buildup of Be at this interface is primarily in the Si_3N_4, since profiles measured with the Si_3N_4 removed show the surface Be peak is nonexistent or less than 100 Å deep. The high background noise level shown in Fig. 3.6 is due to effects associated with SIMS profiling through an insulator into a conducting substrate [72].

The fluence dependence of the diffusion of implanted Be in GaAs is illustrated in Fig. 3.7. In this graph, electrical profiles have been

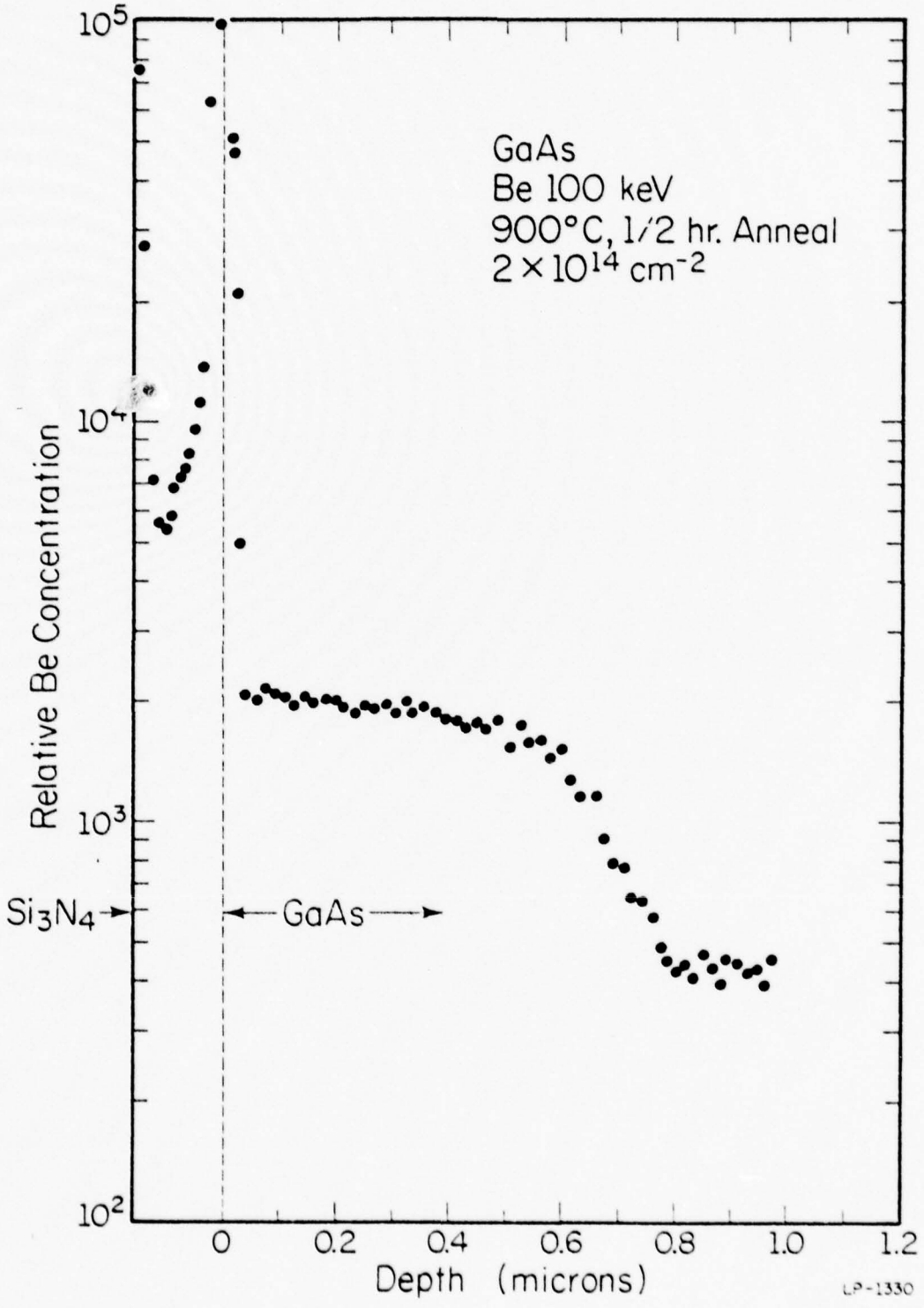

Fig. 3.6. SIMS data of relative Be concentration in the Si_3N_4 encapsulant and the GaAs substrate after the implant and anneal shown.

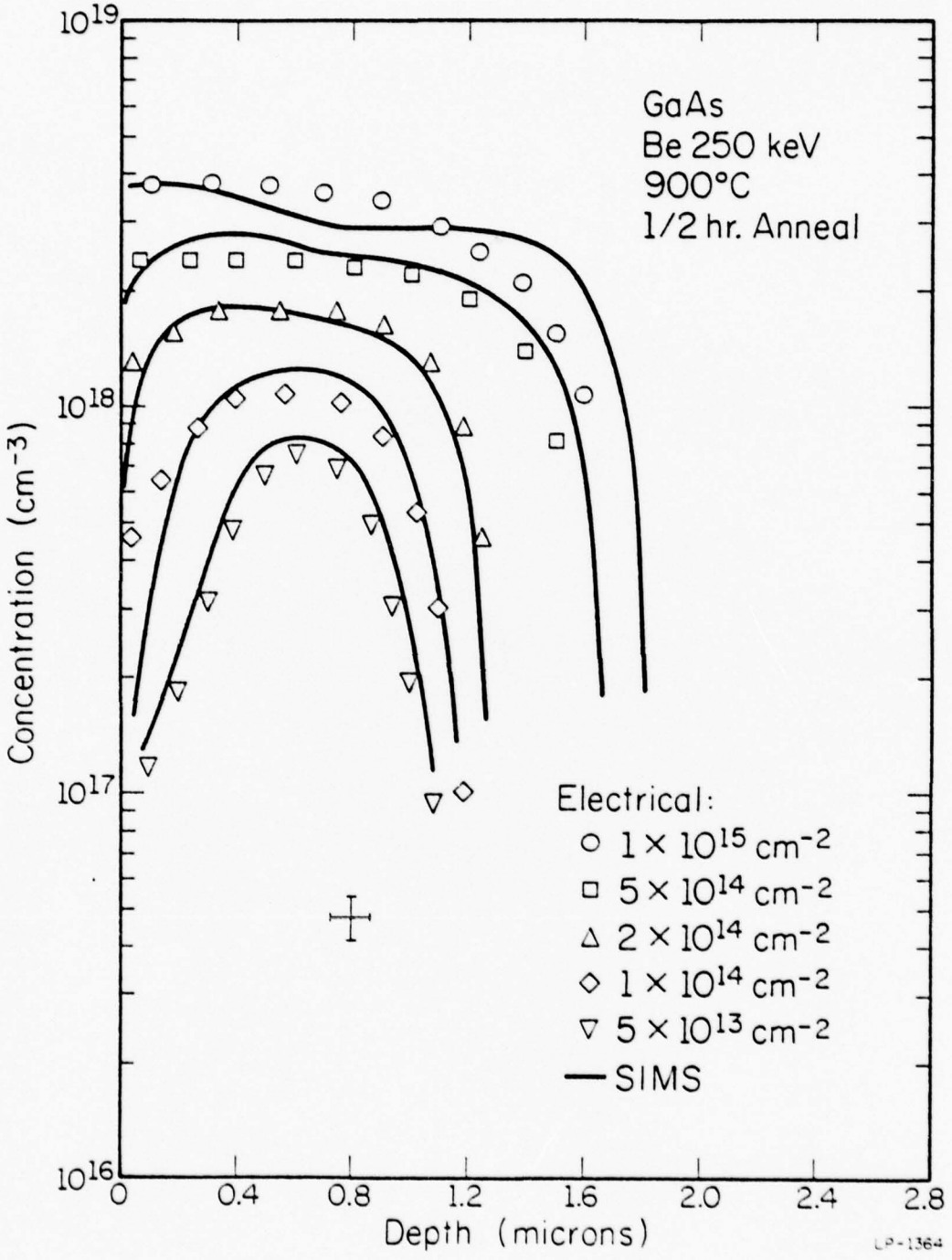

Fig. 3.7. Comparison of SIMS and net acceptor concentration profiles for the 250 keV Be fluences and anneal shown.

plotted with SIMS Be atomic profiles for 900°C, 1/2 hr anneals of five 250 keV Be fluences ranging from 5×10^{13} to 1×10^{15} cm^{-2}. Excellent agreement is observed between SIMS and electrical profiles for all fluences. The sharp diffusion front evident from both SIMS and electrical measurements of the higher dose implants is similar to that observed for Zn diffusion in GaAs [73] and is indicative of a concentration-dependent diffusion. Diffusion is minimal for the lowest dose of 5×10^{13} cm^{-2}, which corresponds to a peak implanted Be concentration before annealing of 1×10^{18} cm^{-3}. As the dose is increased, the distribution begins to flatten as Be diffuses toward the surface and deeper into the substrate during the anneal. The three lower fluences of 5×10^{13} to 2×10^{14} cm^{-2} result in electrical activation efficiencies of 90-100% of the implanted dose, indicating no significant outdiffusion of Be is occurring. For higher fluences, substantial outdiffusion of Be at the surface is observed and the measured electrical activation has decreased to 65% of the implanted dose for a 5×10^{14} cm^{-2} fluence, and to 50% for a 1×10^{15} cm^{-2} fluence. Deeper indiffusion is also observed for the higher doses. However, the close agreement between the SIMS Be atomic distributions and the electrical data for these fluences indicates 85-100% of the Be present after annealing is electrically active. The outdiffusion at the surface is first observed when the Be concentration at the surface during the anneal reaches ~ 1×10^{18} cm^{-3}.

Because the outdiffusion of Be into the Si_3N_4 encapsulant is most strongly related to the Be concentration at the surface during the anneal, the effect of the outdiffusion is more noticeable for shallower implants. This is illustrated in Fig. 3.8, which compares SIMS Be distributions with

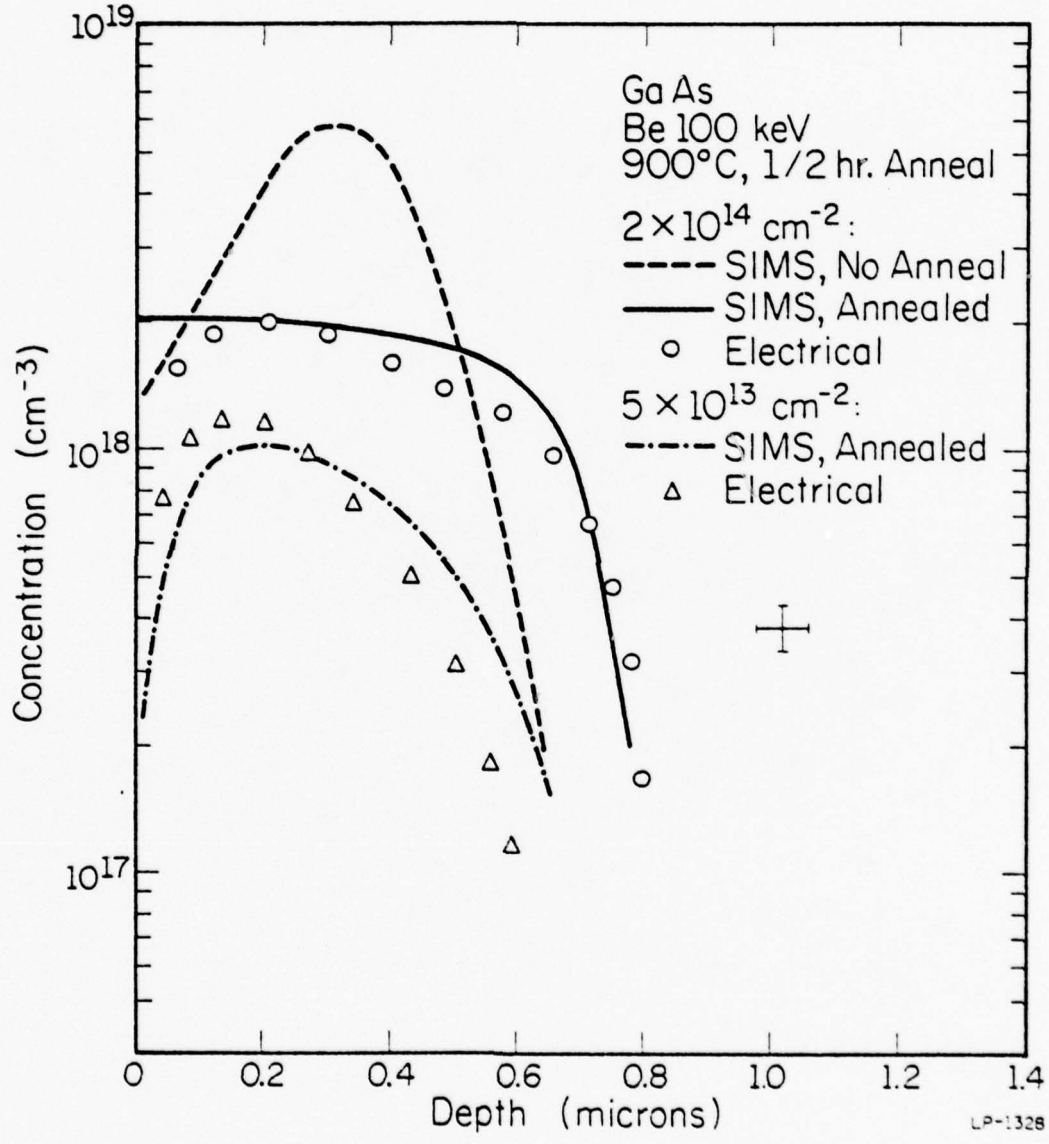

Fig. 3.8. Comparison of SIMS and net acceptor concentration profiles for the 100 keV Be fluences and anneal shown.

corresponding electrical profiles for two 100 keV Be fluences with annealing at 900°C for 1/2 hr. For a relatively low dose of 5×10^{13} cm^{-2}, some skewing of the profile toward the surface is seen in both the SIMS and electrical measurements, but the integrated areas both correspond to ~ 90% of the implanted dose. For the higher fluence of 2×10^{14} cm^{-2}, however, considerable outdiffusion occurs during the anneal, resulting in a measured electrical activation and atomic distribution corresponding to only ~ 60% of the implanted dose. Although significant diffusion occurs for an identical fluence (2×10^{14} cm^{-2}) at 250 keV (Fig. 3.7), the Be surface concentration is still low after annealing in that case due to the greater depth of that implant. In both Figs. 3.7 and 3.8, the onset of the outdiffusion is not observed until the Be surface concentration has exceeded ~ 1×10^{18} cm^{-3}.

Very high dose Be implants of $2\text{-}5 \times 10^{15}$ cm^{-2} at 250 keV were also examined in this work. These fluences correspond to peak implanted Be concentrations of $4\text{-}10 \times 10^{19}$ cm^{-3}. Anomalous diffusion was observed in SIMS profiles, with multiple peaks characteristically seen in the Be distribution after 900°C, 1/2 hr anneals. This multiple peak structure has also been observed using $^{9}Be(p,\alpha)^{6}Li$ nuclear-reaction methods [64]. A large dip in the Be distribution was commonly seen at a depth roughly corresponding to the projected range for these very high dose implants. Deeper indiffusion and a definite pileup of Be near the surface was also observed.

Reproducible electrical profiles for $2\text{-}5 \times 10^{15}$ cm^{-2} implants at 250 keV annealed at 900°C for 1/2 hr could not be obtained because of excessive pitting of the GaAs surface during etching. Such pitting is

presumed to be damage-related, since it was not observed for lower dose implants. However, an electrical profile obtained from differential Hall measurements for a ~ 10^{16} cm^{-2} Be implant at 400 keV annealed at 900°C for 15 min has been published by Donnelly [74]. A flat distribution with carrier concentration ~ 5 x 10^{18} cm^{-3} and junction depth of ~ 3 μm was reported. This is the highest reported net acceptor concentration in Be-implanted GaAs annealed at 900°C.

The anomalous diffusion during annealing observed in heavy-dose Be implants is not surprising considering the damage and concentration dependence involved. Witmeyer et al. [75], utilizing transmission electron microscopy (TEM), have correlated anomalous Be diffusion observed in SIMS with high defect densities still remaining after annealing at 550-800°C. The photoluminescence results reported in Sec. 3.1 also indicate residual lattice damage is still present after 900°C, 1/2 hr anneals of higher dose implants.

3.2.3. Attempts to Inhibit Diffusion

To determine if the Be outdiffusion at the surface is related to the encapsulant, annealing in a controlled ambient was investigated. Samples were annealed by Marc Ilegems, Bell Laboratories, in evacuated sealed ampoules under Ga-liquidus equilibrium conditions (excess Ga and GaAs). Electrical profiles of these samples indicated diffusion behavior identical to that observed with Si_3N_4 encapsulation.

To investigate the possibility that the diffusion of Be is damage dependent, experiments with a two-step annealing procedure were done. Since Be becomes electrically active and diffuses negligibly at low anneal temperatures, it was hoped that by doing long anneals (1-2 hr) at

temperatures of 600-700°C, diffusion during a subsequent 900°C anneal would be restrained. This was found not to be the case, however, as electrical profiles indicated a two-step anneal did nothing to slow the Be diffusion.

It has been reported that significantly higher electron concentrations can be achieved for donor implants into GaAs if the substrate is heated during implantation [74]. Less indiffusion of Cd [76] and a higher substitutional fraction of Cd on lattice sites as determined by backscattering [77] has also been observed for hot substrate implants into GaAs. These effects are presumably related to annealing taking place during the implant. The results of such a study to inhibit the diffusion of implanted Be in GaAs are shown in Fig. 3.9. Electrical and atomic profiles for room temperature and 350°C implants are presented. Both implants were done in GaAs taken from the same wafer, and all processing steps except for the implant temperature were identical. For surface protection, ~300 Å of Si_3N_4 was deposited on all samples prior to the implantation. The samples were implanted with 250 keV Be to a fluence of 5×10^{14} cm^{-2} and were annealed at 900°C for 1/2 hr with ~ 1000 Å Si_3N_4 encapsulation. As shown in Fig. 3.9, the 350°C implant resulted in a somewhat higher peak concentration and slightly less indiffusion. The electrical activation observed was 85% for the 350°C implant as compared with 65% for the 25°C implant. The primary effect of the 350°C implant, however, was only to inhibit the outdiffusion of Be at the surface. Similar studies of lower dose ($\leq 2 \times 10^{14}$ cm^{-2}) 250 keV implants, where the outdiffusion is not observed, revealed no significant difference between room temperature and hot implant profiles after annealing. A larger dose of 10^{15} cm^{-2} also resulted in identical profiles, indicating the higher peak

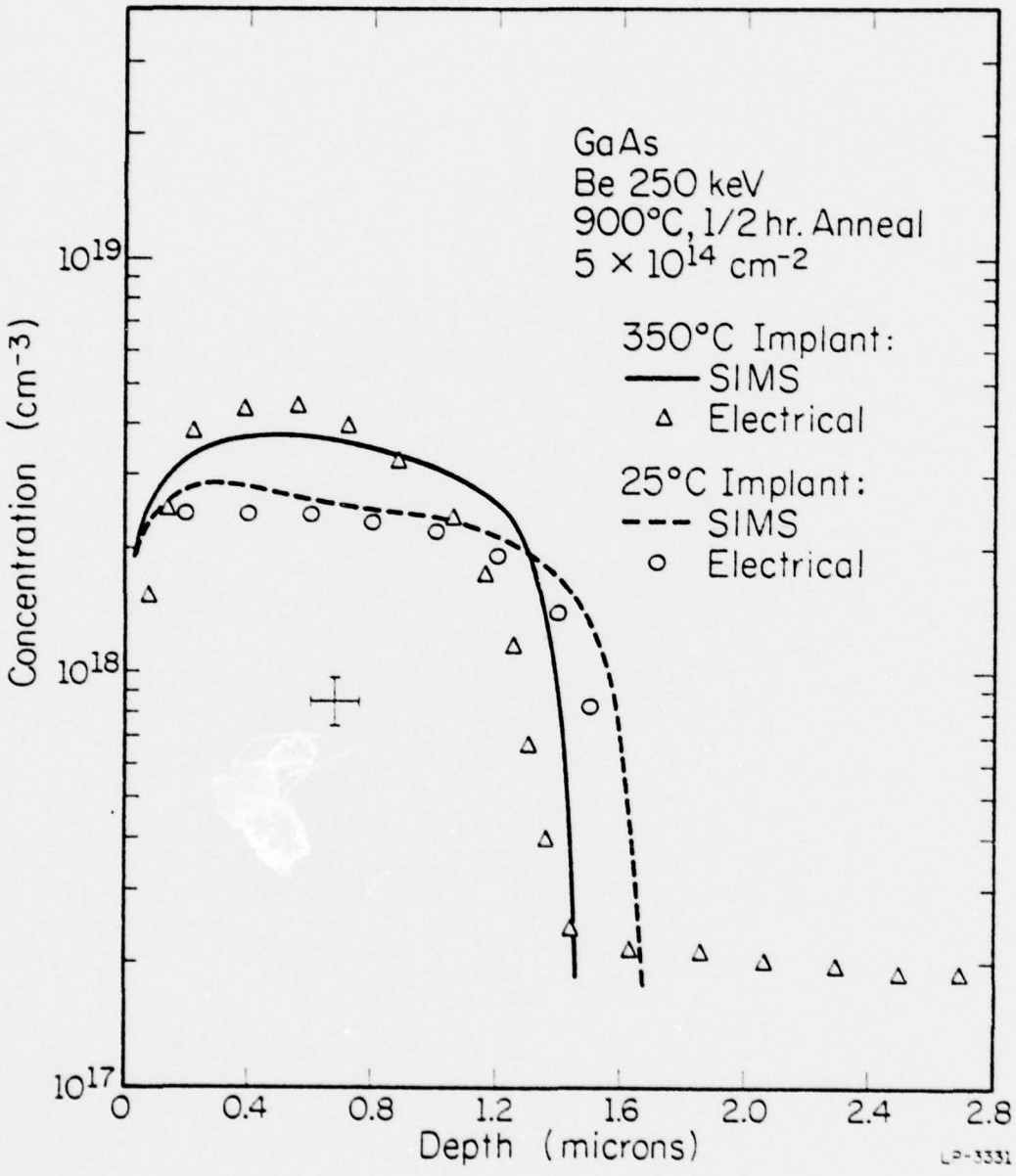

Fig. 3.9. SIMS and electrical concentration profiles for two implantation temperatures for the implant fluence and anneal shown.

concentration shown in Fig. 3.9 for a 350°C implant is a small effect not observable in more heavily damaged implanted layers.

A most disturbing consequence of the heated implants was the formation of a deep p-type tail on the distribution, as is evident in Fig. 3.9. This tail, which was found to extend throughout the ~ 8 μm thick epitaxial layer, was not observed for room temperature implants. A similar result has been reported by Hunsperger and Marsh [78] for Zn and Cd implants into bulk GaAs substrates held at 400°C. They observed the formation of a deep (~ 120 μm), semi-insulating tail beneath the implanted layer after a 10 min 900°C anneal. This was attributed to the deep diffusion of defects and vacancies during the implantation and subsequent anneal. Itoh and Kushiro [79] found that this effect could be eliminated by first performing a room temperature As implant prior to a Cd implant at 500°C. They postulated that the preimplantation of As helped prevent As vacancy formation and diffusion in the following high temperature Cd implant. In the present case the n-type VPE layers used were unintentionally doped, and the most likely principal contaminant was Si. We speculate the p-type conversion observed was due to defect diffusion, causing Si to change sites in the GaAs lattice. It is likely the electrical carrier concentration observed in the tail region is strongly dependent on the nature of the epitaxial layer involved, and further work is necessary to understand this phenomenon.

3.2.4. Estimation of Diffusion Coefficients

It is apparent from the SIMS and electrical profiles presented in this chapter that the annealing of Be-implanted GaAs does not result in simple diffusion of the implanted distribution. Because of surface out-diffusion, concentration dependences, and possible defect-enhanced migration

effects, the diffusion mechanism is extremely complex and is not presently understood. However, some interesting observations can be made by comparing the observed Be distributions after annealing with calculated Gaussian diffusion profiles. In Fig. 3.10, profiles illustrating the diffusion of a Gaussian are shown for various diffusion coefficients. The initial profile roughly corresponds to a 10^{15} cm^{-2} Be implant at 250 keV. The diffusion time is 1/2 hr. These profiles were calculated using the equation

$$N(x) = \frac{\phi}{\sqrt{2\pi}\,\sigma} \exp \frac{-(x-R_p)^2}{2\sigma^2} \tag{3.1}$$

where

$$\sigma^2 = (\Delta R_p)^2 + 2Dt \tag{3.2}$$

These equations represent a Gaussian distribution N(x) centered at $x = R_p$ with integrated area ϕ and standard deviation ΔR_p at time $t = 0$. D is the assumed diffusion coefficient. The computer program written to perform these diffusion calculations is given in Appendix 3.

By comparing the Be concentration near the peaks of the distributions presented in Fig. 3.7 with the peaks of the diffusion profiles in Fig. 3.10, a first-order estimate of the diffusion coefficients can be obtained. These estimates represent a rough average of the diffusion coefficient in the concentration range over which the Be has diffused during the 1/2 hr anneal, and would most accurately describe the diffusion coefficient for a concentration near the middle of this range. For example, the average diffusion coefficient for the 10^{15} cm^{-2} implant profile in Fig. 3.7 is ~ 2-3 x 10^{-12} cm^2/sec, and the corresponding concentration range is from 2 x 10^{19} cm^{-3} to ~ 3.5 x 10^{18} cm^{-3}. By similarly estimating

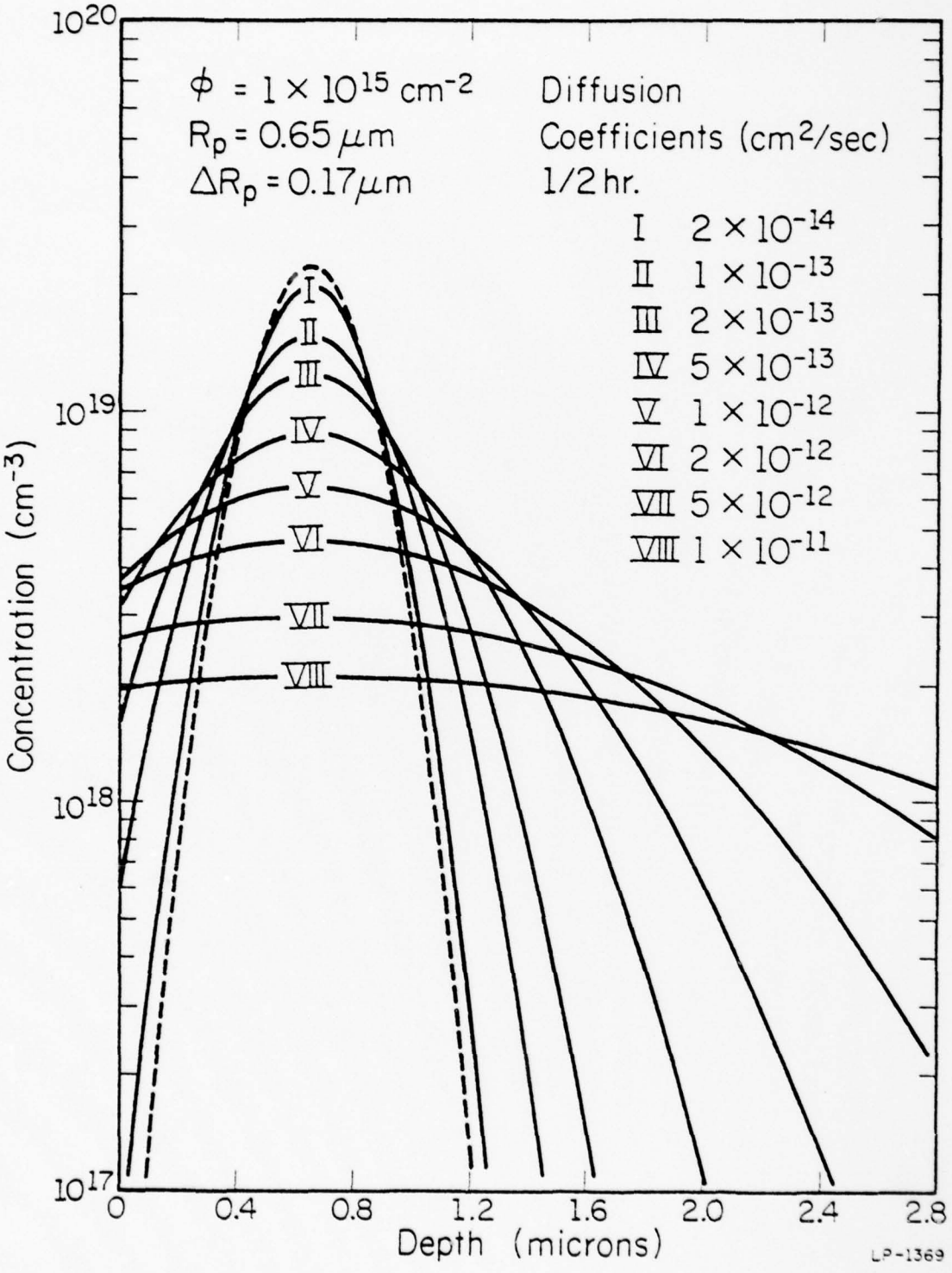

Fig. 3.10. Theoretical diffusion profiles of a Gaussian distribution for the diffusion coefficients shown.

the diffusion coefficients for the other fluence profiles shown in Fig. 3.7, and plotting the results on a log-log graph of diffusion coefficient versus Be concentration, Fig. 3.11 is thereby obtained. It should be noted the horizontal lines on the data in Fig. 3.11 represent the extent of the concentration range for the given average diffusion coefficient and are therefore not true error bars.

The heavy solid line drawn through the data in Fig. 3.11 corresponds to a square-law dependence of the diffusion coefficient on the Be concentration, which appears to accurately describe the data. It is interesting to note that the diffusion coefficient of Zn in GaAs also depends on the square of the Zn concentration [73,80]. Zn in GaAs is known to diffuse by the interstitial-substitutional mechanism [73]. However, lacking further experimental evidence, it is not known if such a diffusion model can be used to explain the observed Be diffusion. An additional complication in attempting a theoretical analysis of implanted Be diffusion is that the Boltzmann-Matano [73,81] method, typically used to study concentration-dependent diffusion, cannot be used since it only applies to diffusion from a constant source at a surface.

The values of the diffusion coefficient for various Be concentrations, as determined from Fig. 3.11, can be compared with other values given in the literature. Zölch [26] estimates a 900°C diffusion coefficient of $\sim 2 \times 10^{-12}$ cm^2/sec for a 10^{15} cm^{-2} Be implant at 150 keV. This is within a factor of 2 of the value given by Fig. 3.11 for a 10^{15} cm^{-2} implant at 250 keV. Poltoratskii and Stuchebnikov [25] fit their Be diffusion data to a complementary error function and calculated a 900°C diffusion coefficient of $\sim 10^{-11}$ cm^2/sec [82]. If one assumes their value to be most accurate around Be concentrations of $\sim 10^{19}$ cm^{-3}, which was roughly the peak acceptor concentration measured, this value is within a factor of 3 of that given by Fig. 3.11.

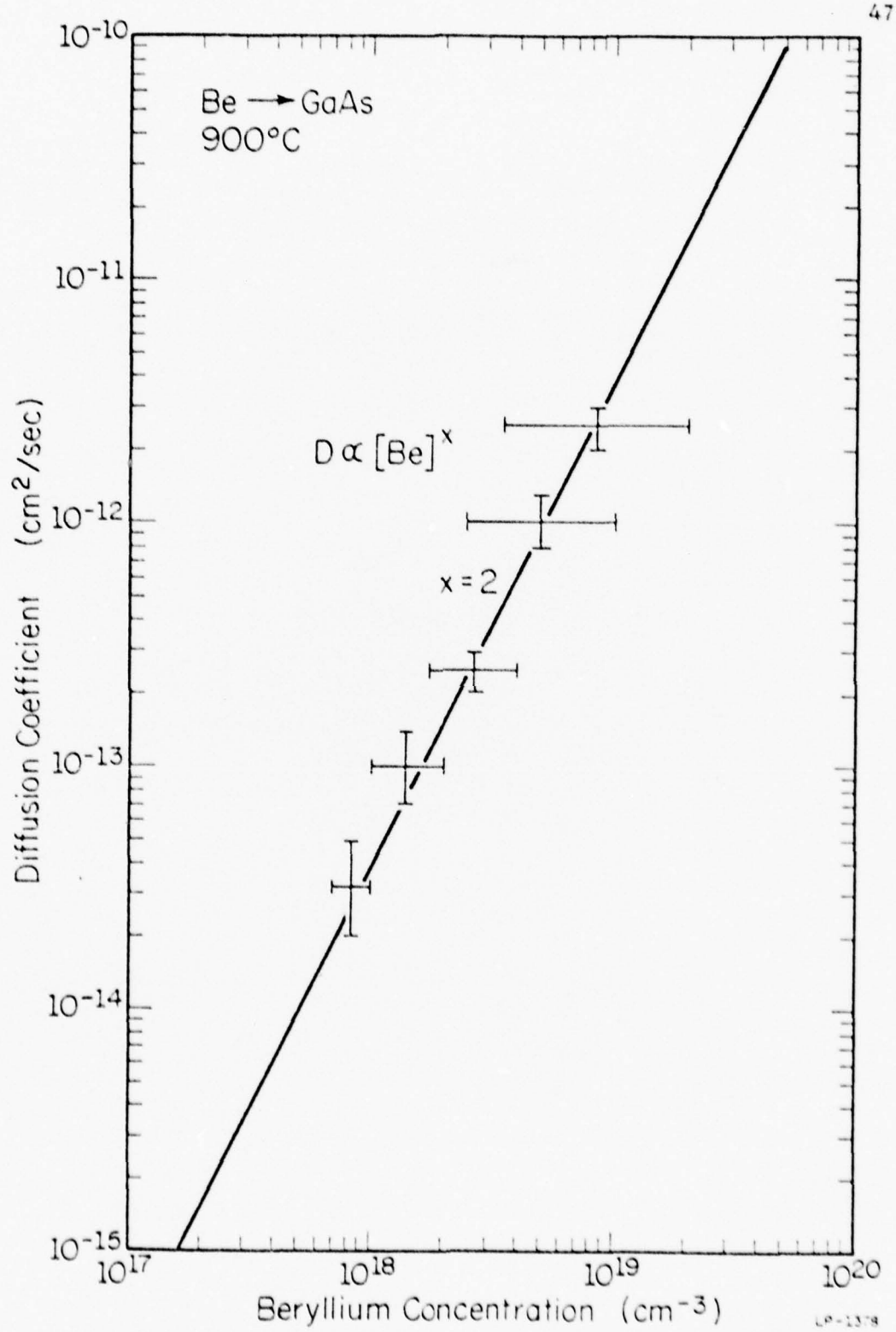

Fig. 3.11. Variation of the 900°C diffusion coefficient with implanted Be concentration in GaAs, as estimated from a Gaussian diffusion approximation.

The Be diffusion coefficients in Fig. 3.11 are approximately two orders of magnitude lower than values given by Casey et al. [80] for Zn diffusion in GaAs. For Zn concentrations of 10^{19} cm^{-3}, the diffusion coefficient at 900°C is 2-4 x 10^{-10} cm^2/sec. For comparable implanted Be concentrations, the diffusion coefficient is ~ 4 x 10^{-12} cm^2/sec. Although no diffusion coefficient data could be found for implanted Zn in GaAs, the profile information available [26,78,83] indicates that implanted Zn diffuses to a depth several times the projected range of the implant during annealing at 900°C. In such cases, the implant may be considered a pre-deposition which is followed by a drive-in diffusion. The diffusion coefficient of implanted Zn is therefore expected to be considerably higher than reported here for Be.

4. ANNEALING STUDIES OF Be-IMPLANTED $GaAs_{0.6}P_{0.4}$

VPE $GaAs_{0.6}P_{0.4}$ obtained from Monsanto was used in this work. This particular composition (x = 0.4) of $GaAs_{1-x}P_x$ is the standard material commercially employed in the fabrication of red light-emitting diodes (LEDs). The epitaxial layers studied had a background donor concentration $N_d = 2.6 \times 10^{16} cm^{-3}$, and were grown on n^+ GaAs substrates. All anneals were performed with Si_3N_4 encapsulation as described in Sec. 2.2.

4.1. Photoluminescence and Be-Implanted LED Results

A considerable amount of photoluminescence data on the annealing of Be-implanted $GaAs_{0.62}P_{0.38}$ has previously been published by Chatterjee et al. [5,7,27]. In those studies, measurements of the integrated intensity of the Be-related luminescence centered at 1.955 eV at 6°K were obtained as a function of annealing temperature from 600 to 900°C for implant fluences from 5×10^{12} to 5×10^{14} cm^{-2} at 250 keV. It was shown that annealing at 900°C results in maximum Be luminescence and lattice recovery.

The results mentioned above were verified in the present work, and additional information was obtained on the annealing of very high dose implants ($1\text{-}5 \times 10^{15}$ cm^{-2} at 250 keV). These implants were of interest for the possible fabrication of LEDs continuing previous work by Chatterjee et al. [7,17], who first demonstrated the feasibility of making red LEDs by Be implantation. The photoluminescence experiments carried out on these samples indicated the integrated intensity of the Be-related luminescence decreases steadily as the implant dose is increased from 5×10^{14} cm^{-2} at 250 keV. Longer anneal times of 1-2 hours increased the luminescence slightly, but the integrated intensities were still 2-10 times lower than that from an

unimplanted sample. These results correlate with that observed in Be-implanted GaAs (Sec. 3.1), and suggest that some residual lattice damage is still present after 900°C annealing of high dose implants.

The apparent inability to anneal out all of the implantation-induced defects was also reflected in the performance of red LEDs fabricated in this work. These Be-implanted LEDs were made using standard photolithographic processing by Monsanto as described previously [7]. Implants of 2×10^{15} cm^{-2} at 250 keV annealed for either 1 or 2 hours at 900°C resulted in LED luminous intensities at 10 mA of ~ 50 µcd. This value is somewhat less than the maximum luminous intensity found by Chatterjee [7] of ~80 µcd for a multiple Be implant which, considering the diffusion discussed in the next section, would be roughly equivalent to a $\sim 10^{15}$ implant at 290 keV annealed at 900°C for 1/2 hr. These luminous intensity valves are still well below the ~400 µcd at 10 mA typically measured for commercial Zn diffused devices.

4.2. Electrical and Atomic Profiles

In this section, SIMS Be atomic profiles and net acceptor distributions obtained from differential resistivity and Hall effect measurements of Be-implanted $GaAs_{0.6}P_{0.4}$ are presented. These results will be compared with those for Be-implanted GaAs in Sec. 4.3.

Because of the ~ 500-1000 Å striations often present on the surface of VPE $GaAs_{0.6}P_{0.4}$, and problems encountered with the uniformity of the etch rate as mentioned in Sec. 2.4.2, the experimental uncertainties involved in profiling Be-implanted $GaAs_{0.6}P_{0.4}$ are greater than those in profiling GaAs. These uncertainties are reflected in the larger error bars on the graphs presented in this section.

In Fig. 4.1, SIMS Be atomic profiles of a 5 x 10^{13} cm^{-2} Be implant at 250 keV before and after annealing at 900°C for 1/2 hr are compared with electrical profiles after annealing from 600 to 900°C. For this low-dose case, in which the peak implanted Be concentration before annealing is ~1 x 10^{18} cm^{-3}, the electrical activation is observed to be only 20% of the implanted dose for a 600°C, 1/2 hr anneal. The electrical activation increases to 60% for a 700°C, 1/2 hr anneal, and to 90% for both 800 and 900°C, 1/2 hr anneals. The highest net acceptor concentration (~7 x 10^{17} cm^{-3}) occurs for the 800°C anneal, since diffusion at 900°C reduces that distribution to a flat profile with concentration ~ 4.5 x 10^{17} cm^{-3}. The flat diffusion profile at 900°C is also observed in the SIMS Be atomic distribution. It appears that the amount of indiffusion is somewhat less than the diffusion towards the surface, suggesting the mechanism is damage-related.

The values for the electrical activation given in Fig. 4.1 are in agreement with previous findings published by Chatterjee et al. [6,7] for the annealing of low dose Be implants in $GaAs_{0.62}P_{0.38}$. However, the profile data presented by Chatterjee et al. [6,7] for a 6 x 10^{13} cm^{-2} implant at 250 keV annealed at 900°C for 1/2 hr has not been reproduced. This discrepancy is believed to be due to the poor reproducibility of the anodic oxidation technique [84] and of the method of depth calibration [85] used, although effects due to differences in the Si_3N_4 encapsulants may also be involved.

Electrical profiles for a 1 x 10^{15} cm^{-2} fluence of Be at 250 keV annealed from 700 to 900°C for 1/2 hr are given in Fig. 4.2. These profiles are also compared with the unannealed Be distribution as determined by SIMS. In this high dose case, the highest net acceptor concentration

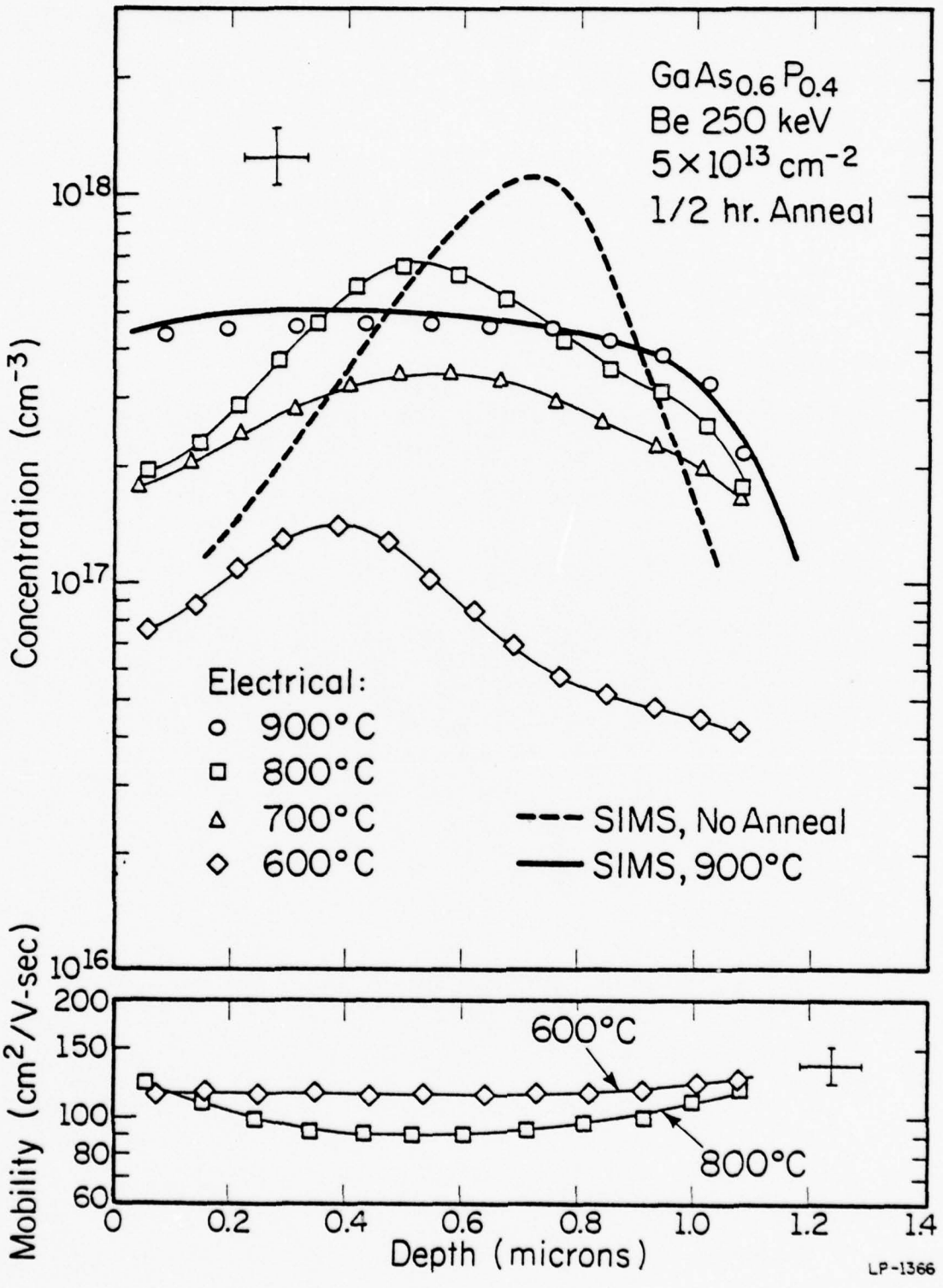

Fig. 4.1. Net acceptor concentration, SIMS, and mobility profiles for the low fluence implant and isochronal anneals shown.

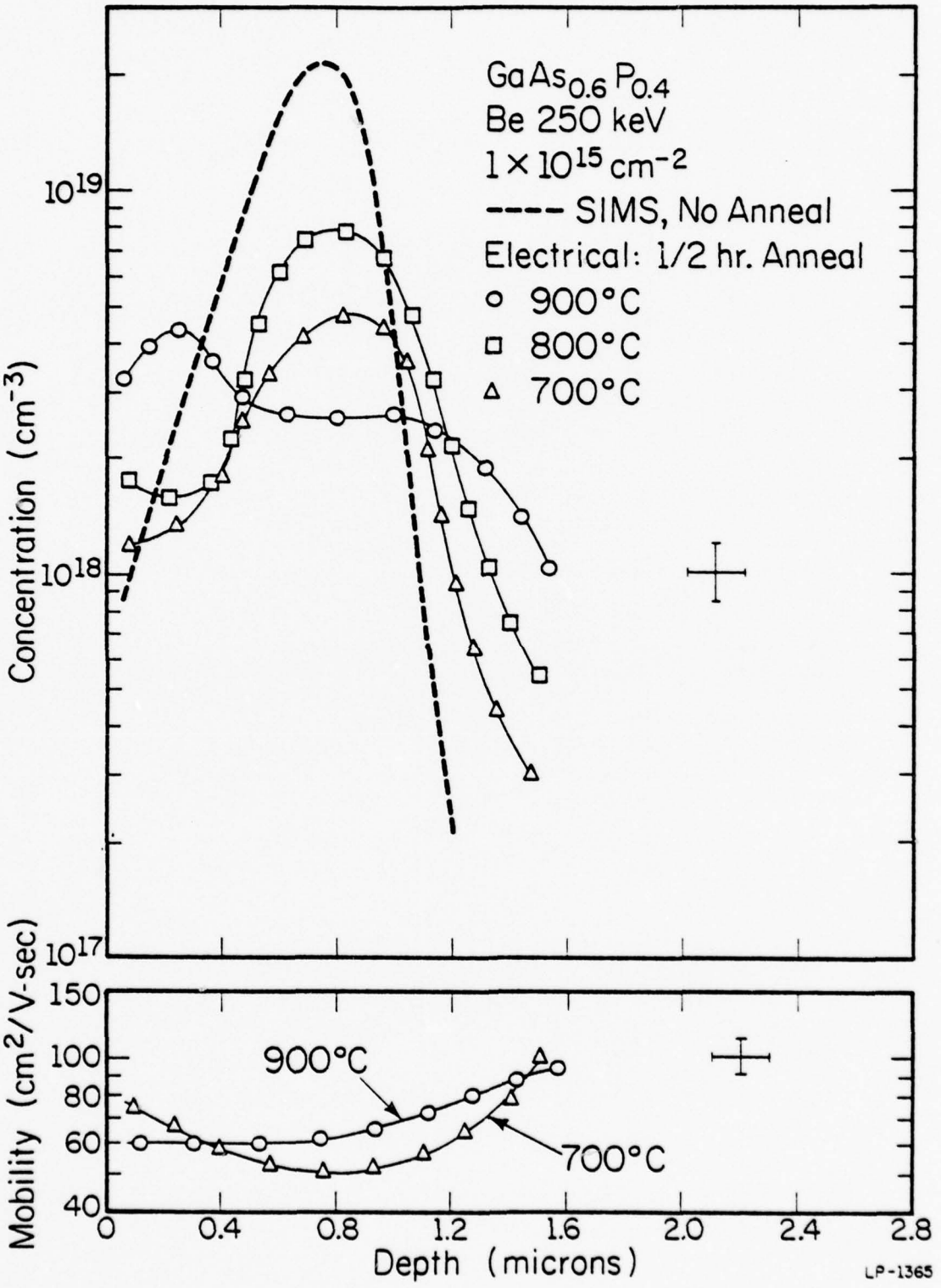

Fig. 4.2. Net acceptor concentration, SIMS, and mobility profiles for the high fluence implant and isochronal anneals shown.

also occurs for the 800°C anneal, with considerable diffusion taking place at 900°C. The electrical activations observed are 35% for a 700°C anneal, 60% for a 800°C anneal, and 40% for a 900°C anneal. The decrease in the electrical activation for the 900°C anneal is due to outdiffusion of Be into the Si_3N_4 encapsulant, which is also observed for high dose Be implants into GaAs (Sec. 3.2).

The higher electrical activation for the 800°C anneal also occurs for an implant of 5×10^{14} cm^{-2} at 250 keV. For this fluence, 70% activation is observed with 800°C, 1/2 hr annealing, and 60% with 900°C, 1/2 hr annealing. This 900°C data is in agreement with previous results reported by Chatterjee et al. [6,7]. However, the lower activation at 800°C reported by Chatterjee et al. [6,7] has not been reproduced. A similar discrepancy was noted in Sec. 3.2.1 for the low temperature annealing of Be-implanted GaAs.

The SIMS unannealed Be profiles in both Figs. 4.1 and 4.2 are skewed considerably toward the surface, as they are for Be-implanted GaAs (Sec. 3.2). This indicates calculation of higher order moments [70,71] is again necessary to correct LSS theory and accurately predict the implanted profile of Be in $GaAs_{0.6}P_{0.4}$.

The time dependence of the 900°C diffusion of implanted Be in $GaAs_{0.6}P_{0.4}$ is shown in Fig. 4.3. This graph compares SIMS Be atomic profiles with net acceptor distributions for a 1×10^{15} cm^{-2} implant at 250 keV annealed for various times from 5 min to 1 hr. The agreement between SIMS and electrical measurements is quite good in each case, except for the 5 min anneal, in which the net acceptor concentration appears slightly less than the Be atomic concentration near the peak of

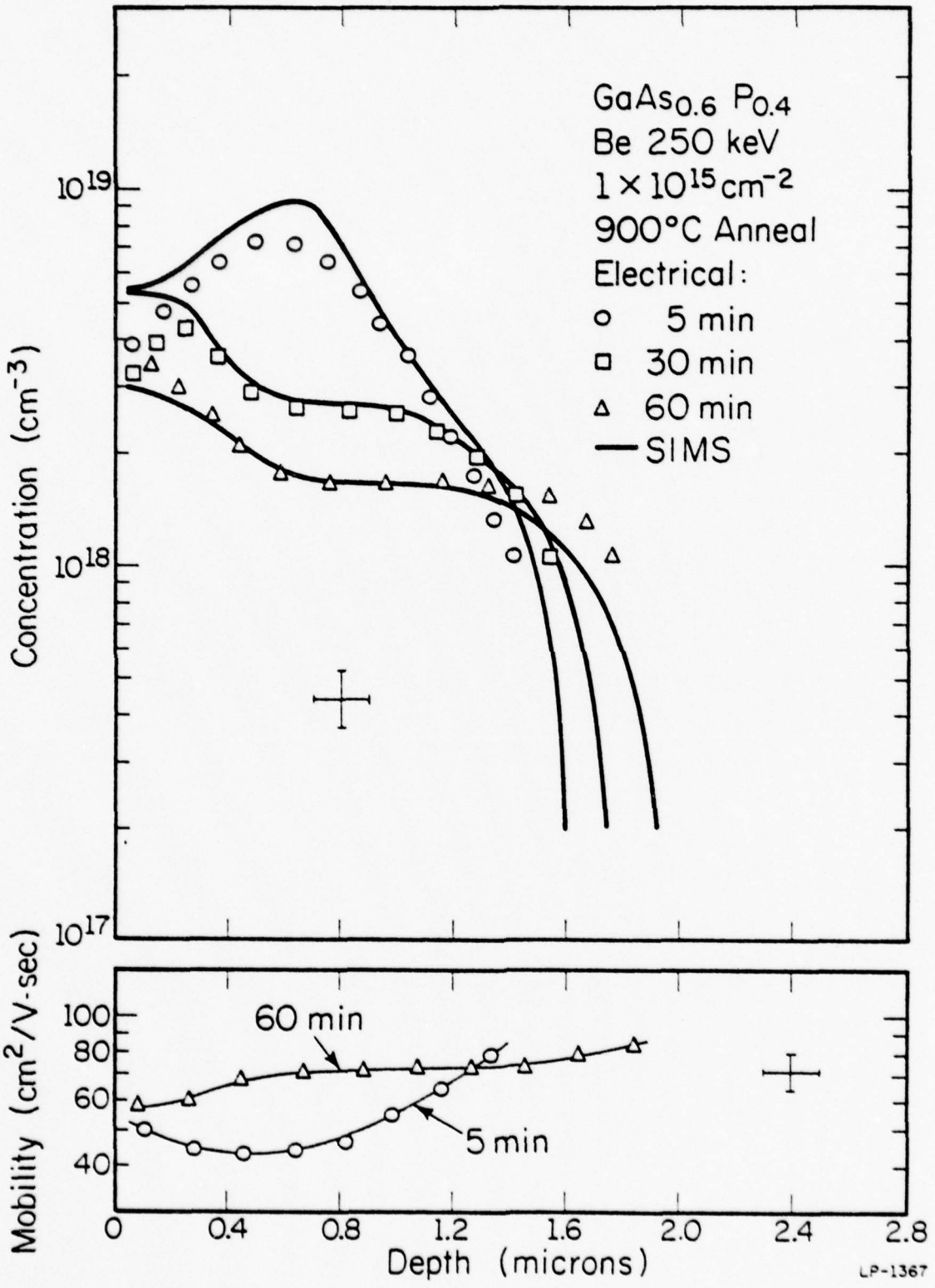

Fig. 4.3. Net acceptor concentration, SIMS, and mobility profiles for the high fluence implant and isothermal anneals shown.

the profile. The measured electrical activation is 65% for a 5 min anneal, 40% for a 1/2 hr anneal, and 35% for a 1 hr anneal. The Be continues to diffuse out at the surface and also diffuses deeper inward with increasing anneal time. The electrical profile for the 1/2 hr anneal has a slight dip at the surface not observed in the SIMS profile, which indicates some of the Be at the surface is not electrically active. The higher Be concentration extending ~ 4000 Å in from the surface for both the 1/2 and 1 hr anneals is also observed in SIMS and electrical profiles of 5×10^{14} and 2×10^{15} cm^{-2} Be implants at 250 keV annealed at 900°C for 1/2 hr. This effect is presumably defect-related and associated with the Si_3N_4 encapsulant and the outdiffusion of Be.

The mobilities shown in Figs. 4.1, 4.2 and 4.3 are comparable to those reported by others for Be [6,26], Zn [26,86,87], Cd [26], and Mg [26] implants into $GaAs_{0.6}P_{0.4}$. The observed mobilities range from ~ 120 cm^2/V-sec for net acceptor concentrations near 10^{17} cm^{-3} to 40-50 cm^2/V-sec for concentrations of $7-8 \times 10^{18}$ cm^{-3}. The lower mobilities measured in $GaAs_{0.6}P_{0.4}$ compared to GaAs are consistent with other reports of lower hole mobilities in GaP [66,88].

SIMS profiles of $GaAs_{0.6}P_{0.4}$ implanted with Be to fluences of $2-5 \times 10^{15}$ cm^{-2} at 250 keV showed anomalous diffusion during annealing identical to that observed for similar dose implants in GaAs (Sec. 3.2.2). Multiple peaks, a surface pileup of Be, and ~ 2μm junction depths were observed after annealing at 900°C for 1/2 hr.

4.3. Comparison with Be-Implanted GaAs

In general, the annealing behavior of implanted Be in GaAs and $GaAs_{0.6}P_{0.4}$ is quite similar. However, some significant differences are observed.

In Table 4.1, values for sheet carrier concentration and Hall mobility are tabulated for various fluences of Be-implants into GaAs and $GaAs_{0.6}P_{0.4}$, with annealing at various temperatures and times. The electrical activations are also given as a percentage of the implant dose in each case. The most notable difference observed between the annealing of Be-implanted GaAs and $GaAs_{0.6}P_{0.4}$ is that the low temperature (600-700°C) electrical activation of implanted Be in $GaAs_{0.6}P_{0.4}$ is substantially less than that in GaAs. However, the electrical activation for a 900°C, 1/2 hr anneal is only slightly less (5-15%) in $GaAs_{0.6}P_{0.4}$. As mentioned in Sec. 4.2 and evident from Table 4.1, the mobilities in $GaAs_{0.6}P_{0.4}$ are lower by about a factor of 2 compared with GaAs.

The diffusion profiles presented in Sec. 3.2 for Be-implanted GaAs can be compared with those in Sec. 4.2 for Be-implanted $GaAs_{0.6}P_{0.4}$. For the low fluence of 5×10^{13} cm^{-2} at 250 keV, profiles in GaAs are given in Fig. 3.2 while those for $GaAs_{0.6}P_{0.4}$ are shown in Fig. 4.1. Different electrical activations at 600 and 700°C are clearly evident: 80 and 85%, respectively, for Be in GaAs, and only 20 and 60% for Be in $GaAs_{0.6}P_{0.4}$. The extent of the diffusion taking place during a 900°C, 1/2 hr anneal is considerably greater in $GaAs_{0.6}P_{0.4}$. In GaAs, this implant and anneal results in a profile which remains Gaussian in shape. However, in $GaAs_{0.6}P_{0.4}$ this anneal gives a flat Be distribution, as shown in Fig. 4.1. A similarly flat profile was observed in both SIMS and electrical measurements of $GaAs_{0.6}P_{0.4}$ for 1 and 2×10^{14} cm^{-2} fluence implants at 250 keV annealed at 900°C for 1/2 hr.

A comparison of the low temperature activation and diffusion observed for a high fluence Be implant of 1×10^{15} cm^{-2} at 250 keV in

Table 4.1. Comparison of Electrical Measurements of Be-Implanted GaAs and $GaAs_{0.6}P_{0.4}$

Beryllium Fluence 250 keV N_D (cm^{-2})	Anneal		GaAs			$GaAs_{0.6}P_{0.4}$		
	Temp. (°C)	Time (min)	Sheet Carrier Concentration N_s (cm^{-2})	Electrical Activation $\frac{N_s}{N_D}$ (%)	Sheet Hall Mobility (cm^2/V-sec)	Sheet Carrier Concentration N_s (cm^{-2})	Electrical Activation $\frac{N_s}{N_D}$ (%)	Sheet Hall Mobility (cm^2/V-sec)
5×10^{13}	600	30	4.0×10^{13}	80	200	1.0×10^{13}	20	110
	700	30	4.2×10^{13}	85	210	3.0×10^{13}	60	90
	800	30	-	-	-	4.5×10^{13}	90	100
	900	30	4.8×10^{13}	95	210	4.5×10^{13}	90	100
1×10^{14}	900	30	9.5×10^{13}	95	180	8.5×10^{13}	85	90
2×10^{14}	700	30	1.8×10^{14}	90	150	-	-	-
	900	30	1.9×10^{14}	95	160	1.6×10^{14}	80	80
5×10^{14}	800	30	-	-	-	3.5×10^{14}	70	60
	900	30	3.2×10^{14}	65	150	3.0×10^{14}	60	70
1×10^{15}	600	30	7.0×10^{14}	70	110	-	-	-
	700	30	7.5×10^{14}	75	110	3.5×10^{14}	35	60
	800	30	5.0×10^{14}	50	120	6.0×10^{14}	60	50
	900	5	6.5×10^{14}	65	110	6.5×10^{14}	65	50
	900	30	5.0×10^{14}	50	140	4.0×10^{14}	40	70
	900	60	4.0×10^{14}	40	150	3.5×10^{14}	35	70

GaAs and $GaAs_{0.6}P_{0.4}$ can be made by examining Fig. 3.3 (GaAs) and Fig. 4.2 ($GaAs_{0.6}P_{0.4}$). For a 700°C, 1/2 hr anneal, such an implant results in 75% electrical activation in GaAs, but only 35% in $GaAs_{0.6}P_{0.4}$. However, for an 800°C, 1/2 hr anneal, the electrical activation is 50% in GaAs and 60% in $GaAs_{0.6}P_{0.4}$. The decrease in activation for Be-implanted GaAs at this anneal temperature is due to outdiffusion of Be into the encapsulant. Strangely, the diffusion of implanted Be at 800°C is less in $GaAs_{0.6}P_{0.4}$ than in GaAs, although the tail on the 700°C profile in Fig. 4.2 for $GaAs_{0.6}P_{0.4}$ extends deeper than the corresponding tail in Fig. 3.3 for GaAs.

The annealing behavior of implanted Be at 900°C in this high fluence (1×10^{15} cm^{-2} at 250 keV) case is found by comparing Fig. 3.4 (GaAs) with Fig. 4.3 ($GaAs_{0.6}P_{0.4}$). For a 5 min anneal, the electrical activation in both materials is 65%, although a slightly higher peak concentration and less diffusion is observed in Fig. 4.3 for Be-implanted $GaAs_{0.6}P_{0.4}$. However, the outdiffusion of Be at the surface, once it begins to take place, appears to be greater with $GaAs_{0.6}P_{0.4}$. In GaAs the electrical activation is 50% of the implanted dose after a 1/2 hr anneal, and 40% after a 1 hr anneal. The corresponding activation in $GaAs_{0.6}P_{0.4}$ is 40% after 1/2 hr and 35% after 1 hr. These anneals both result in a ~ 4000 Å deep Be peak near the surface in $GaAs_{0.6}P_{0.4}$, an effect not observed in GaAs. The extent of the indiffusion in both cases is nearly identical, however. The extremely rapid diffusion (a 900°C diffusion coefficient of 2×10^{-8} cm^2/sec for 10^{19} cm^{-3} Be concentrations) previously reported for Be in GaP [89] is not observed for either Be-implanted GaAs or $GaAs_{0.6}P_{0.4}$.

The unusual annealing properties observed for Be-implanted $GaAs_{0.6}P_{0.4}$ compared to Be-implanted GaAs may be due to a greater dependence of the electrical activation and diffusion on temperature, defect, and surface-related effects in the ternary. However, it is clear from the close agreement between SIMS and electrical measurements for 900°C, 1/2 hr anneals that, in spite of substantial diffusion for all fluences into $GaAs_{0.6}P_{0.4}$ studied, and the concentration-dependent diffusion observed for Be-implanted GaAs, nearly all (85-100%) of the Be remaining after the anneal is electrically active for both materials.

5. ANNEALING STUDIES OF Be-DOPED MBE GaAs

Ilegems [28] has recently demonstrated the feasibility of molecular beam epitaxial (MBE) growth of p-type GaAs using Be doping. A unity sticking coefficient was observed, and net acceptor concentrations of up to 5×10^{19} cm^{-3} were obtained. Mobilities were comparable with values measured in p-GaAs grown by other techniques. MBE-grown p-n junctions fabricated using Be as the p-dopant were found to have promising current-voltage characteristics.

Annealing experiments [28] on Be-doped MBE GaAs have established a very low diffusion coefficient of $\leq 10^{-15}$ cm^2/sec at 800°C for Be concentrations near 10^{17} cm^{-3}. This diffusion is one order of magnitude slower than found for Zn, if the 800°C Zn diffusion coefficients given by Casey et al. [90] are extrapolated to a concentration of $\sim 10^{17}$ cm^{-3}. The Be diffusion was independent of the As overpressure used, suggesting the mechanism may be different from that observed for Zn in GaAs. It has been shown that the diffusion coefficient of Zn in GaAs is inversely proportional to the fourth root of the As_4 overpressure under As-rich diffusion conditions [73]. However, it should be mentioned that such As pressure dependence is also associated with the indiffusion of Zn from an outside source, and may not be applicable to the diffusion within an MBE-grown layer.

Of particular interest to the present work is the comparison of the annealing behavior of Be incorporated during the MBE growth process with implanted Be in GaAs. The annealing of MBE-grown Be concentrations above 2×10^{17} cm^{-3} has not been studied prior to the present work

because of the limitations of the differential capacitance-voltage technique [91] in profiling heavily-doped layers. Differential resistivity and Hall effect measurements and SIMS are well suited for the study of higher doping concentrations, and therefore have been used in this work. All the MBE samples investigated here were grown by M. Ilegems of Bell Laboratories.

5.1. Annealing of a Buried Rectangular Be Distribution

A major advantage of MBE is the capability to fabricate rapidly varying doping profiles. An example of a Be-doped "buried spike" grown by MBE is shown in Fig. 5.1. This structure consists of a heavily Be-doped region $\sim$ 3200 Å wide centered at $\sim$ 4800 Å, with lightly Be-doped regions on both sides. This structure was grown on a lightly doped n-type MBE GaAs layer. In this figure, SIMS Be atomic distributions are compared with electrical profiles before and after annealing at 900°C for 1/2 hr with Si_3N_4 encapsulation. In the absence of an absolute SIMS calibration of Be concentration, the electrical data are used for this calibration. The SIMS data are plotted with the electrical data, assuming the peak concentrations of the as-grown profiles are equal for the two types of measurement. As is evident from Fig. 5.1, some diffusion of the Be has occurred during the 900°C anneal, but the peak concentration has not changed drastically. The peak net acceptor concentration before annealing was $\sim 3.3 \times 10^{19}$ cm^{-3}, compared with $\sim 2.1 \times 10^{19}$ cm^{-3} following the anneal. This concentration is about 5 times the maximum Be concentration observed for implanted Be in GaAs after an identical 900°C, 1/2 hr anneal. The SIMS and electrical profiles of the annealed samples agree reasonably well, although the electrical data appear to show slightly more diffusion.

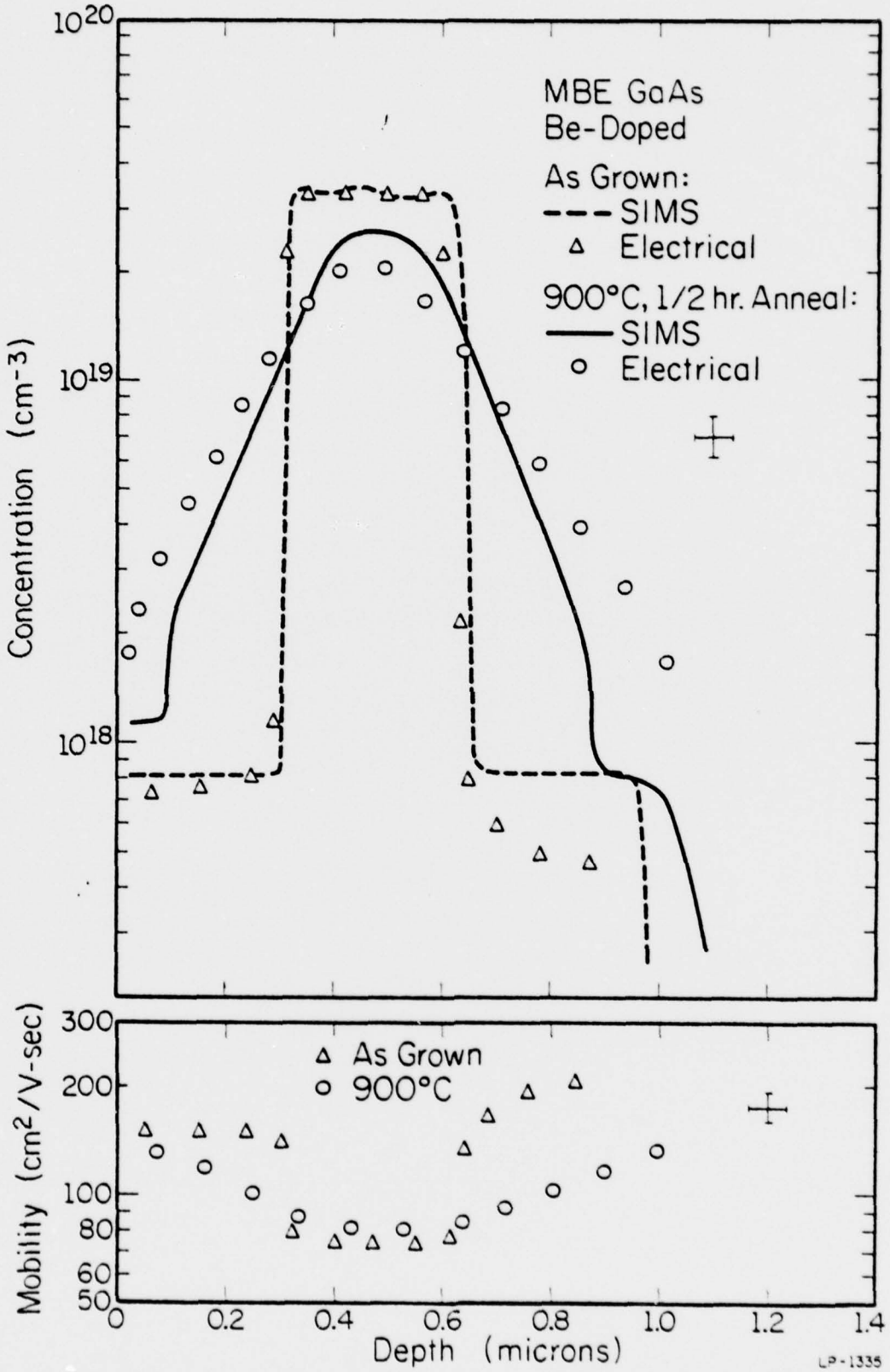

Fig. 5.1. Comparison of net acceptor concentration, SIMS, and mobility profiles for an MBE-grown "buried spike" before and after a 900°C, 1/2 hr anneal.

The mobilities corresponding to the as-grown and annealed profiles are also plotted in Fig. 5.1. The observed mobilities compare exceptionally well with hole mobilities found experimentally for GaAs grown by other techniques [66], and range from 75-85 $cm^2/V\text{-sec}$ for acceptor concentrations of 2-3 x 10^{19} cm^{-3} to $\sim$ 200 $cm^2/V\text{-sec}$ for concentrations of $\sim$ 5 x 10^{17} cm^{-3}. These values are also in agreement with mobilities reported previously for Be-doped MBE GaAs [28].

The diffusion profile in Fig. 5.1 appears to be roughly Gaussian in shape, hence a standard diffusion coefficient calculation can be made. The equation describing the diffusion with time of an initially rectangular distribution of width 2w and peak concentration C_o centered at x = 0 is given by [92]

$$C(x) = \frac{1}{2} C_o \left\{ \mathrm{erf}\left(\frac{w+x}{2\sqrt{Dt}}\right) + \mathrm{erf}\left(\frac{w-x}{2\sqrt{Dt}}\right) \right\} \qquad (5.1)$$

where C is the concentration at depth x, D is the diffusion coefficient, and t is time. In Appendix 3, a computer program that performs the calculation given by Eqn. (5.1) for arbitrary diffusion coefficients and times is presented. This program was used to generate diffusion profiles, shown in Fig. 5.2, for the initially rectangular distribution given in Fig. 5.1. By comparing the diffusion profiles in Figs. 5.1 and 5.2, a good estimate of the diffusion coefficient can be made. The SIMS data in Fig. 5.1 correspond to a diffusion coefficient of $\sim$ 5 x 10^{-14} cm^2/sec, while the electrical data correspond to a diffusion coefficient of $\sim$ 1 x 10^{-13} cm^2/sec. Therefore, the diffusion coefficient of Be in MBE GaAs at 900°C is $\sim$ 0.5-1 x 10^{-13} cm^2/sec for the Be concentration range of $\sim$ 0.2-3 x 10^{19} cm^{-3}. This value is two orders of magnitude lower than

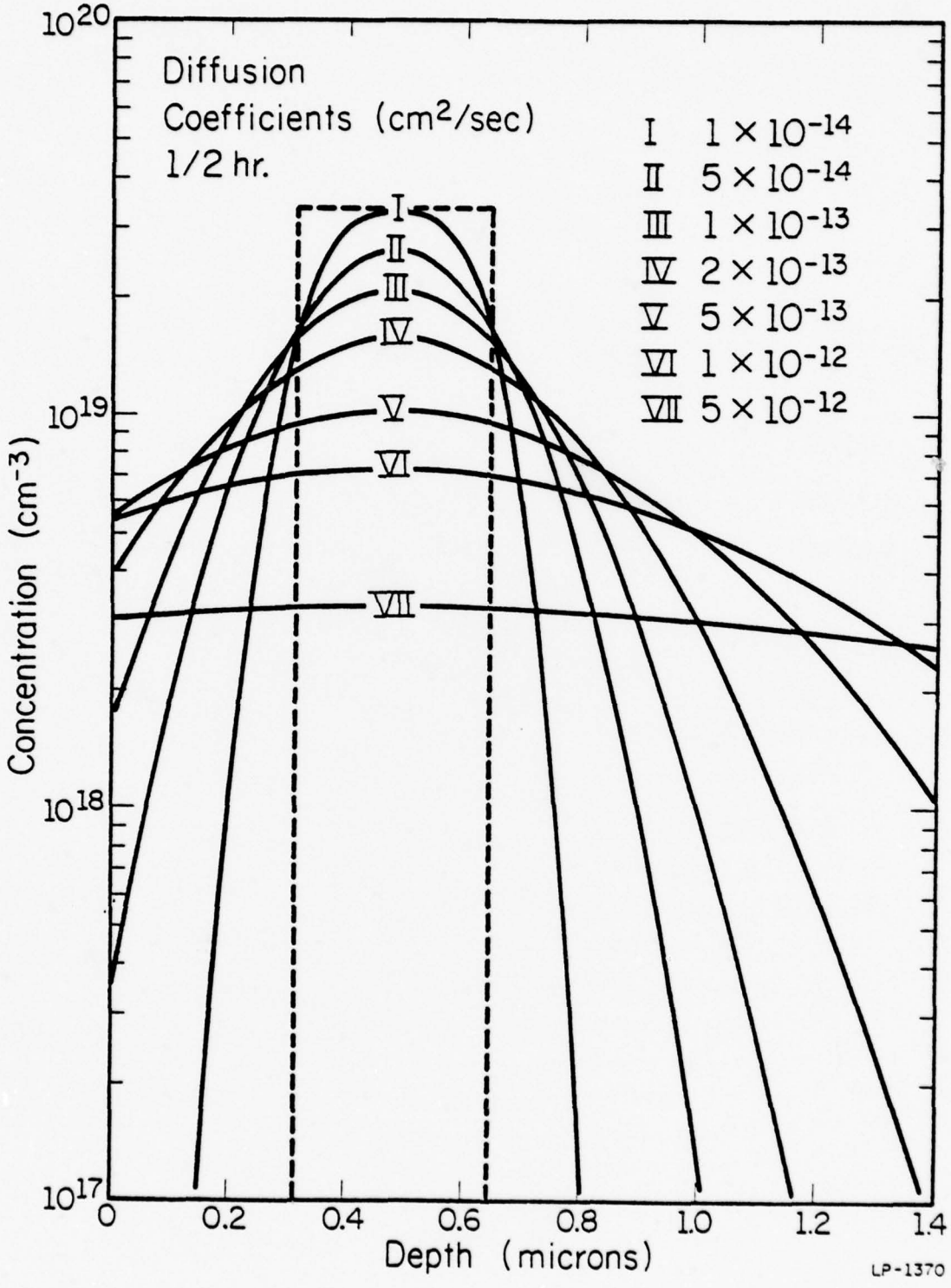

Fig. 5.2. Theoretical diffusion profiles of an initially rectangular distribution for the diffusion coefficients shown.

the diffusion coefficient found for implanted Be in GaAs as given by Fig. 3.11 in Sec. 3.2.4. From Fig. 3.11, an implanted Be concentration of 2-3 x 10^{19} cm^{-3} would have a diffusion coefficient of ~ 10^{-11} cm^2/sec at 900°C. Such a large difference between the diffusion coefficients for implanted and MBE-grown Be clearly indicates a different diffusion process is involved in these two cases.

Electrical profiles were also obtained after 800°C, 1/2 hr anneals of the same MBE-grown distribution described in Fig. 5.1. The diffusion coefficient at this temperature is 0.5-1 x 10^{-14} cm^2/sec, which is 5-10 times higher than reported by Ilegems [28] for much lower Be concentrations of ~ 10^{17} cm^{-3}. This indicates some concentration dependence of the diffusion of MBE-grown Be in GaAs. However, it should be noted that this concentration dependence is substantially less than the square-law dependence described in Sec. 3.2.4 for implanted Be in GaAs.

To ensure that the diffusion described in Chapter 3 for implanted Be in VPE GaAs was not a substrate-related effect, Be implants were also performed into undoped MBE GaAs layers. SIMS and electrical profiles of Be-implanted and annealed MBE samples were identical to those obtained for VPE material.

To investigate the possibility that the diffusion of Be is damage dependent, a helium implant of 1 x 10^{15} cm^{-2} at 130 keV was performed on unannealed samples with the same buried rectangular Be distribution shown in Fig. 5.1. Helium was chosen since it is an inert atom and can be implanted deep enough to create damage throughout the ~ 1 μm thick Be-doped MBE layer. The implant used corresponds to a peak implanted

He concentration of $\sim 2 \times 10^{19}$ cm^{-3} at a projected range of $\sim$ 7500 Å. Both SIMS and electrical profiles performed on these He-damaged samples after 900°C, 1/2 hr annealing indicated no significant change in the diffusion behavior from that observed for unimplanted samples annealed in the same manner. In 5°K photoluminescence measurements performed on these samples, a four-fold decrease in the integrated intensity of the Be-related luminescence was observed in the He-implanted and annealed samples compared to unimplanted but identically annealed samples. Thus significant lattice damage resulted from the He implant. The fact that no significant increase in Be diffusion was observed in the presence of such damage strongly suggests that the diffusion of Be, whether introduced during growth by MBE or implanted, is not simply related to damage. This experiment is not completely definitive, however, in that damage from the He implant only approximates the type and extent of damage caused by implantation of Be.

5.2. Annealing of a Thin Be-Doped Surface Layer

Figure 5.3 illustrates SIMS and electrical profiles of Be grown in a $\sim$ 3500 Å deep surface layer on an undoped MBE layer. The concentration of Be in the surface layer is $\sim 2 \times 10^{19}$ cm^{-3}. This graph compares the Be profiles before and after annealing at 900°C for 1/2 hr, and also shows a SIMS profile of a He-damaged sample annealed similarly. A double He implant was employed, composed of 1.5×10^{15} cm^{-2} at 220 keV followed by 1×10^{15} cm^{-2} at 90 keV. This implant was designed to result in an essentially flat He distribution of 2×10^{19} cm^{-3} to a depth of $\sim$ 1.2 μm. The SIMS data were not calibrated in terms of absolute Be concentration,

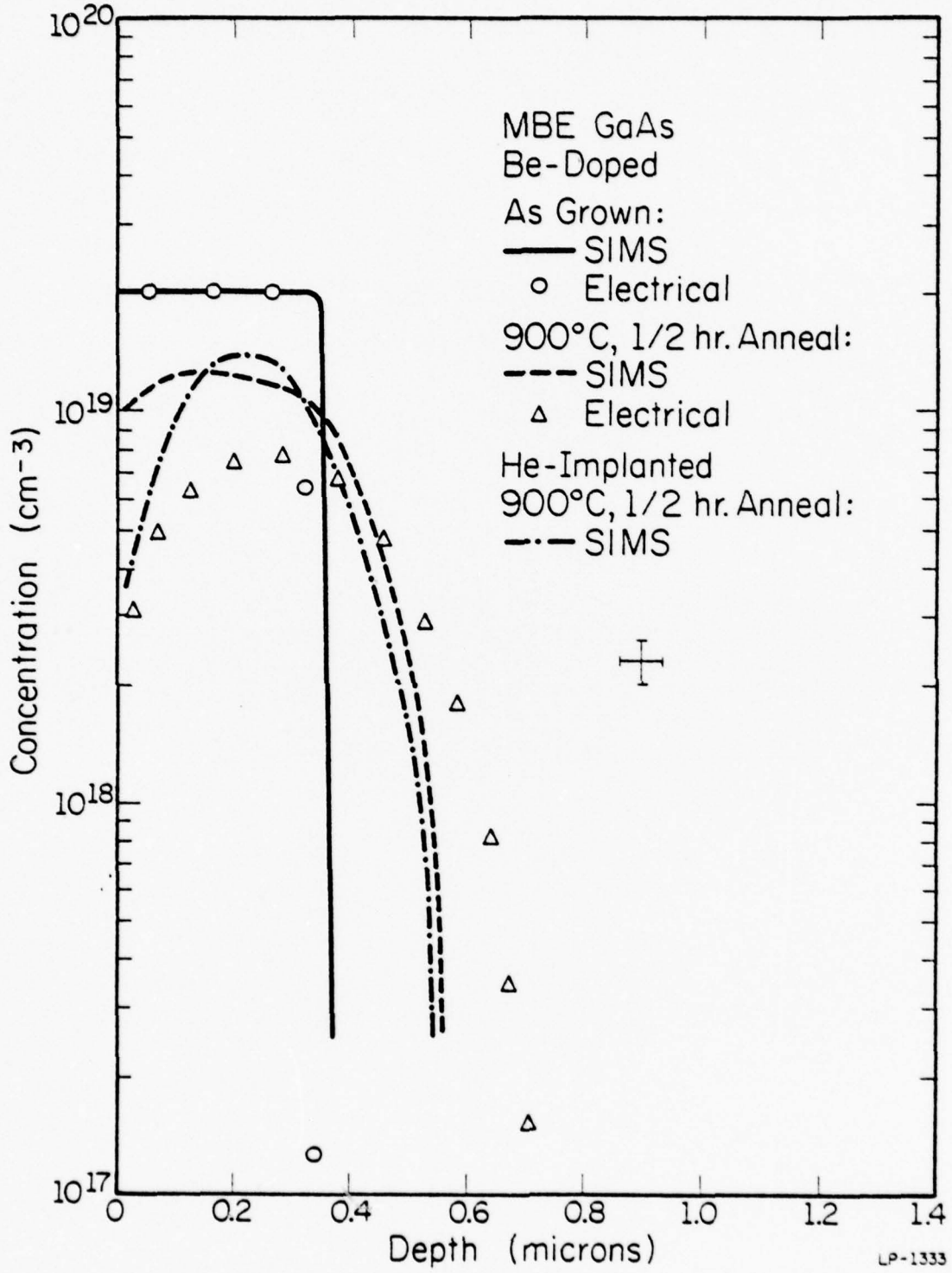

Fig. 5.3. Comparison of net acceptor concentration and SIMS profiles for an MBE-grown Be-doped surface layer before and after a 900°C, 1/2 hr anneal. A SIMS profile after a helium damage-implant and similar anneal is also shown.

and are therefore plotted with the electrical data points by assuming the peak concentrations are equal.

Unlike Fig. 5.1, where reasonably close agreement between SIMS and the electrical data was observed, the profiles in Fig. 5.3 exhibit substantial differences. The electrical data for the 900°C, 1/2 hr anneal show a considerably lower net acceptor concentration in the ~ 4000 Å region near the surface and somewhat deeper indiffusion than the SIMS profile. The reason for this discrepancy is not clear. The apparent compensation near the surface may be related to the encapsulant. The deeper indiffusion of the electrical profile suggests that other acceptors besides Be may be present. A slightly deeper indiffusion was also noted for the electrical profile in Fig. 5.1. Even though some uncertainty exists in interpreting the electrical data, the SIMS Be atomic profiles in Figs. 5.1 and 5.3 show roughly similar redistribution behavior. Both figures indicate the 900° diffusion coefficient of MBE-grown Be in GaAs is substantially less than that observed for implanted Be.

As shown by the SIMS profile in Fig. 5.3 for the He-implanted sample, damaging the crystal lattice does not significantly affect the indiffusion of the Be. However, the lower concentration at the surface observed after annealing the He-implanted sample suggests that outdiffusion into the encapsulant is enhanced by lattice damage. However, as mentioned in Sec. 5.1, it is not clear that the damage resulting from such a He implant is equivalent to that accompanying a Be implant.

Photoluminescence (5°K) measurements performed on the as-grown sample of Fig. 5.3 indicated the presence of a luminescence peak centered at 1.474 eV in addition to the usual band-to-acceptor luminescence at

1.493 eV associated with Be. These two luminescence peaks were approximately of equal intensity. The lower energy peak (1.474 eV) corresponds to a center with a binding energy of ~ 47 meV, which is too deep to be any known simple acceptor [93]. Presumably this peak is defect-related, since its intensity diminishes by a factor of ~ 10 after annealing at 900°C for 1/2 hr. The discrepancy found between electrical measurements and SIMS in Fig. 5.3 may be associated with this defect.

5.3. Annealing of a Thick Be-Doped Layer

In Fig. 5.4, SIMS and electrical profiles of a 1.4 μm thick heavily Be-doped MBE layer grown on an undoped MBE layer are compared before and after annealing at 900°C for 1/2 hr. In this graph, the SIMS data were calibrated by comparing with SIMS measurements of an unannealed 1×10^{15} cm^{-2} Be implant at 250 keV into undoped MBE GaAs. Such an implant corresponds to a peak Be concentration of 2×10^{19} cm^{-3}.

Figure 5.4 shows substantial differences between the SIMS Be atomic profiles and the net acceptor distributions found from electrical measurements, as was the case in Fig. 5.3. For the unannealed profile, electrical data indicate the net acceptor concentration is $\sim 4 \times 10^{19}$ cm^{-3}, while the SIMS data correspond to a Be concentration of $\sim 5.5 \times 10^{19}$ cm^{-3}. This suggests that not all of the Be is electrically active for such high Be concentrations. In the annealed profile, the SIMS Be concentration has dropped considerably, to $\sim 3 \times 10^{19}$ cm^{-3}, and a large pileup of Be is observed at the surface. Strangely, the SIMS data indicate no significant indiffusion of the Be, although the outdiffusion is substantial. In contrast to the SIMS data, the electrical profiles in

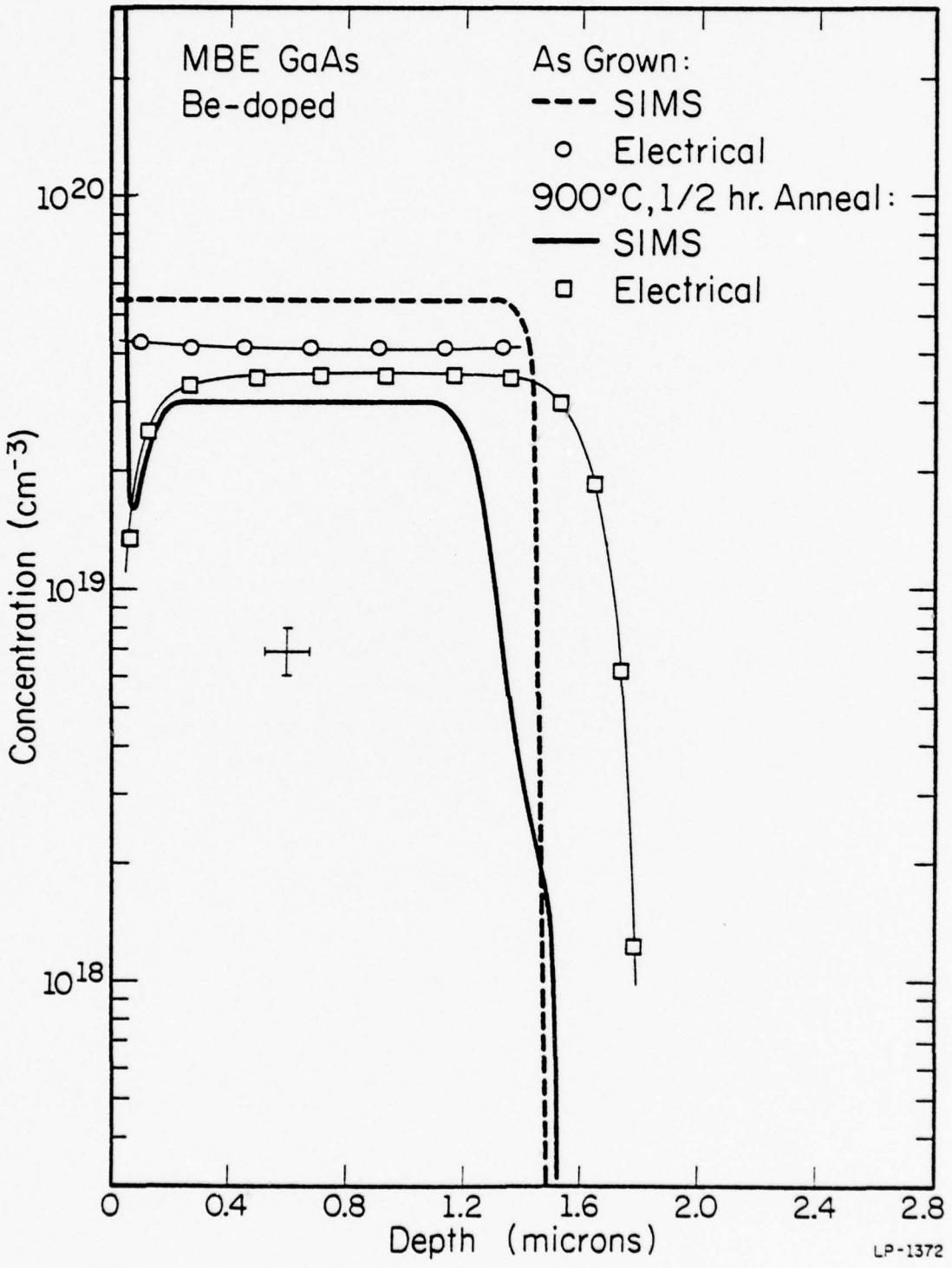

Fig. 5.4. Comparison of net acceptor concentration and SIMS profiles for a Be-doped MBE layer before and after a 900°C, 1/2 hr anneal.

Fig. 5.4 show only a slight decrease in peak concentration with the anneal, and a significant amount of indiffusion. The peak net acceptor concentration changes from $\sim 4 \times 10^{19}$ cm^{-3} to $\sim 3.5 \times 10^{19}$ cm^{-3} after the 900°C anneal. The tail on the distribution moves from ~ 1.4 μm initially to ~ 1.8 μm after the anneal. The extent of this indiffusion is consistent with that observed for the electrical data in Figs. 5.1 and 5.3. The substantial differences between the SIMS and electrical data are not understood, and may be due in part to measurement uncertainties. Since all three cases presented in Figs. 5.1-5.4 exhibit a noticeably deeper indiffusion of acceptors than is observed for atomic Be, the possibility exists that there are other acceptors besides Be involved.

Electrical profiles for 700, 800, and 900°C, 1/2 hr anneals are compared in Fig. 5.5 for the same MBE layer shown in Fig. 5.4. The electrical carrier concentration is observed to decrease slightly as the annealing temperature is increased. The diffusion front is also observed to move steadily inward, to ~ 1.6 μm for an 800° anneal, and to ~ 1.8 μm for a 900° anneal. The mobilities of all samples studied are $\sim$ 70-80 $cm^2/V\text{-sec}$, which is in agreement with previously reported values [28].

As has been observed in the other MBE samples described previously in this chapter, the diffusion of Be in the samples of Figs. 5.4 and 5.5 does not appear to be enhanced by He implant damage. Electrical profiles obtained after implanting a He fluence of 2×10^{15} cm^{-2} at 250 keV and annealing at 900°C for 1/2 hr actually showed slightly less Be indiffusion. The junction depth after the implant and anneal was ~ 1.6 μm, compared to ~ 1.8 μm found for unimplanted but identically annealed samples.

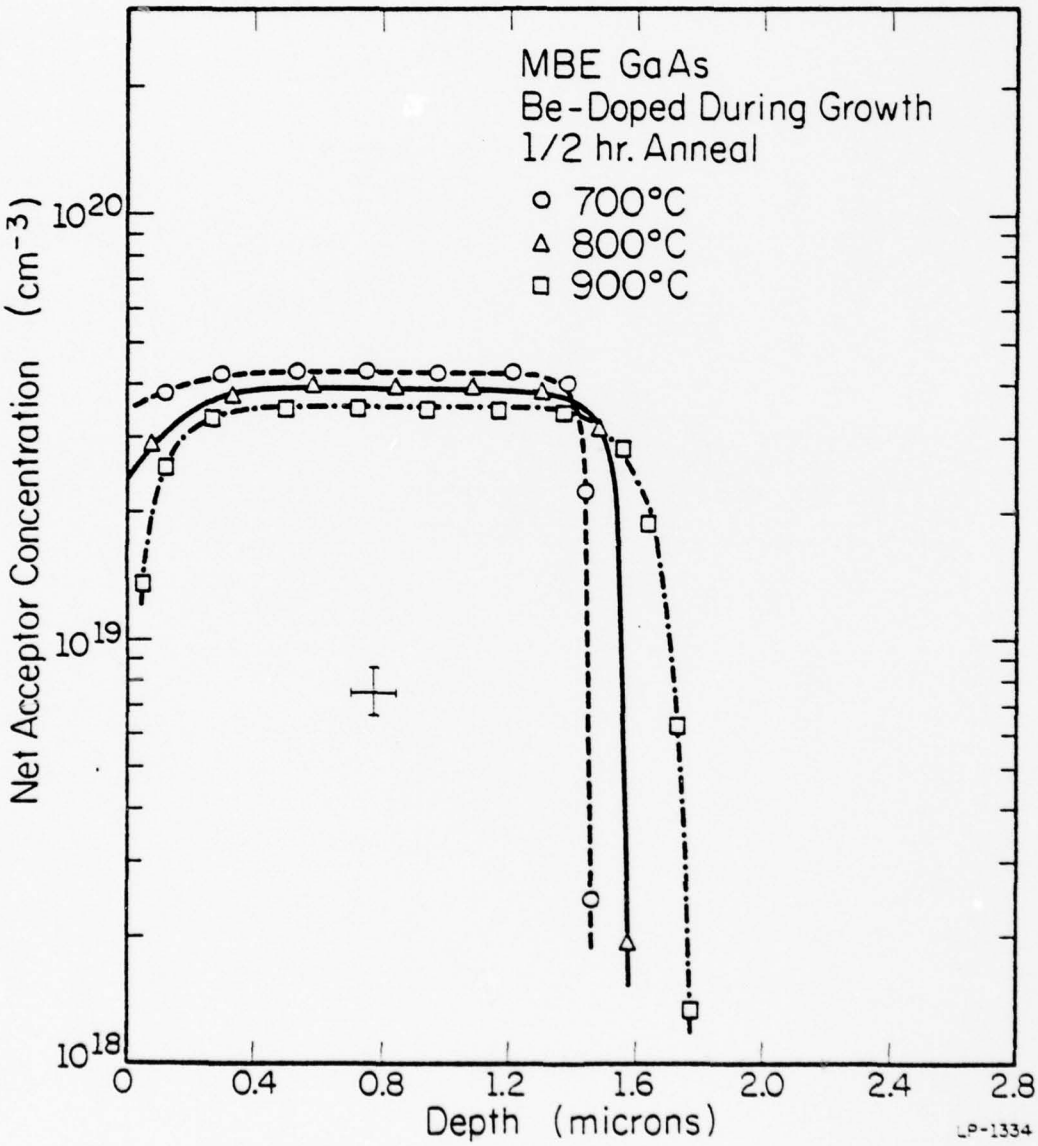

Fig. 5.5. Net acceptor concentration profiles for a Be-doped MBE layer annealed at the temperatures shown for 1/2 hr.

Photoluminescence ($5^{o}K$) spectra on unannealed samples from the same wafer from which the profiles in Figs. 5.4 and 5.5 were obtained exhibited a broad luminescence band peaked at 1.463 eV, containing the Be-related luminescence at 1.493 eV as a small shoulder. A similar low energy peak at 1.474 eV was noted in the photoluminescence spectra for the MBE sample discussed in Sec. 5.2. The peak at 1.463 eV corresponds to a binding energy of $\sim$ 58 meV, which also is too deep to be a simple acceptor, and is therefore presumed to be defect-related.

The discrepancies between SIMS Be atomic profiles and electrically active carrier distributions observed in heavily Be-doped MBE layers may be associated with the unusual low energy photoluminescence peaks observed in these materials. However, measurement uncertainties cannot be ruled out. The indiffusion observed in the electrical data appears to be consistent for all three cases studied in this chapter. The SIMS data presented in Figs. 5.1 and 5.3 are also consistent, although the diffusion appears to be slightly less than that observed in the electrical profiles. Despite these uncertainties, it is clear that the diffusion of Be incorporated during growth by MBE is substantially less than that observed for implanted Be in GaAs.

6. SUMMARY AND CONCLUSIONS

In this work, differential resistivity and Hall effect measurements, secondary ion mass spectrometry (SIMS), and low temperature (5°K) photoluminescence have been used to study and compare the annealing behavior of beryllium-implanted GaAs and $GaAs_{0.6}P_{0.4}$, and the diffusion of beryllium incorporated during the growth process by molecular beam epitaxy (MBE). In the following sections the results and conclusions of this work are summarized, and recommendations for further studies are noted.

6.1. Be-Implanted GaAs

Photoluminescence studies of Be-implanted GaAs, as reported previously by Chatterjee et al. [2] and further substantiated by this work, indicate an anneal temperature of 900°C using appropriate Si_3N_4 encapsulation results in optimum Be optical activation and lattice recovery. The increase in integrated intensity of the Be-related luminescence band at 1.493 eV for anneals between 600 and 900°C becomes even more pronounced for implant fluences above $5 \times 10^{13} cm^{-2}$ at 250 keV. For heavy dose implants ($\geq 1 \times 10^{15} cm^{-2}$ at 250 keV), some residual lattice damage may be unannealable even at 900°C. Annealing temperatures above 900°C were not investigated in this work because of problems with the Si_3N_4 encapsulant at such temperatures, such as indiffusion of Si from the encapsulant [67,94].

The optimum annealing time at 900°C is a trade-off between the reliability of the Si_3N_4 encapsulant used and the slight increase in luminescence observed for longer anneal times. In this work, a 1/2 hr anneal appeared to be the best compromise. Further work is necessary to investigate the possibility and effect of indiffusion of Si or N from the

Si_3N_4 encapsulant during the anneal. Complications arising from the outdiffusion of Be into the encapsulant during the anneal of high dose implants must also be considered.

A heavily fluence-dependent diffusion of implanted Be in GaAs is observed. For low fluences ($\leq 5 \times 10^{13}$ cm^{-2} at 250 keV), no significant diffusion occurs during annealing up to 900°C, and the highest electrical activation (90-100%) occurs at 900°C. However, for high fluences ($\geq 5 \times 10^{14}$ cm^{-2} at 250 keV), substantial diffusion is observed at anneal temperatures $\geq$ 800°C, resulting in an apparent maximum in electrical activity (~75%) near 700°C. The decreased activation at higher anneal temperatures is due to outdiffusion of the implanted Be into the Si_3N_4 encapsulant. The extent of the outdiffusion is dependent on the Be concentration near the surface during the anneal, and is most pronounced when the surface concentration exceeds 1×10^{18} cm^{-3}. The excellent agreement found between electrical and atomic profiles demonstrates that, although considerable outdiffusion of Be occurs for higher dose implants, 85-100% of the Be present after annealing is electrically active.

The excellent mobilities (up to 300 cm^2/V-sec for Be concentrations of $\sim 10^{17}$ cm^{-3}) and the high electrical activation efficiencies observed for 600-700°C anneals indicate the requirements for electrical activation of Be-implanted GaAs are much less stringent than those for efficient luminescence. For applications in which only electrical activation is desired, low anneal temperatures of 600-700°C may be sufficient. However, the photoluminescence results indicate that optoelectronic devices fabricated with Be implantation will require an anneal temperature of 900°C for successful removal of residual lattice damage. Therefore, depending on the desired application, both the annealing time and temperature may

have to be adjusted to result in optimum device performance.

The outdiffusion of Be at the GaAs surface is also observed for anneals performed without Si_3N_4 encapsulation in evacuated sealed ampoules under Ga-liquidus equilibrium conditions (excess Ga and GaAs). Electrical profiles indicate diffusion behavior identical to that observed with Si_3N_4 encapsulation. Further studies of the outdiffusion and possible pileup of Be at the surface are necessary. Additional information may be gained by varying the partial pressures of Ga and As in sealed ampoule anneals [73], or experimenting with other encapsulants [94].

It is difficult to distinguish between concentration and defect-dependent diffusion effects because of the increased lattice damage accompanying higher dose implants. However, a two-step anneal does not reduce the diffusion of implanted Be at 900°C. In this method, a long anneal (1-2 hr.) at a low temperature (600-700°C) is first done to electrically activate most of the implanted Be, and then is followed by a 900°C, 1/2 hr anneal. Implants into heated (350°C) substrates, in which some annealing would be expected to take place during the implant, also do not significantly affect the diffusion of the implanted Be. These results demonstrate the diffusion is not simply damage related. The sharp diffusion fronts observed in both SIMS and electrical profiles of higher dose implants annealed at 900°C are indicative of a concentration-dependent diffusion. First order estimates of the diffusion coefficient of implanted Be at 900°C (Fig. 3.11) suggest the diffusion coefficient is proportional to the square of the Be concentration. The measured diffusion coefficients range from 10^{-14} cm^2/sec for Be concentrations of $\sim 5 \times 10^{17}$ cm^{-3}, to 10^{-11} cm^2/sec for concentrations of $\sim 2 \times 10^{19}$ cm^{-3}. However, considering

the substantially lower diffusion coefficient observed with MBE-grown Be-doped GaAs (Chap. 5), defect-enhanced migration effects cannot be ruled out. Although not presently understood, the diffusion mechanism for implanted Be in GaAs apparently involves a complex combination of defect and concentration-dependent effects.

The data presented here can form the basis for future theoretical and experimental work on the subject of Be diffusion in GaAs. The fact that both Zn and Be diffusion appear to have a square-law concentration-dependence is intriguing. It is not known if this is merely coincidental or indicative of a basic similarity in the diffusion mechanisms involved. An interesting experiment in this regard would be to perform the anneal with the sample in an electric field, and determine the charge state, if any, of the diffusing Be.

The diffusion coefficient for implanted Be at 900°C is approximately two orders of magnitude lower than that reported for diffused Zn in GaAs (Sec. 3.2.4). However, further studies similar to that described in refs. [11-12] are necessary to more thoroughly characterize the lateral diffusion properties of implanted Be. The extremely low leakage currents, high breakdown voltages, and greatly reduced lateral diffusion that have been reported [4,12,14] for p-n junctions fabricated by Be implantation in GaAs clearly indicate that device quality p-type layers are obtainable.

6.2. Be-Implanted $GaAs_{0.6}P_{0.4}$

In general, the annealing behavior of implanted Be in $GaAs_{0.6}P_{0.4}$ is very similar to that in GaAs. The most notable difference between the annealing of the two materials is that low temperature (600-700°C) electrical activation of implanted Be in $GaAs_{0.6}P_{0.4}$ is substantially less than that

in GaAs. However, the electrical activation for a 900°C, 1/2 hr anneal is only slightly less (5-15%) in $GaAs_{0.6}P_{0.4}$. Although the extent of the indiffusion of Be during a 900°C anneal is nearly identical for both GaAs and $GaAs_{0.6}P_{0.4}$, the outdiffusion of Be into the Si_3N_4 encapsulant is slightly greater in $GaAs_{0.6}P_{0.4}$, and results in the lower electrical activation measured. Even a low fluence of 5×10^{13} cm^{-2} at 250 keV into $GaAs_{0.6}P_{0.4}$ results in a completely flat distribution after 900°C annealing, while an identical implant and anneal in GaAs gives a profile still roughly Gaussian in shape. The excellent agreement observed between SIMS and electrical profiles in GaAs and $GaAs_{0.6}P_{0.4}$ indicates that, in spite of the substantial diffusion which is observed for all the fluences into $GaAs_{0.6}P_{0.4}$ studied in this work, nearly all (85-100%) of the Be remaining after the anneal is electrically active for both materials.

Some aspects of the annealing behavior of Be-implanted $GaAs_{0.6}P_{0.4}$ are peculiar compared to Be-implanted GaAs. The diffusion of implanted Be at 800°C is less in $GaAs_{0.6}P_{0.4}$ than in GaAs, although the reverse appears to be true at 700°C. For 900°C anneals of low fluence implants in $GaAs_{0.6}P_{0.4}$, the diffusion of Be towards the surface is noticeably greater than the indiffusion into the substrate. Higher fluences ($\geq 5 \times 10^{14}$ cm^{-2}) at 250 keV annealed at 900°C for 1/2 hr result in a significant Be peak in the $\sim$ 4000 Å region next to the surface, an effect not observed in GaAs. The unusual annealing properties of Be-implanted $GaAs_{0.6}P_{0.4}$ compared to Be-implanted GaAs are presumably due to a greater dependence of the electrical activation and diffusion on temperature, defect, and surface-related effects in the ternary.

The hole mobilities observed for Be-implanted $GaAs_{0.6}P_{0.4}$ are

comparable to those reported for Zn implants into $GaAs_{0.6}P_{0.4}$ [26,86,87]. The observed mobilities range from ~ 120 cm^2/V-sec for concentrations near 10^{17} cm^{-3} to 40-50 cm^2/V-sec for concentrations of 7-8 x 10^{18} cm^{-3}. These mobilities are a factor of 2 or more below those for similar hole concentrations in GaAs.

Photoluminescence (5°K) measurements show annealing behavior for Be-implanted $GaAs_{0.6}P_{0.4}$ similar to that observed for Be-implanted GaAs. As reported previously by Chatterjee et al. [5], an anneal temperature of 900°C using Si_3N_4 encapsulation is necessary for optimum Be optical activation and lattice recovery. High fluence implants ($\geq$ 1 x 10^{15} cm^{-2} at 250 keV) result in some residual lattice damage which may be unannealable even at 900°C. This was reflected in the lower performance of Be-implanted red LEDs fabricated in this work compared to those made previously [7,17] by lower fluence Be implantation.

Device quality p-n junctions and greatly reduced lateral diffusion have been reported for Be-implanted $GaAs_{0.6}P_{0.4}$ [7,11,15,17]. Further studies, similar to those mentioned in Sec. 6.1 for Be-implanted GaAs, would be helpful to fully exploit the potential of Be implantation in $GaAs_{0.6}P_{0.4}$.

6.3. Be-Doped MBE GaAs

Two dramatic differences in the annealing behavior of Be incorporated during the growth process by MBE and implanted Be in GaAs are observed. Much higher electrically active Be concentrations can be achieved with MBE, and a substantially lower diffusion coefficient at 900°C is observed for MBE-grown Be compared to implanted Be. For Be-doped MBE GaAs, a peak net acceptor concentration of ~ 3.5 x 10^{19} cm^{-3} is obtainable even after a 900°C, 1/2 hr anneal. This doping level is approximately one order of magnitude

higher than can be achieved with Be implantation and similar annealing. The diffusion coefficient of MBE-grown Be in GaAs at 900° is ~ 0.5 - 1 x 10^{-13} cm^2/sec for the Be concentration range of ~0.2 - 3 x 10^{19} cm^{-3}. This value is two orders of magnitude lower than the diffusion coefficient observed for Be-implanted GaAs for concentrations of 2 - 3 x 10^{19} cm^{-3}. Only a slight concentration-dependence of the diffusion in MBE GaAs is noted, in contrast to the square-law dependence of the diffusion coefficient for implanted Be concentrations.

The hole mobilities observed for Be-doped MBE GaAs compare exceptionally well with those found experimentally for GaAs grown by other techniques. The mobilities range from 75-85 cm^2/V-sec for acceptor concentrations of 2 - 3 x 10^{19} cm^{-3} to ~ 200 cm^2/V-sec for concentrations of ~ 5 x 10^{17} cm^{-3}.

Be implants into undoped MBE layers show annealing behavior identical to that for VPE material, indicating the diffusion effects reported here for Be-implanted GaAs are not substrate-dependent. The implantation of He in heavily Be-doped MBE GaAs layers to create lattice damage has no substantial effect on the Be diffusion in a subsequent anneal. This suggests the diffusion of Be, whether introduced during crystal growth by MBE or implanted, is not a simple damage-dependent phenomenon. However, a comparison between the diffusion of implanted Be and the diffusion in He-damaged Be-doped MBE layers may not be definitive, since it is not known whether the damage resulting from He implants properly approximates the damage accompanying Be implants.

Photoluminescence (5°K) measurements on unannealed samples of heavily Be-doped MBE layers indicate the presence of a broad, low energy

luminescence peak in addition to the usual band-to-acceptor luminescence at 1.493 eV associated with Be. The low energy luminescence peak was observed at 1.474 eV in one set of samples, and at 1.463 eV in another. Both of these luminescence peaks correspond to energy levels too deep to be simple acceptors, and are therefore presumed to be defect-related. Their intensity was found to decrease after 900^{o}C annealing.

There is evidence to suggest that not all the Be is electrically active in MBE layers with Be doping levels above 3 - 4 x 10^{19} cm^{-3}. Some discrepancies are also observed between SIMS and electrical profiles, including deeper indiffusion of net acceptor distributions compared to SIMS Be atomic profiles. These discrepancies may be associated with the unusual photoluminescence peaks observed. Further studies are necessary to resolve these uncertainties.

The differences in the annealing behavior of implanted Be and MBE-grown Be in GaAs are not understood. The diffusion mechanisms are clearly different for the two cases, and further work in this area is needed. However, the present findings demonstrate that high doping levels, good mobilities, and very low diffusion coefficients are obtainable with Be doping of GaAs by MBE. This relatively new technology is therefore expected to find significant applications as it continues to develop.

REFERENCES

1. R. G. Hunsperger, R. G. Wilson, and D. M. Jamba, "Mg and Be ion implanted GaAs," J. Appl. Phys., Vol. 43, pp. 1318-20, 1972.

2. P. K. Chatterjee, K. V. Vaidyanathan, W. V. McLevige, and B. G. Streetman, "Photoluminescence from Be-implanted GaAs," Appl. Phys. Lett., Vol. 27, pp. 567-9, 1975.

3. P. K. Chatterjee, W. V. McLevige, K. V. Vaidyanathan, and B. G. Streetman, "Temperature dependence of photoluminescence from Be-implanted GaAs," Appl. Phys. Lett., Vol. 28, pp. 509-12, 1976.

4. J. P. Donnelly, F. J. Leonberger, and C. O. Bozler, "Uniform-carrier-concentration p-type layers in GaAs produced by beryllium ion implantation," Appl. Phys. Lett., Vol. 28, pp. 706-8, 1976.

5. P. K. Chatterjee, W. V. McLevige, and B. G. Streetman, "Luminescence properties of Be-implanted $GaAs_{1-x}P_x$ ($x \sim 0.38$)," J. Appl. Phys., Vol. 47, pp. 3003-9, 1976.

6. P. K. Chatterjee, W. V. McLevige, and B. G. Streetman, "Electrical properties of Be-implanted $GaAs_{1-x}P_x$," Solid State Electronics, Vol. 19, pp. 961-4, 1976.

7. P. K. Chatterjee, "Acceptor behavior of implanted beryllium in gallium arsenide and gallium arsenide phosphide," Ph.D. Thesis, University of Illinois, 1976. Also Coordinated Science Laboratory Report R-721, available from NTIS, Springfield, Va. 22151 (Report #ADA025607).

8. J. A. Hutchby and K. V. Vaidyanathan, "Temperature dependence of electrical properties in Be-implanted semi-insulating GaAs," J. Appl. Phys., Vol. 48, pp. 2559-64, 1977.

9. W. V. McLevige, M. J. Helix, K. V. Vaidyanathan, and B. G. Streetman, "Electrical profiling and optical activation studies of Be-implanted GaAs," J. Appl. Phys., Vol. 48, pp. 3342-6, 1977.

10. B. J. Baliga and S. K. Ghandhi, "Lateral diffusion of zinc and tin in gallium arsenide," IEEE Trans. Electron Devices, Vol. ED-21, pp. 410-5, 1974.

11. P. K. Chatterjee and B. G. Streetman, "Reduced lateral diffusion and reverse leakage in Be-implanted $GaAs_{1-x}P_x$ diodes," Solid State Electronics, Vol. 20, pp. 305-6, 1977.

12. M. J. Helix, K. V. Vaidyanathan, B. G. Streetman, and P. K. Chatterjee, "Planar GaAs p-n junctions by Be ion implantation," 1977 IEDM Technical Digest, IEEE, New York, 1977, pp. 195-7.

13. F. J. Leonberger, J. P. Donnelly, and C. O. Bozler, "Low-loss GaAs $P^+n^-n^+$ three-dimensional optical waveguides," Appl. Phys. Lett., Vol. 28, pp. 616-9, 1976.

14. A. A. Immorlica, Jr. and F. H. Eisen, "Planar passivated GaAs hyperabrupt varactor diodes," Sixth Biennial Conference on Active Microwave Semiconductor Devices and Circuits, Cornell University, Ithaca, N. Y., August 1977.

15. R. K. Ahrenkiel, F. Moser, T. J. Coburn, S. L. Lyu, K. V. Vaidyanathan, P. K. Chatterjee, W. V. McLevige, and B. G. Streetman, "Low dark current photosensors based on $GaAs_{0.6}P_{0.4}$," 1976 IEDM Technical Digest, IEEE, New York, 1976, pp. 426-8.

16. E. E. Barrowcliff, L. O. Bubulac, D. T. Cheung, W. E. Tennant, and A. M. Andrews, "GaSb metal-insulator-semiconductor field-effect-transistors," 1977 IEDM Technical Digest, IEEE, New York, 1977, pp. 559-62.

17. P. K. Chatterjee, B. G. Streetman, D. L. Keune, and A. H. Herzog, "Be-implanted $GaAs_{1-x}P_x$ light emitting diodes," 1975 IEDM Technical Digest, IEEE, New York, 1975, pp. 187-91.

18. S. T. Picraux, "Vaporization of ion-implanted GaAs," Ion Implantation in Semiconductors and Other Materials, edited by B. L. Crowder, Plenum Press, New York, 1973, pp. 641-54.

19. J. P. Donnelly, W. T. Lindley, and C. E. Hurwitz, "Silicon- and selenium-ion-implanted GaAs reproducibly annealed at temperatures up to 950°C," Appl. Phys. Lett., Vol. 27, pp. 41-3, 1975.

20. J. S. Harris, F. H. Eisen, B. Welch, J. D. Haskell, R. D. Pashley, and J. W. Mayer, "Influence of implantation temperature and surface protection on tellurium implantation in GaAs," Appl. Phys. Lett., Vol. 21, pp. 601-3, 1972.

21. R. M. Malbon, D. H. Lee, and J. M. Whelan, "Annealing of ion-implanted GaAs in a controlled atmosphere," J. Electrochem. Soc., Vol. 123, pp. 1413-5, 1976.

22. J. Gyulai, J. W. Mayer, I. V. Mitchell, and V. Rodriguez, "Outdiffusion through silicon oxide and silicon nitride layers on gallium arsenide," Appl. Phys. Lett., Vol. 17, pp. 332-4, 1970.

23. K. Gamo, T. Inada, S. Krekeler, J. W. Mayer, F. H. Eisen, and B. M. Welch, "Selenium implantation in GaAs," Solid State Electronics, Vol. 20, pp. 213-7, 1977.

24. K. V. Vaidyanathan, M. J. Helix, D. J. Wolford, B. G. Streetman, R. J. Blattner, and C. A. Evans, Jr., "Study of encapsulants for annealing GaAs," J. Electrochem Soc., Vol. 124, pp. 1781-4, 1977.

25. E. A. Poltoratskii and V. M. Stuchebnikov, "Diffusion of beryllium in gallium arsenide," Sov. Phys.-Solid State, Vol. 8, pp. 770-1, 1966.

26. R. Zölch, H. Ryssel, H. Franz, H. Reichl, and I. Ruge, "Implantation of Be, Cd, Mg and Zn in GaAs and $GaAs_{1-x}P_x$," Ion Implantation in Semiconductors 1976, edited by F. Chernow, J. A. Borders, and D. K. Brice, Plenum Press, New York, 1977, pp. 593-601.

27. P. K. Chatterjee, W. V. McLevige, B. G. Streetman, and K. V. Vaidyanathan, "Electrical and photoluminescence properties of Be-implanted GaAs and $GaAs_{0.62}P_{0.38}$," Ion Implantation in Semiconductors 1976, edited by F. Chernow, J. A. Borders, and D. K. Brice, Plenum Press, New York, 1977, pp. 611-19.

28. M. Ilegems, "Beryllium doping and diffusion in molecular-beam epitaxy of GaAs and $Al_xGa_{1-x}As$," J. Appl. Phys., Vol. 48, pp. 1278-87, 1977.

29. A. Y. Cho and J. R. Arthur, "Molecular beam epitaxy," Prog. Solid-State Chem., Vol. 10, pp. 157-91, 1975.

30. L. L. Chang, L. Esaki, W. E. Howard, and R. Ludeke, "The growth of a GaAs-GaAlAs superlattice," J. Vac. Sci. Technol., Vol. 10, pp. 11-16, 1973.

31. A. Y. Cho, C. N. Dunn, R. L. Kuvas, and W. E. Schroeder, "GaAs IMPATT diodes prepared by molecular beam epitaxy," Appl. Phys. Lett., Vol. 25, pp. 224-6, 1974.

32. A. Y. Cho and H. C. Casey, Jr., "GaAs-$Al_xGa_{1-x}As$ double-heterostructure lasers prepared by molecular-beam epitaxy," Appl. Phys. Lett., Vol. 25, pp. 288-90, 1974.

33. J. R. Arthur, "Adsorption of Zn on GaAs," Surface Sci., Vol. 38, pp. 394-412, 1973.

34. A. Y. Cho and M. B. Panish, "Magnesium-doped GaAs and $Al_xGa_{1-x}As$ by molecular beam epitaxy," J. Appl. Phys., Vol. 43, pp. 5118-23, 1972.

35. N. Matsunaga, M. Naganuma, and K. Takahashi, "Molecular beam epitaxy with ionized beam doping," Jap. J. Appl. Phys., Vol. 16, Suppl. 16-1, pp. 443-9, 1977.

36. J. F. Gibbons, "Ion implantation in semiconductors - Part I: Range distribution theory and experiments," Proc. IEEE, Vol. 56, pp. 295-319, 1968.

37. J. F. Gibbons, "Ion implantation in semiconductors - Part II: Damage production and annealing," Proc. IEEE, Vol. 60, pp. 1062-96, 1972.

38. J. W. Mayer, L. Ericksson, and J. A. Davies, Ion Implantation in Semiconductors, Academic Press, New York, 1970.

39. J. Lindhard, M. Scharff, and H. Schiott, "Range concepts and heavy ion ranges (notes on atomic collisions II)," K. Dan. Vidensk. Selsk. Mat. Fys. Medd., Vol. 33, pp. 1-39, 1963.

40. J. F. Gibbons, W. S. Johnson, and S. V. Mylroie, Projected Range Statistics, Semiconductors and Related Materials, 2nd edition, Dowden, Hutchinson, and Ross, Stroudsburg, 1975.

41. This program was adapted from the formulation of Johnson, Gibbons, and Mylorie (ref. 40) by W. E. Miller of NASA Langley and was modified for this work by A. J. Rosa.

42. M. J. Helix, K. V. Vaidyanathan, and B. G. Streetman, "A low temperature reactive plasma system for depositing silicon nitride layers," Extended Abstracts of the 152nd Meeting of the Electrochemical Society, Atlanta, October 1977, #156.

43. R. S. Rosler, W. C. Benzing, and J. Baldo, "A production reactor for low temperature plasma-enhanced silicon nitride deposition," Solid State Technology, Vol. 19, pp. 45-50, June 1976.

44. H. B. Bebb and E. W. Williams, "Photoluminescence I: theory," Semiconductors and Semimetals, Vol. 8, edited by R. K. Willardson and A. C. Beer, Academic Press, New York, 1975, pp. 181-320.

45. E. W. Williams and H. B. Bebb, "Photoluminescence II: GaAs," Semiconductors and Semimetals, Vol. 8, edited by R. K. Willardson and and A. C. Beer, Academic Press, New York, 1975, pp. 321-392.

46. N. Holonyak, Jr. and D. R. Scifres, "Window heat sink sandwich for optical experiments: diamond (or sapphire) - semiconductor-indium sandwich," Rev. Sci. Instrum., Vol. 42, pp. 1885-6, 1971.

47. J. W. Mayer, O. J. Marsh, G. A. Shifrin, and R. Baron, "Ion implantation of silicon: II. Electrical evaluation using Hall-effect measurements," Can. J. Phys. Vol. 45, pp. 4073-89, 1967.

48. N.G.E. Johansson, J. W. Mayer, and O. J. Marsh, "Technique used in Hall effect analysis of ion implanted Si and Ge," Solid-State Electronics, Vol. 13, pp. 317-35, 1970.

49. B. L. Crowder and J. M. Fairfield, "High-dose implantations of P, As, and Sb in silicon: A comparison of room-temperature implantations followed by a 550°C anneal and implantations conducted at 600°C," J. Electrochem. Soc., Vol. 117, pp. 363-7, 1970.

50. H. Muller, F. H. Eisen, and J. W. Mayer, "Anodic oxidation of GaAs as a technique to evaluate electrical carrier concentration profiles," J. Electrochem. Soc., Vol. 122, pp. 621-5, 1975.

51. W. V. McLevige, P. K. Chatterjee, and B. G. Streetman, "Versatile

double AC Hall effect system for profiling impurities in semiconductors," J. Phys. E: Sci. Instrum., Vol. 10, pp. 335-7, 1977.

52. B. R. Russell and C. Wahlig, "A new method for the measurement of Hall coefficients," Rev. Sci. Instrum., Vol. 21, pp. 1028-9, 1950.

53. T. Kaneda, S. Kobayashi, and K. Shimoda, "A double AC method for sensitive measurement of the Hall effect," Jap. J. Appl. Phys., Vol. 12, pp. 1335-7, 1973.

54. N. Z. Lupu, N. M. Tallan, and D. S. Tannhauser, "Apparatus for measuring the Hall effect of low-mobility samples at high temperatures," Rev. Sci. Instrum., Vol. 38, pp. 1658-61, 1967.

55. M. Altwein, H. Finkenrath, and T. Stockel, "Low temperature Hall measurements in a cryostat with a built-in magnet," J. Phys. E: Sci. Instrum., Vol. 6, pp. 623-7, 1973.

56. C. J. Nuese and J. J. Gannon, "Silver-manganese evaporated ohmic contacts to p-type gallium arsenide," J. Electrochem. Soc., Vol. 115, pp. 327-8, 1968.

57. L. J. van der Pauw, "A method of measuring specific resistivity and Hall effect of discs of arbitrary shape," Philips Res. Repts., Vol. 13, pp. 1-9, 1958.

58. R. Chwang, B. J. Smith, and C. R. Crowell, "Contact size effects on the van der Pauw method for resistivity and Hall coefficient measurement," Solid-State Electronics, Vol. 17, pp. 1217-27, 1974.

59. R. L. Petritz, "Theory of an experiment for measuring the mobility and density of carriers in the space-charge region of a semiconductor surface," Phys. Rev., Vol. 110, pp. 1254-62, 1958.

60. D. R. Myers, "Properties of silicon implanted with arsenic through silicon dioxide," Ph.D. thesis, University of Illinois, 1977. Also Coordinated Science Laboratory Report R-756, available from NTIS, Springfield, Va. 22151 (Report #ADA040683).

61. G. E. Stillman, C. M. Wolfe, and J. O. Dimmock, "Hall coefficient factor for polar mode scattering in n-type GaAs," J. Phys. Chem. Solids, Vol. 31, pp. 1199-204, 1970.

62. G. H. Morrison and G. Slodzian, "Ion microscopy," Anal. Chem., Vol. 47, pp. 932A-943A, 1975.

63. W. K. Hofker, H. W. Werner, D. P. Oosthoek, and H.A.M. de Grefte, "Profiles of boron implantations in silicon measured by secondary ion mass spectrometry," Rad. Eff., Vol. 17, pp. 83-90, 1973.

AD-A057 645 ILLINOIS UNIV AT URBANA-CHAMPAIGN COORDINATED SCIENCE LAB F/G 20/12
ANNEALING STUDIES OF BERYLLIUM IN GALLIUM ARSENIDE AND GALLIUM --ETC(U)
DEC 77 W V MCLEVIGE DAAB07-72-C-0259
UNCLASSIFIED R-802 NL

2 OF 2
AD
A057 645

END
DATE
FILMED
9-78
DDC

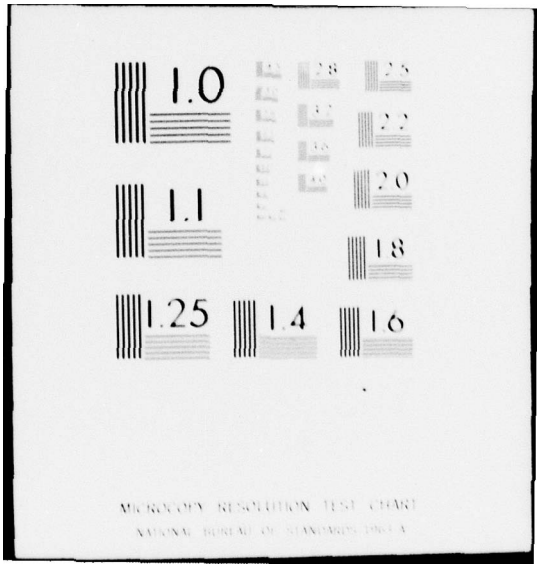
1.0
1.1
1.25
1.4
1.6
2.0
1.8
MICROCOPY RESOLUTION TEST CHART
NATIONAL BUREAU OF STANDARDS 1963-A

64. G. K. Hubler, J. Comas, and L. Plew, "Profiles of ion-implanted Be in GaAs by means of p,α nuclear reaction and SIMS methods," Nucl. Instrum. Meth., to be published.

65. H. Brooks, "Theory of the electrical properties of germanium and silicon," Adv. Electron. Electron Phys., Vol. 7, pp. 85-182, 1955.

66. J. D. Wiley, "Mobility of holes in III-V compounds," Semiconductors and Semimetals, Vol. 10, edited by R. K. Willardson and A. C. Beer, Academic Press, New York, 1975, pp. 91-174.

67. J. Comas and L. Plew, "Beryllium and sulfur ion-implanted profiles in GaAs," J. Electron. Mater., Vol. 5, pp. 209-21, 1976.

68. J. Comas, L. Plew, P. K. Chatterjee, W. V. McLevige, K. V. Vaidyanathan, and B. G. Streetman, "Impurity distribution of ion-implanted Be in GaAs by SIMS, photoluminescence, and electrical profiling," Ion Implantation in Semiconductors 1976, edited by F. Chernow, J. A. Borders, and D. K. Brice, Plenum Press, New York, 1977, pp. 141-8.

69. J. Comas and L. Plew, unpublished data.

70. W. K. Hofker, D. P. Oosthoek, N. J. Koeman, and H.A.M. de Grefte, "Concentration profiles of boron implantations in amorphous and polycrystalline silicon," Rad. Effects, Vol. 24, pp. 223-31, 1975.

71. J. Gibbons and S. Mylroie, "Estimation of impurity profiles in ion-implanted amorphous targets using joined half-Gaussian distributions," Appl. Phys. Lett., Vol. 22, pp. 568-9, 1973.

72. L. Plew, Naval Weapons Support Center, private communication.

73. H. C. Casey, Jr., "Diffusion in the III-V compound semiconductors," Atomic Diffusion in Semiconductors, edited by D. Shaw, Plenum, New York, 1973, pp. 351-430.

74. J. P. Donnelly, "Ion implantation in GaAs," Gallium Arsenide and Related Compounds (St. Louis) 1976, edited by L. F. Eastman, Institute of Physics, Bristol and London, 1977, pp. 166-90.

75. R. J. Witmeyer, R. B. Benson, Jr., M. A. Littlejohn, and J. Comas, "Correlation of defect density and atomic concentration profiles of Be ion implanted layers in GaAs," 19th Electronic Materials Conference, Cornell University, June 1977.

76. V. M. Zelevinskaya, G. A. Kachurin, N. P. Bogomyakov, B. S. Azikov, and L. L. Shirokov, "Capture of impurity atoms by vacancies in implanted layers," Sov. Phys. - Semicond., Vol. 8, pp. 164-6, 1974.

77. M. Takai, K. Gamo, K. Masuda, and S. Namba, "Lattice site location of cadmium and tellurium implanted in gallium arsenide," Jap. J. Appl. Phys., Vol. 14, pp. 1935-41, 1975.

78. R. G. Hunsperger and O. J. Marsh, "Anneal behavior of defects in ion-implanted GaAs diodes," Met. Trans., Vol. 1, pp. 603-7, 1970.

79. T. Itoh and Y. Kushiro, "Arsenic and cadmium implantations into n-type gallium arsenide," J. Appl. Phys., Vol. 42, pp. 5120-4, 1971.

80. H. C. Casey, Jr., M. B. Panish, and L. L. Chang, "Dependence of the diffusion coefficient on the Fermi level: zinc in gallium arsenide," Phys. Rev., Vol. 162, pp. 660-8, 1967.

81. P. G. Shewmon, Diffusion in Solids, McGraw-Hill, New York, 1963.

82. The value quoted is based on the data in Fig. 2 of Ref. 25, rather than on the equation for D which appears to be incorrect.

83. V. M. Zelevinskaya, G. A. Kachurin, N. B. Pridachin, and L. S. Smirnov, "Doping of gallium arsenide by implantation of zinc ions," Sov. Phys. - Semicond., Vol. 4, pp. 1529-32, 1971.

84. E. B. Stoneham, "A nonaqueous electrolyte for anodizing GaAs and $GaAs_{0.6}P_{0.4}$," J. Electrochem. Soc., Vol. 121, p. 1382, 1974.

85. D. Z. Tsang, "Anodic oxidation of gallium arsenide and gallium arsenide phosphide," M.S. Thesis, University of Illinois, 1975. Also Coordinated Science Laboratory Report R-708, available from NTIS, Springfield, Va. 22151 (Report #ADA019447).

86. H. Okabayashi, "Electrical and photoluminescent properties of zinc implanted $GaAs_{0.62}P_{0.38}$," Ion Implantation in Semiconductors, edited by S. Namba, Plenum Press, New York, 1974, pp. 95-100.

87. E. B. Stoneham, "The effects of ion-implanted gallium, arsenic, and phosphorus on the diffusion of ion-implanted zinc in gallium arsenide phosphide," Stanford Electronics Lab. Tech. Report 4733-1, Stanford University, 1975. It should be noted, however, that while the Hall mobilities in this reference are probably accurate, the net acceptor concentration profiles were obtained using 1.93 as the Hall coefficient factor (the ratio of Hall mobility to drift mobility), which is incorrect.

88. H. C. Casey, Jr., F. Ermanis, and K. B. Wolfstirn, "Variation of electrical properties with Zn concentration in GaP," J. Appl. Phys., Vol. 40, pp. 2945-58, 1969.

89. M. Ilegems and W. C. O'Mara, "Diffusion of beryllium into gallium phosphide," J. Appl. Phys., Vol. 43, pp. 1190-7, 1972.

90. H. C. Casey, Jr. and G. L. Pearson, "Diffusion in Semiconductors," Point Defects in Solids, Vol. 2, edited by J. H. Crawford and L. M. Slifkin, Plenum Press, New York, 1975, pp. 163-255.

91. W. C. Johnson and P. T. Panousis, "The influence of Debye length on the C-V measurement of doping profiles," IEEE Trans. Electron Devices, Vol. ED-18, pp. 965-73, 1971.

92. J. Crank, Mathematics of Diffusion, 2nd ed. Clarendon, Oxford, 1975.

93. D. J. Ashen, P. J. Dean, D.T.J. Hurle, J. B. Mullin, A. M. White, and P. D. Greene, "The incorporation and characterization of acceptors in epitaxial GaAs," J. Phys. Chem. Solids, Vol. 36, pp. 1041-53, 1975.

94. A. Lidow, J. F. Gibbons, and T. Magee, "A double-layered encapsulant for annealing ion-implanted GaAs up to 1100°C," Appl. Phys. Lett., Vol. 31, pp. 158-61, 1977.

APPENDIX 1

Projected Range Statistics of Implanted Be in GaAs and $GaAs_{0.6}P_{0.4}$

LSS RANGE STATISTICS FOR BERYLLIUM

IN GALLIUM ARSENIDE

SUBSTRATE PARAMETERS-

	GALLIUM	ARSENIDE
Z	31	33
M	69.720	74.920
N	.2214E+23	.2214E+23
RHO/R	.4991E+01	.4564E+01
EPS/E	.6603E-01	.6149E-01
CNSE	.1014E+02	.1027E+02
MU	7.747	8.324
GAMMA	.4050	.3830
SNO	.4890E+02	

ION-BERYLLIUM

Z	4
M	9.000

CROSS SECTION SUB. E= 4.00

ELECTRONIC CROSS SECTIONS OF
LINDHARD,SCHARFF,SCHIOTT

ENERGY (KEV)	PROJECTED RANGE (MICRONS)	PROJECTED STANDARD DEVIATION (MICRONS)	RANGE (MICRONS)	STANDARD DEVIATION (MICRONS)	NUCLEAR ENERGY LOSS (KEV/MICRON)	ELECTRONIC ENERGY LOSS (KEV/MICRON)
10	0.0308	0.0103	0.1069	0.0178	0.5924E+02	0.6453E+02
20	0.0615	0.0410	0.1821	0.0267	0.5035E+02	0.9125E+02
30	0.0936	0.0555	0.2492	0.0331	0.4433E+02	0.1118E+03
40	0.1262	0.0678	0.3108	0.0380	0.3937E+02	0.1291E+03
50	0.1590	0.0788	0.3683	0.0419	0.3548E+02	0.1443E+03
60	0.1917	0.0885	0.4223	0.0450	0.3267E+02	0.1581E+03
70	0.2240	0.0971	0.4733	0.0476	0.2991E+02	0.1707E+03
80	0.2564	0.1051	0.5221	0.0498	0.2727E+02	0.1825E+03
90	0.2887	0.1123	0.5688	0.0517	0.2499E+02	0.1936E+03
100	0.3209	0.1188	0.6136	0.0534	0.2308E+02	0.2041E+03
110	0.3528	0.1248	0.6569	0.0549	0.2154E+02	0.2140E+03
120	0.3842	0.1303	0.6986	0.0563	0.2037E+02	0.2235E+03
130	0.4151	0.1353	0.7389	0.0575	0.1957E+02	0.2327E+03
140	0.4452	0.1400	0.7779	0.0586	0.1913E+02	0.2414E+03
150	0.4744	0.1444	0.8157	0.0595	0.1907E+02	0.2499E+03
160	0.5026	0.1486	0.8523	0.0604	0.1887E+02	0.2581E+03
170	0.5305	0.1525	0.8879	0.0612	0.1790E+02	0.2661E+03
180	0.5582	0.1562	0.9227	0.0619	0.1702E+02	0.2738E+03
190	0.5856	0.1597	0.9567	0.0626	0.1620E+02	0.2813E+03
200	0.6128	0.1630	0.9900	0.0633	0.1546E+02	0.2886E+03
220	0.6662	0.1691	1.0544	0.0644	0.1420E+02	0.3027E+03
240	0.7185	0.1745	1.1163	0.0655	0.1324E+02	0.3161E+03
260	0.7695	0.1794	1.1759	0.0664	0.1257E+02	0.3290E+03
280	0.8191	0.1839	1.2334	0.0672	0.1219E+02	0.3414E+03
300	0.8673	0.1880	1.2891	0.0679	0.1211E+02	0.3534E+03
320	0.9139	0.1919	1.3429	0.0686	0.1197E+02	0.3650E+03
340	0.9596	0.1955	1.3952	0.0692	0.1131E+02	0.3763E+03
360	1.0045	0.1988	1.4462	0.0697	0.1071E+02	0.3872E+03
380	1.0486	0.2019	1.4958	0.0702	0.1015E+02	0.3978E+03
400	1.0920	0.2047	1.5442	0.0707	0.9648E+01	0.4081E+03
420	1.1347	0.2074	1.5916	0.0711	0.9193E+01	0.4182E+03
440	1.1767	0.2099	1.6379	0.0715	0.8788E+01	0.4280E+03
460	1.2180	0.2122	1.6832	0.0719	0.8432E+01	0.4376E+03
480	1.2587	0.2143	1.7275	0.0722	0.8127E+01	0.4471E+03
500	1.2987	0.2164	1.7711	0.0726	0.7872E+01	0.4563E+03
550	1.3961	0.2210	1.8763	0.0733	0.7452E+01	0.4785E+03
600	1.4896	0.2251	1.9770	0.0740	0.7345E+01	0.4998E+03
650	1.5796	0.2289	2.0737	0.0745	0.7196E+01	0.5202E+03
700	1.6666	0.2322	2.1668	0.0750	0.6812E+01	0.5399E+03
750	1.7511	0.2352	2.2567	0.0755	0.6466E+01	0.5588E+03
800	1.8332	0.2380	2.3438	0.0759	0.6157E+01	0.5771E+03
850	1.9132	0.2405	2.4282	0.0762	0.5879E+01	0.5949E+03
900	1.9911	0.2428	2.5103	0.0766	0.5627E+01	0.6122E+03
950	2.0672	0.2449	2.5901	0.0769	0.5397E+01	0.6289E+03
1000	2.1416	0.2468	2.6680	0.0772	0.5188E+01	0.6453E+03

LSS RANGE STATISTICS FOR BERYLLIUM

IN GALLIUM ARSENIDE PHOSPHIDE40%

SUBSTRATE PARAMETERS-

	GALLIUM	ARSENIDE	PHOSPHIDE40%
Z	31	33	15
M	69.720	74.920	30.970
N	.2313E+23	.1388E+23	.9300E+22
RHO/R	.5214E+01	.2662E+01	.5202E+01
EPS/E	.6603E-01	.6149E-01	.1433E+00
CNSE	.1059E+02	.6436E+01	.3561E+01
MU	7.747	8.324	3.441
GAMMA	.4050	.3830	.6979

SNO .5281E+02

ION-BERYLLIUM

Z 4

M 9.000

CROSS SECTION SUB. E= 4.00

ELECTRONIC CROSS SECTIONS OF
LINDHARD,SCHARFF,SCHIOTT

ENERGY (KEV)	PROJECTED RANGE (MICRONS)	PROJECTED STANDARD DEVIATION (MICRONS)	RANGE (MICRONS)	STANDARD DEVIATION (MICRONS)	NUCLEAR ENERGY LOSS (KEV/MICRON)	ELECTRONIC ENERGY LOSS (KEV/MICRON)
10	0.0326	0.0241	0.1001	0.0182	0.6004E+02	0.6511E+02
20	0.0651	0.0407	0.1744	0.0276	0.5116E+02	0.9208E+02
30	0.0986	0.0545	0.2410	0.0342	0.4435E+02	0.1128E+03
40	0.1324	0.0666	0.3021	0.0391	0.3950E+02	0.1302E+03
50	0.1662	0.0772	0.3592	0.0430	0.3542E+02	0.1456E+03
60	0.1999	0.0867	0.4128	0.0461	0.3211E+02	0.1595E+03
70	0.2335	0.0952	0.4637	0.0487	0.2955E+02	0.1723E+03
80	0.2658	0.1028	0.5118	0.0509	0.2850E+02	0.1842E+03
90	0.2976	0.1098	0.5578	0.0527	0.2677E+02	0.1953E+03
100	0.3288	0.1162	0.6020	0.0543	0.2520E+02	0.2059E+03
110	0.3597	0.1221	0.6444	0.0558	0.2378E+02	0.2159E+03
120	0.3901	0.1276	0.6854	0.0570	0.2251E+02	0.2255E+03
130	0.4201	0.1326	0.7251	0.0582	0.2140E+02	0.2348E+03
140	0.4496	0.1373	0.7636	0.0592	0.2042E+02	0.2436E+03
150	0.4792	0.1416	0.8010	0.0602	0.1908E+02	0.2522E+03
160	0.5081	0.1456	0.8373	0.0611	0.1845E+02	0.2604E+03
170	0.5365	0.1494	0.8727	0.0619	0.1785E+02	0.2685E+03
180	0.5644	0.1530	0.9072	0.0626	0.1728E+02	0.2762E+03
190	0.5919	0.1563	0.9409	0.0633	0.1673E+02	0.2838E+03
200	0.6189	0.1595	0.9738	0.0639	0.1621E+02	0.2912E+03
220	0.6719	0.1653	1.0374	0.0650	0.1524E+02	0.3054E+03
240	0.7235	0.1705	1.0986	0.0660	0.1438E+02	0.3190E+03
260	0.7737	0.1753	1.1575	0.0669	0.1362E+02	0.3320E+03
280	0.8228	0.1796	1.2144	0.0677	0.1295E+02	0.3445E+03
300	0.8708	0.1836	1.2695	0.0684	0.1223E+02	0.3566E+03
320	0.9179	0.1872	1.3229	0.0691	0.1156E+02	0.3683E+03
340	0.9640	0.1905	1.3748	0.0697	0.1094E+02	0.3797E+03
360	1.0092	0.1935	1.4254	0.0702	0.1037E+02	0.3907E+03
380	1.0536	0.1964	1.4746	0.0707	0.9849E+01	0.4014E+03
400	1.0973	0.1990	1.5227	0.0712	0.9375E+01	0.4118E+03
420	1.1401	0.2014	1.5696	0.0716	0.8948E+01	0.4220E+03
440	1.1823	0.2036	1.6155	0.0720	0.8567E+01	0.4319E+03
460	1.2237	0.2057	1.6604	0.0724	0.8232E+01	0.4416E+03
480	1.2644	0.2076	1.7044	0.0727	0.7943E+01	0.4511E+03
500	1.3045	0.2095	1.7476	0.0731	0.7699E+01	0.4604E+03
550	1.4019	0.2137	1.8519	0.0738	0.7286E+01	0.4829E+03
600	1.4954	0.2174	1.9518	0.0745	0.7152E+01	0.5043E+03
650	1.5853	0.2207	2.0476	0.0750	0.6924E+01	0.5249E+03
700	1.6723	0.2237	2.1400	0.0755	0.6549E+01	0.5448E+03
750	1.7567	0.2264	2.2291	0.0760	0.6214E+01	0.5639E+03
800	1.8388	0.2289	2.3155	0.0764	0.5915E+01	0.5824E+03
850	1.9186	0.2311	2.3992	0.0767	0.5646E+01	0.6003E+03
900	1.9964	0.2331	2.4806	0.0771	0.5402E+01	0.6177E+03
950	2.0723	0.2350	2.5597	0.0774	0.5180E+01	0.6346E+03
1000	2.1464	0.2367	2.6369	0.0776	0.4978E+01	0.6511E+03

APPENDIX 2

Computer Programs for Analysis of Differential Resistivity and Hall Effect Data

```
00100   C       NEWDA.F4
00200   C
00300   C       NEWDA.F4 IS THE SAME AS HDATI.F4 EXCEPT THE DATA IS READ IN
00400   C       AND OUT THROUGH DATA FILES (DA1.DAT AND DA2.DAT)
00500   C       THIS PROGRAM COMPUTES SHEET RESISTIVITY AND HALL COEFFICIENTS
00600   C       FOR DIFFERENTIAL DOUBLE AC VAN DER PAUW DATA
00700   C       NOTE: LPT 10 MUST BE ASSIGNED
00800   C       TO ENTER VAN DER PAUW DATA:  SOS DA1.DAT
00900   C       5F FORMAT:  VABCD(MV)  VBCDA(MV)  DELTAVBDAC(MV)  VAN DER PAUW
01000   C       FACTOR  CURRENT(MA)
01100   C       WHEN FINISHED ENTERING DATA IN DA1.DAT, TYPE ES TO DELETE
01200   C       LINE NUMBERS;  THEN  EX NEWDA.F4
01300   C       VALUES FOR SHEET RESISTIVITY AND HALL COEFFICIENT ARE
01400   C       AUTOMATICALLY ENTERED IN DA2.DAT
01500           REAL I(50)
01600           DIMENSION V1(50),V2(50),DV(50),F(50),RS(50),RH(50),US(50),CS(50)
01700
01800           OPEN(UNIT=20,ACCESS='SEQIN',MODE='ASCII',FILE='DA1.DAT')
01900           OPEN(UNIT=21,ACCESS='SEQOUT',MODE='ASCII',FILE='DA2.DAT')
02000           TYPE 1
02100      1    FORMAT(2X,'TYPE IN',/,2X,'B(GAUSS)',2X,
02200        1  '# OF DATA POINTS',2X,'HALL COEFFICIENT FACTOR'/)
02300           ACCEPT 2,B,N,HCF
02400      2    FORMAT(F,I,F)
02500           WRITE(10,6) B,HCF
02600      6    FORMAT(3X,'B =',2X,F6.1,' GAUSS',5X,'HALL COEFFICIENT FACTOR = '
02700        1  ,F5.2/)
02800           DO 4 M=1,N
02900           READ(20,5,END=4) V1(M),V2(M),DV(M),F(M),I(M)
03000      5    FORMAT (5F)
03100      4    CONTINUE
03200           WRITE(10,30)
03300     30    FORMAT(3X,'SHEET RESISTIVITY',3X,'HALL COEFFICIENT',5X,
03400        1  'MOBILITY',7X,'SHEET CARRIER CONC',3X,'VABCD',5X,'VBCDA',6X,
03500        1  'DVBDAC',6X,'F',7X,'I'/)
03600           WRITE(10,35)
```

```
03700    35       FORMAT(7X,'(OHM/SQ)',8X,'(CM**2/COUL)',7X,'(CM**2/V/SEC)',
03800           1 7X,'(CM**-2)',12X,'MV',8X,'MV',9X,'MV',16X,'MA'/)
03900             DO 15 K=1,N
04000             RS(K)=3.14159/ALOG(2.)*(V1(K)+V2(K))/(2.*I(K))*F(K)
04100             RH(K)=DV(K)/(I(K)*B*1.0E-8)*SQRT(2.0)
04200             US(K)=RH(K)/(RS(K)*HCF)
04300             CS(K)=HCF/(1.60219E-19*RH(K))
04400             WRITE(10,40) RS(K),RH(K),US(K),CS(K),V1(K),V2(K),DV(K),F(K),I(K)
04500             WRITE(21,101)  RS(K),RH(K)
04600     101     FORMAT(5X,E11.5,9X,E11.5)
04700    40       FORMAT(5X,E11.5,9X,E11.5,8X,F8.2,9X,E11.5,7X,F7.3,3X,F7.3,2X,
04800           1 E10.4,2X,F5.3,3X,E8.3)
04900      15     CONTINUE
05000             END
```

```
00100    C        NEWPR.F4
00200    C
00300    C        NEWPR.F4 IS THE SAME AS HPRFL.F4 EXCEPT THE DATA IS READ IN
00400    C        THROUGH A DATA FILE (DA2.DAT)
00500    C        THIS PROGRAM COMPUTES CARRIER CONCENTRATION PROFILES FROM
00600    C        DIFFERENTIAL RESISTIVITY AND HALL COEFFICIENT DATA
00700    C        NOTE: LPT 10 MUST BE ASSIGNED
00800    C        TO ENTER DATA:  SOS DA2.DAT
00900    C        2F FORMAT:  SHEET RESISTIVITY(OHM/SQ)  SHEET HALL COEFFICIENT
01000    C        (CM**2/COUL)
01100    C        WHEN FINISHED ENTERING DATA IN DA2.DAT, TYPE ES TO DELETE LINE
01200    C        NUMBERS;  THEN  EX NEWPR.F4
01300             DIMENSION SIGMA(50),UH(50),UC(50),CC(50),DEP(50)
01400             DIMENSION RS(50),RH(50)
01500             TYPE 1
01600       1     FORMAT(2X,'TYPE IN',/,2X,'STEP SIZE (A)',5X,'# OF DATA POINTS',
01700           1 5X,'HALL COEFFICIENT FACTOR'/)
```

```
01800            ACCEPT 2,D,N,HCF
01900       2    FORMAT( F,I,F)
02000            WRITE(10,12) HCF
02100       12   FORMAT(2X,'HALL COEFFICIENT FACTOR = ',F5.2/)
02200            WRITE(10,6) D
02300        6   FORMAT(2X,'RS (OHM/SQ)',5X,'RH (CM**2/COUL)',5X,'STEP SIZE ='
02400          1 ,F7.1,2X,'(A)'/)
02500            OPEN(UNIT=21,ACCESS='SEQIN',MODE='ASCII',FILE='DA2.DAT')
02600            DO 4 M=1,N
02700            READ (21,5) RS(M),RH(M)
02800       5    FORMAT (2F)
02900            WRITE(10,7) RS(M),RH(M)
03000        7   FORMAT(2X,E10.5,7X,E11.5)
03100       4    CONTINUE
03200            WRITE(10,30)
03300       30   FORMAT (2X,///,2X,'DEPTH (A)',3X,'MOBILITY (CM**2/V/SEC)',3X,'
03400          1  CARRIER CONC (CM**-3)'/)
03500            DO 15 K=1,N
03600            IF (K-1) 20,15,20
03700       20   SIGMA(K)=1.E8/D*(1./RS(K-1)-1./RS(K))
03800            UH(K)=RH(K-1)/RS(K-1)+RH(K)/RS(K)-(RH(K)-RH(K-1))/(RS(K)-RS(K-1))
03900            UC(K)=UH(K)/HCF
04000            CC(K)=SIGMA(K)/(1.60219E-19*UC(K))
04100            DEP(K)=D*(K-1.5)
04200            WRITE (10,35) DEP(K),UC(K),CC(K)
04300       35   FORMAT(3X,F7.1,12X,F6.1,17X,E)
04400       15   CONTINUE
04500            END
```

APPENDIX 3

Computer Programs for Diffusion Analysis of Gaussian and Rectangular Distributions

```
00100    C      GAUSDF.F4
00200    C      THIS PROGRAM COMPUTES THE DIFFUSION PROFILE OF A GAUSSIAN
00300    C      DISTRIBUTION WITH INTEGRATED AREA Q AND CENTERED AT R WITH
00320    C      STANDARD DEVIATION SD
00500           DIMENSION CONC(150)
00600     5     CONTINUE
00700           TYPE 10
00800    10     FORMAT(' SUPPLY INPUT PARAMETERS'//' INTEGRATED',3X,'CENTERED',3X
00900          1 ,'STANDARD',5X,'DIFFUSION'/4X,'AREA',9X,'AT',6X,'DEVIATION',3X,
01000          1 'COEFFICIENT',4X,'TIME'/'  (CM**-2)   (MICRONS)',3X,'(MICRONS)',
01100          1 3X,'(CM**2/SEC)  (MINUTES)')
01200           ACCEPT 20,Q,R,SD,D,T
01300    20     FORMAT(5F)
01400           WRITE(3,30) Q,R,SD,D,T
01500    30     FORMAT('1','INTEGRATED',3X,'CENTERED',3X,'STANDARD',5X,'DIFFUSION'
01600          1 /4X,'AREA',9X,'AT',6X,'DEVIATION',3X,'COEFFICIENT',4X,'TIME'/
01700          1 '  (CM**-2)',3X,'(MICRONS)',3X,'(MICRONS)',3X,'(CM**2/SEC)',
01800          1 2X,'(MINUTES)'//1X,E10.4,F9.4,5X,F6.4,5X,E10.4,4X,F6.1)
01900           TYPE 40
02000    40     FORMAT('-INCREMENT SIZE (MICRONS)',5X,'NUMBER OF INCREMENTS')
02100           ACCEPT 50,SIZE,N
02200    50     FORMAT(F,I)
02300           WRITE(3,60)
02400    60     FORMAT('-   DEPTH',4X,'CONCENTRATION'/' (MICRONS)',5X,'(CM**-3)'/)
02500           M=N+1
02600           DO 90 K=1,M
02700           SIGMA=SQRT((SD*1.0E-4)**2+120.0*D*T)
02800           DEP=SIZE*(K-1)
02900           CONC(K)=Q/SQRT(2.0*3.14159265)/SIGMA*EXP(-1.0E-8*(DEP-R)**2
03000          1 /2.0/SIGMA**2)
03100           WRITE(3,70) DEP,CONC(K)
03200    70     FORMAT(1X,F7.4,4X,E10.4)
03300    90     CONTINUE
03400           GO TO 5
03500           END
```

```
00100    C      RECTDF.F4,SYS:IMSL/SEAR
00200    C      THIS PROGRAM COMPUTES THE DIFFUSION PROFILE OF AN INITIALLY
00300    C      RECTANGULAR DISTRIBUTION OF WIDTH W AND CONCENTRATION Q AND
00400    C      CENTERED AT DEPTH R
00500    C
00550           DIMENSION CONC(150)
00600     5     CONTINUE
00700           TYPE 10
00800    10     FORMAT(1X,/' SUPPLY INPUT PARAMETERS'//4X,'INITIAL',7X,'CENTERED'
00900          1 ,6X,'WIDTH',6X, 'DIFFUSION',6X,'TIME'/' CONCENTRATION',7X,'AT',
01000          1 19X,'COEFFICIENT'/3X,'(CM**-3)',6X,'(MICRONS)',4X,'(MICRONS)'
01100          1 ,3X,'(CM**2/SEC)',3X,'(MINUTES)')
01200           ACCEPT 20,Q,R,W,D,T
01300    20     FORMAT(5F)
01400           WRITE(3,30) Q,R,W,D,T
01500    30     FORMAT('1',3X,'INITIAL',9X,'CENTERED',6X,'WIDTH',6X,
01600          1 'DIFFUSION',6X,'TIME'/' CONCENTRATION',9X,'AT',19X,'COEFFICIENT'
01700          1 /3X,'(CM**-3)',9X,'(MICRONS)',3X,'(MICRONS)',3X,'(CM**2/SEC)',
01800          1 2X,'(MINUTES)'//2X,E10.4,9X,F7.4,5X,F7.4,4X,E10.4,5X,F6.1)
01900           TYPE 40
02000    40     FORMAT('-INCREMENT SIZE (MICRONS)',5X,'NUMBER OF INCREMENTS')
02100           ACCEPT 50,SIZE,N
02200    50     FORMAT(F,I)
02300           WRITE(3,60)
02400    60     FORMAT('-   DEPTH',4X,'CONCENTRATION'/' (MICRONS)',5X,'(CM**-3)'/)
02500           M=N+1
02600           DO 90 K=1,M
02700           XK=(SIZE*(K-1)-R)*1.0E-4
02800           DEP=SIZE*(K-1)
02900           ARG1=(W*1.0E-4/2.0+XK)/2.0/SQRT(D*T*60.0)
02940           ARG2=(W*1.0E-4/2.0-XK)/2.0/SQRT(D*T*60.0)
02980           CALL MERF(ARG1,ERF1)
03020           CALL MERF(ARG2,ERF2)
03060           CONC(K)=0.5*Q*(ERF1+ERF2)
03100           WRITE(3,70) DEP,CONC(K)
03200    70     FORMAT(1X,F7.4,4X,E10.4)
03300    90     CONTINUE
03400           GO TO 5
03500           END
```

VITA

William Victor McLevige was born on July 1, 1952 in Rockford, Illinois. Since September 1970 he has been attending the University of Illinois at Urbana-Champaign. He received a Bachelor of Science in Electrical Engineering with highest honors in May 1974. While working towards the Master of Science degree in Electrical Engineering, which was received in May 1975, he held a University Fellowship. Mr. McLevige is a member of the Institute of Electrical and Electronics Engineers.